Title
Baroclinic-Barotropic Interaction in Teleconnections

Author
Ji, Xuan

Publication Date
2016

Peer reviewed|Thesis/dissertation

UNIVERSITY OF CALIFORNIA

Los Angeles

Baroclinic-Barotropic Interaction in Teleconnections

A dissertation submitted in partial satisfaction
of the requirements for the degree Doctor of Philosophy
in Atmospheric and Oceanic Sciences

by

Xuan Ji

2016

ABSTRACT OF THE DISSERTATION

Baroclinic-Barotropic Interaction in Teleconnections

by

Xuan Ji

Doctor of Philosophy in Atmospheric and Oceanic Sciences

University of California, Los Angeles, 2016

Teleconnections are remote impacts from one location to another, which are transmitted through planetary-scale wave motions, e.g., Rossby waves. Teleconnections can be forced by tropical heat sources, for example, El Niño/Southern Oscillation (ENSO), and result in many societally important impacts in remote ocean basins and continents. It is thus important to understand the complex pathway and wave dynamics in teleconnections. This dissertation discusses the role of baroclinic-barotropic interaction in three different aspects of atmospheric teleconnections.

The first major question addressed is what mechanisms control the interhemispheric teleconnections from tropical heat sources. These are investigated using an intermediate complexity model [a Quasi-equilibrium Tropical Circulation Model (QTCM)] and a simple linear two-level model with dry dynamics. Illustrating the interhemispheric teleconnection process with an Atlantic Warm Pool principal case, the heat source directly excites a baroclinic response that spreads across the equator. Three processes involving baroclinic-barotropic interactions—shear advection, surface drag, and vertical advection—then force a cross-equatorial barotropic Rossby wave response. An analysis of these processes in QTCM simulations indicates that: (1) shear advection has a pattern that roughly coincides with the baroclinic signal in the tropics and subtropics; (2) surface drag has large amplitude and spatial extent, and can be very effective in forcing barotropic motions around the globe; (3) vertical advection has a significant contribution locally and remotely where large vertical motions and vertical shear occur. A simple model is modified to perform experiments in which each of these three mechanisms may be included or omitted. By adding surface drag and vertical advection, and comparing each to shear advection, the effects of the three mechanisms on the

generation and propagation of the barotropic Rossby waves are shown to be qualitatively similar to the results in QTCM. It is also found that the moist processes included in the QTCM can feed back on the teleconnection process and alter the teleconnection pattern by enlarging the prescribed tropical heating in both intensity and geographical extent, and by inducing remote precipitation anomalies by interaction with the basic state.

The second major question addressed concerns the dynamics that maintain the sea level pressure (SLP) anomalies in the western Pacific that are an integral part of the classic ENSO pattern. Traditional studies of the ENSO response in the tropics assume a single deep baroclinic mode associated with the tropospheric temperature anomalies. However, the SLP anomalies in the western Pacific are spatially separated from the baroclinic signal in the NCEP-NCAR reanalysis, CMIP5 models, and QTCM. Separation of ENSO SLP anomalies in the tropical Pacific into baroclinic and barotropic components indicates that the barotropic component contributes throughout the tropics and constitutes the primary contribution in the western Pacific. To demonstrate the roles of baroclinic and barotropic modes in ENSO teleconnections within the tropics, a series of QTCM experiments is performed, where anomalies in the interactions between baroclinic and barotropic modes are suppressed over increasingly wider latitudinal bands in the tropical Pacific. If this suppression is done in the 15°N-15°S band, the pressure signals in the western Pacific are only partly removed, whereas if it is done in the 30°N-30°S band, the anomalies in the western Pacific are almost entirely removed. This suggests the following pathway: interactions with sea surface temperature (SST) anomalies create the baroclinic response in the central and eastern Pacific, but baroclinic-barotropic interactions, arising substantially in the subtropical Pacific, generate a barotropic response that yields the SLP anomalies in the western Pacific.

The third major question addressed is by what pathways the baroclinic response forced by El Niño SST anomalies gives rise to the barotropic component of ENSO teleconnections, focusing especially on the subtropical Pacific. This is examined by diagnosing from NCEP-NCAR reanalysis the interaction terms in a vertical mode decomposition that yields an effective Rossby wave source, and by analyzing the response of QTCM to the NCEP-NCAR effective Rossby wave source. Among the three barotropic Rossby wave source contributions (shear advection, vertical advection and surface drag), the leading contribution is from shear advection, and more specifically, the mean baroclinic

zonal wind advecting the anomalous baroclinic zonal wind. Vertical advection is the smallest term, while surface drag tends to cancel and reinforce the shear advection in different regions through damping on baroclinic mode, which spins up a barotropic response. There are also non-trivial impacts of transients in the barotropic wind response to ENSO. Both tropical and subtropical baroclinic vorticity advection contribute to the barotropic component of the Pacific subtropical jet near coast of North America, where the resulting barotropic wind contribution approximately doubles the zonal jet anomaly at upper levels, relative to the baroclinic anomalies alone. In this view, the effective Rossby wave source in the subtropics simply arises from the basic-state baroclinic flow acting on the well-known baroclinic ENSO flow pattern that spreads from the deep tropics into the subtropics over a scale of equatorial radius of deformation. This is inseparably connected to the leading deep tropical Rossby wave source that arises from eastern Pacific climatological baroclinic winds advecting the tropical portion of the same ENSO flow pattern.

The dissertation of Xuan Ji is approved.

James C. McWilliams

Marilyn N. Raphael

Carlos R. Mechoso

J. David Neelin, Committee Chair

University of California, Los Angeles

2016

DEDICATION

to my parents, and husband Lin Cheng

Table of contents

List of figures

ACKNOWLEDGEMENTS

Chapter 1 contains versions of figures from work published in Ma et al. (2013). This work was supported in part by NOAA's MAPP/CPO program under Grant NA100AR4310262. This work was also supported under NSF Grants ATM-0751030, AGS-1041477, AGS-1102838, and AGS-1115506. I would like to thank Hsi-Yen Ma for a chance to participate in his interesting research. I would like to thank Sang-ki Lee for his guidance and support in running the simple model.

Chapter 2 is a version of Ji et al. (2014), which was supported in part by National Science Foundation Grant AGS-1102838 and AGS-1041477. I would like to thank Joyce E. Meyerson and Katrina Hales for their guidance and support in running the QTCM.

Chapter 3 is a version of Ji et al. (2015), This work was supported in part by National Science Foundation Grants AGS-1102838 and AGS-1041477, National Oceanic and Atmospheric Administration Grants NA11OAR4310099 and NA14OAR4310274. I would like to thank Hui Su and Matt Munnich for their unpublished initial QTCM and NCEP analysis (2004) related to this problem, and to Xin Qu for his comments. JDN would like to acknowledge the role of Plate 8 from Wallace et al. (1998) in which the mismatch of sea level pressure and tropospheric temperature patterns led to the puzzle analyzed here.

Chapter 4 is a draft of a manuscript in progress to be coauthored with J. David Neelin and C. Roberto Mechoso. This work was supported by National Science Foundation Grant AGS-1540518, and National Oceanic and Atmospheric Administration Grant NA14OAR4310274.

The first three chapters contain versions of work published in *Journal of Climate*, © Copyright 2013–2015 American Meteorological Society (AMS). I would like to acknowledge a scholarship awarded by the Chinese Scholarship Council to support my doctoral study at the University of California, Los Angeles. I am grateful to Joyce E. Meyerson for her assistance with graphics and with translation from word to latex. Finally, I thank J. David Neelin and C. Roberto Mechoso for their patience and guidance as coauthors and coadvisors.

Xuan Ji

Los Angeles, California

January, 2016

Xuan Ji

EDUCATION

University of California, Los Angeles, CA

M.S. Atmospheric and Oceanic Sciences — June 2012

Nanjing University, Nanjing, China

Sc.B. Atmospheric Science — June 2010

FELLOWSHIPS AND AWARDS

Government-sponsored Study Abroad Scholarship (Chinese Scholarship Council) — 2010–2014

Outstanding Graduates of Nanjing University (Nanjing University) — 2010

People Scholarship (Nanjing University) — 2009

China National Scholarship (Education Ministry of China) — 2008

PUBLICATIONS

Ji, X., J. D. Neelin, and C. R. Mechoso, 2015: El Niño/Southern Oscillation Sea Level Pressure anomalies in the western Pacific: Why are they there? *Journal of Climate*, **28 (22)**, 8860–8872.

Ji, X., J. D. Neelin, S.-K. Lee, and C. R. Mechoso, 2014: Interhemispheric teleconnections from tropical heat sources in intermediate and simple models. *Journal of Climate*, **27 (2)**, 684–697.

Ma, H.-Y., C. R. Mechoso, Y. Xue, H. Xiao, J. D. Neelin, and X. Ji, 2013: On the connection between continental-scale land surface processes and the tropical climate in a coupled ocean–atmosphere–land system. *Journal of Climate*, **26 (22)**, 9006–9025.

Ma, H. Y., X. Ji, J. D. Neelin, and C. R. Mechoso, 2011: Mechanisms for precipitation variability of the eastern Brazil/SACZ convective margin. *Journal of Climate*, **24 (13)**, 3445–3456.

Chapter 1

Introduction

1.1 Background and overview

Teleconnections are remote impacts from one location to another, which are transmitted through planetary-scale wave motions, e.g., Rossby waves. Teleconnections can be forced by tropical heat sources, for example, El Niño/Southern Oscillation (ENSO), and result in many societally important impacts in remote ocean basins and continents. It is thus important to understand the complex wave dynamics in atmospheric teleconnections, and to study the pathway of wave propagations and interactions with basic state, so that we can better simulate and predict the impacts due to teleconnections from different variabilities in the climate system.

This dissertation is based on published and to-be-published work on the fundamental mechanisms at work in atmospheric teleconnections, with an emphasis on the interaction between baroclinic and barotropic components of the flow. Founded in many teleconnection studies using models with different complexities, heating anomalies directly force a baroclinic signal in the vicinity of heating anomalies, with deep tropospheric temperature perturbations and associated vertically varying wind fields. Teleconnections to mid- and high latitudes, however, tend to be dominated by an equivalent barotropic signal, with some temperature contribution but approximately vertically constant wind fields. Barotropic teleconnections can also be important within the tropics. How does the baroclinic mode translate into a barotropic mode in the process? By projecting the primitive equations onto a consistent vertical mode decomposition, a barotropic mode can be forced by three mechanisms due to baroclinic-barotropic interaction: shear advection, vertical advection and surface drag.

Chapter 2 presents results from work done in Ji et al. (2014), which examined how a heat source in the subtropics of the Northern Hemisphere, in particular in the Atlantic Warm Pool, could have impacts into the Southern Hemisphere through teleconnections. Using two different models [an intermediate complexity model for the tropics that includes moist dynamics (QTCM), and a linear, two-level wave model], it is shown that a baroclinic wave mode excited by the subtropical heat source could propagate through the tropics and then excite a barotropic mode in the Southern Hemisphere which can then penetrate to mid- and high latitudes. The effects of the three mechanisms (shear advection, vertical advection and surface drag) for transferring energy from the baroclinic mode into the barotropic teleconnections were studied in detail in this interhemispheric teleconnection case.

Chapter 3 discusses work done in Ji et al. (2015), which identified a hitherto unknown aspect of the atmospheric side of the tropical ENSO phenomenon. Since the earliest days of observational analysis of the Southern Oscillation, sea level pressure anomalies in the western Pacific have been a part of the classical oscillation pattern. Contrary to understanding based on simple models, which assumed that baroclinic dynamics was sufficient to explain the atmospheric response to heating anomalies in the deep tropics, the analysis here show that the pressure anomalies in the western Pacific are primarily barotropic. It is shown that baroclinic-barotropic mode interactions are necessary to explain these anomalies, and that subtropical regions must be included to properly understand the tropical response. The results are based on combined analysis of observations, climate models from the Coupled Model Intercomparison Project Phase 5 (CMIP5), and an intermediate complexity climate model (QTCM).

Chapter 4 discusses current work in preparation to be published. This work continues to identify the impacts of these modal interactions on El Niño teleconnections. The barotropic mode is important in carrying the El Niño impacts to midlatitudes, but it has been difficult to assess how energy is transferred from the directly-forced baroclinic response in the tropics to the barotropic dynamics that can propagate to higher latitudes. Diagnoses using the NCEP-NCAR reanalysis, as well as several simulations using an intermediate complexity climate model (QTCM) have been performed to assess the relative importance of each of the three mechanisms (shear advection, vertical advection and surface drag) and the sum of the three as a whole in generating El Niño

teleconnections from tropics to mid- and high latitudes.

The remainder of the current chapter discusses published work to which I have contributed analysis, as well as some of the major conclusions.

1.2 On the Connection between Continental-Scale Land Surface Processes and the Tropical Climate in a Coupled Ocean-Atmosphere-Land System (Ma et al., 2013)

This teleconnection study by Ma et al. (2013) examines in a climate model how the perturbations in land surface processes can transfer to other regions. It is found that perturbations in the tropical African continent have the largest impact on the tropical Pacific. This connection can be explained by the convective heating anomalies associated with perturbed surface heat fluxes in African continent triggering global teleconnections through equatorial wave dynamics. One very interesting aspect of this study is that impacts from Africa to the Pacific Ocean could be amplified by ocean-atmosphere interaction within the Pacific.

Some of my main contribution to this paper involve using a simple atmospheric model developed by Lee et al. (2009) to gain insights into the remote response to the convective heating in Africa. This is a steady-state two-level primitive equation model, linearized about a prescribed background mean state. This model has been used in several theoretical studies by Lee et al. (2009) and Wang et al. (2010) on the impact of convection heating associated with the Atlantic Warm Pool. In this experiment, the prescribed mean states correspond to the large-scale flows at 250 and 750 hPa from the JJA climatology of the NCEP-NCAR reanalysis (Kalnay et al., 1996). A thermal forcing of Gaussian shape at middle level (500 hPa), where the intensity ~ 2.5 K day^{-1} is prescribed centered at 108°N, 258°E to mimic the anomalous convective heating. More details of this model are presented in Lee et al. (2009).

Figures 1.1a and 1.1b show the anomalous velocity potential and divergent winds at 250 hPa in the simple model, together with the streamfunction and rotational winds at 750 hPa. With the thermal forcing placed over the African continent, the response of large-scale flows demonstrates the typical equatorial wave solution. The equatorial Kelvin waves extend eastward over the tropical Pacific and modify the intensity of subtropical highs and the equatorial trade winds. Therefore,

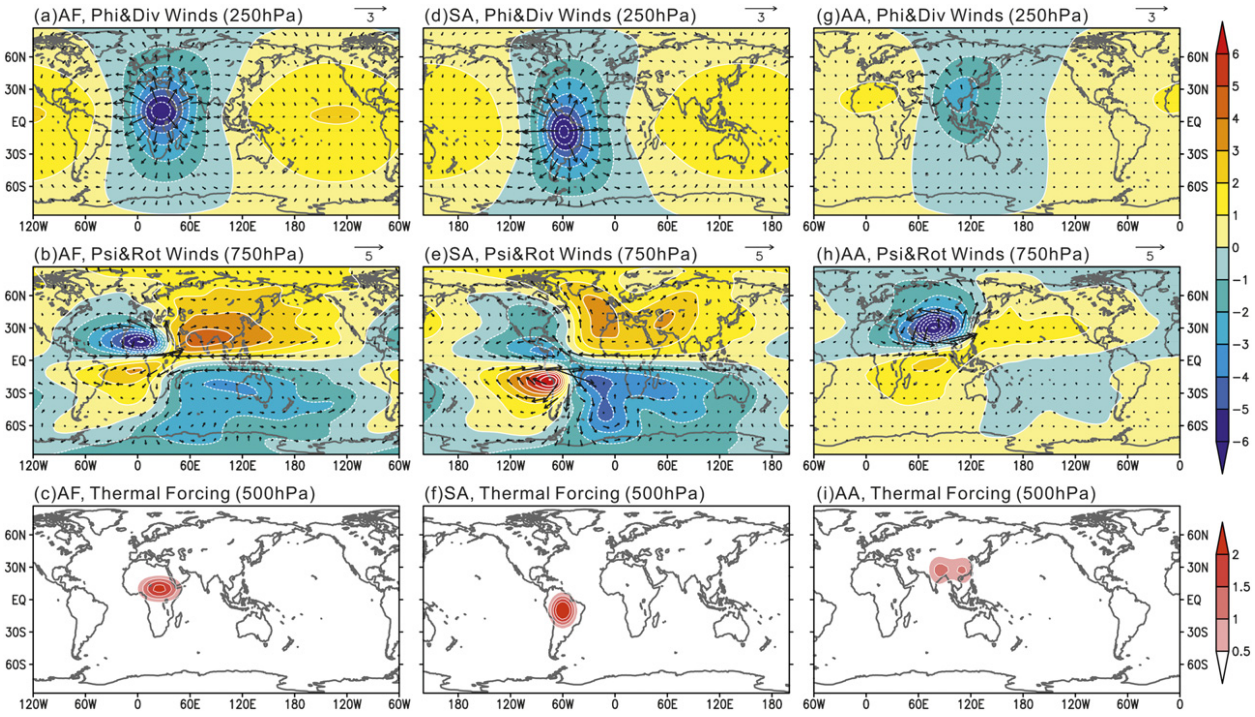

Figure 1.1: (a),(d),(g) Anomalous velocity potential ($m^2\ s^{-1}$) and divergent winds ($m\ s^{-1}$) at 250 hPa and (b),(e),(h) streamfunction ($m^2\ s^{-1}$) and rotational winds ($m\ s^{-1}$) at 750 hPa from a two-layer shallow water model with a prescribed thermal forcing (K) at 500 hPa over (c) Africa, (f) South America, and (i) Asia. See text for more details of experimental setup.

the equatorial easterlies at low level over the western and central Pacific are enhanced through the anomalous convective heating over Africa. The simple model lacks the convective interactions of moist teleconnections but it establishes that eastward wave propagation can yield surface easterlies over the equatorial Pacific where they can initiate ocean-atmosphere feedbacks.

We also performed another two simple model tests (Figs. 1.1d-i) with prescribed heating centers located over South America ($\sim$ 2.5 K day^{-1}, DJF climatological winds) or South and Southeast Asia ($\sim$ 1.25 K day^{-1}, JJA climatological winds). In the South America experiment, the largest impacts of low-level flows are over the equatorial eastern Pacific, Atlantic, and Indian Ocean. The impacts over the western and central Pacific are very small. In the Asia experiment, the impacts of low-level flows are over the equatorial Indian and Pacific Oceans. There are westerly anomalies over the Indian Ocean and easterly anomalies over the Pacific.

Chapter 2

Interhemispheric teleconnections from tropical heat sources in intermediate and simple models

Abstract

The mechanisms that control the interhemispheric teleconnections from tropical heat sources are investigated using an intermediate complexity model (a Quasi-Equilibrium Tropical Circulation Model, QTCM) and a simple linear two-level model with dry dynamics. Illustrating the interhemispheric teleconnection process with an Atlantic Warm Pool principal case, the heat source directly excites a baroclinic response that spreads across the equator. Three processes involving baroclinic-barotropic interactions—shear advection, surface drag, and vertical advection—then force a cross-equatorial barotropic Rossby wave response. An analysis of these processes in QTCM simulations indicates that: (1) shear advection has a pattern that roughly coincides with the baroclinic signal in the tropics and subtropics; (2) surface drag has large amplitude and spatial extent, and can be very effective in forcing barotropic motions around the globe; (3) vertical advection has a significant contribution locally and remotely where large vertical motions and vertical shear occur. The simple model is modified to perform experiments in which each of these three mechanisms may be included or omitted. By adding surface drag and vertical advection, and comparing each to shear advection, the effects of the three mechanisms on the generation and propagation of the barotropic Rossby waves are shown to be qualitatively similar to the results in QTCM. It is also found that the moist processes included in the QTCM can feed back on the teleconnection process and alter the teleconnection pattern by enlarging the prescribed tropical heating in both intensity and geographical extent, and by inducing remote precipitation anomalies by interaction with the

basic state.

2.1 Introduction

Tropical heat sources can remotely influence ocean basins and continents through atmospheric teleconnections (e.g., Horel and Wallace, 1981; Ropelewski and Halpert, 1987; Wallace et al., 1998; Trenberth et al., 1998). In addition to many teleconnection studies in general circulation models (GCMs; e.g., Lau, 1985; Mechoso et al., 1987; Kumar and Hoerling, 1998; Barnston et al., 1999; Goddard and Graham, 1999; Latif et al., 1999; Saravanan and Chang, 2000), much has been learned from simpler models. In the tropics, heating anomalies directly force a baroclinic signal that tends to remain trapped in latitude. Thus, highly damped shallow water models (Matsuno, 1966; Webster, 1972; Gill, 1980), which assume a vertical structure of a single deep baroclinic mode, can give a plausible first approximation to the low-level wind field in the vicinity of heating anomalies. In mid- and high latitudes, teleconnections tend to be dominated by an equivalent barotropic signal for two reasons. First, barotropic stationary or low-frequency Rossby waves in westerly flow tend to be less equatorially trapped than their baroclinic counterparts (Salby and Garcia, 1987). Second, vertical propagation tends to reduce the contribution of baroclinic modes in the midlatitude troposphere, leaving the signal far from the source dominated by an equivalent barotropic mode (Held et al., 1985). Thus barotropic models have been widely used to study the teleconnection response at midlatitudes (e.g., Hoskins and Karoly, 1981; Simmons, 1982; Simmons et al., 1983; Held and Kang, 1987). However, because the heating does not directly force a barotropic response, barotropic models used to study teleconnections must prescribe a vorticity source or "Rossby wave source" (Sardeshmukh and Hoskins, 1988), which can be based, for instance, on baroclinic divergence at upper levels or on baroclinic transient motions diagnosed from a GCM simulation (Held and Kang, 1987). This diagnosed Rossby wave source is one convenient approach that permits the barotropic processes to be examined while deferring investigation of the complex baroclinic-to-barotropic pathway in the tropics-to-midlatitudes teleconnection process. However, many of the terms that are specified as a fixed source in this approach are dynamical quantities whose scales, spatial form, and so on depend on the interaction of the baroclinic mode with the basic state in ways that can be interesting to elucidate. Multilevel linear, steady-state wave models with both

baroclinic and barotropic components comprise part of a model hierarchy (Hoskins and Karoly, 1981; Ting and Held, 1990; DeWeaver and Nigam, 2004) that can capture at least some aspects of the tropical/baroclinic to midlatitude/barotropic transition. Interactions with baroclinic transient eddies (Held et al., 1989; Hoerling and Ting, 1994) can also alter the teleconnection pattern in a manner that is not easily captured by stationary wave models.

The energy exchange between equatorially trapped baroclinic modes and equivalent barotropic modes with a significant projection on midlatitudes needs, therefore, to be addressed in a more sophisticated way. Instead of prescribing a Rossby wave source based on upper-level divergent flow in the one-level barotropic vorticity equation (e.g., Sardeshmukh and Hoskins, 1988; Held and Kang, 1987), a series of studies have been examining this problem from the point of view of baroclinic-barotropic interaction terms and studying the effect of each mechanism at work in the baroclinic-to-barotropic transition. Majda and Biello (2003) develop a set of simplified asymptotic equations describing the nonlinear interaction of near-resonant long-wavelength barotropic wave trains and equatorial baroclinic wave trains in the presence of sheared zonal mean winds, and emphasize the central role of baroclinic mean shear for sufficiently rapid nonlinear exchange of energy between the tropics and midlatitudes. Biello and Majda (2004a) further examine this resonant nonlinear interaction in the presence of vertically and meridionally sheared zonal mean winds [i.e., including both meridionally symmetric and antisymmetric (about the equator) vertical mean shear] and find that the effect of moderate antisymmetric winds is to shift the barotropic waves meridionally. Biello and Majda (2004b) incorporate the dissipative mechanisms arising from radiative cooling and atmospheric boundary layer drag, to explain how this mechanism creates barotropic/baroclinic spin up/spin down in the teleconnection process. Their results indicate that although the dissipation slightly weakens the tropics to midlatitude connection, strong localized wave packets are nonetheless able to exchange energy between barotropic and baroclinic waves on intraseasonal timescales in the presence of baroclinic mean shear. Wang et al. (2010) examine how, in the presence of background vertical shear, the transition from equatorial baroclinic mode to equivalent barotropic mode at midlatitudes establishes the interhemispheric influence of the Atlantic Warm Pool (AWP) in the Northern Hemisphere on the southeastern Pacific.

In this work, we aim at directly diagnosing and assessing the relative importance of the

interaction terms between the baroclinic and barotropic modes that appear as source terms in the barotropic equation. These interaction terms are similar to a Rossby wave source approach in that these terms appear as a vorticity source in the barotropic equation, but the "source" can be quantitatively and conceptually quite different from approaches based on upper-level divergent flow in a single-level vorticity equation. For instance, if there is no vertical shear and no damping on the baroclinic mode associated with surface stress, then upper-level divergence in the baroclinic mode does not produce any linear forcing of the barotropic mode. At the same time, by explicitly modeling the gravest baroclinic mode, the teleconnection pathway can be followed as the two modes interact, for instance with the baroclinic mode producing a teleconnection across the equator, and then interactions yielding a barotropic mode that can propagate to higher latitudes in the opposite hemisphere. Building on previous work with idealized asymptotic equations, we use realistic background states and more detailed physics including moist processes to analyze teleconnections arising from tropical heat sources.

We use two numerical models with different complexity, in both of which the baroclinic-barotropic interactions are explicitly formulated. The more complex one is a quasi-equilibrium (QE) tropical circulation model (QTCM, Neelin and Zeng, 2000), in which part of the quasi-equilibrium convective closure is used to carry forward analytically the model solution for the baroclinic vertical structure in the convective regions. The full primitive equations are then projected on the resulting baroclinic-plus-barotropic basis functions for vertical structure. This intermediate complexity model retains some of the simplicity of the analytical solutions while keeping full nonlinearity from the primitive equations and a consistent representation of moist processes including a deep convective parameterization. The consistent vertical mode decomposition yields three mechanisms (Neelin and Zeng, 2000) for excitation terms in the barotropic equations due to baroclinic terms: interactions of vertical shear in horizontal advection terms, vertical advection of vertically sheared motions, and interactions via surface stress in the boundary layer. Thus, the QTCM allows for quantifying the effect of each of those mechanisms and for assessing the role of feedbacks associated with moist processes. The simpler model we use is based on that of Lee et al. (2009), which is a two-level steady-state wave model linearized about background flows. In preparation for the present study, the Lee et al. (2009) version was extended to include the three mechanisms for excitation of

barotropic modes present in the QTCM. The simple model permits experiments in which mechanisms may be included or omitted. Therefore, an assessment of individual impacts is obtained by retaining the forcing terms one at a time in the barotropic equation, and inspecting the differences in the teleconnection patterns obtained with each mechanism. Our primary focus is on the heat source region above the Atlantic Warm Pool (AWP) because previous studies have shown that it has significant interhemispheric influences (e.g., Wang et al., 2010).

The remainder of the text is organized as follows. Section 2 gives a brief introduction of the two models as well as the modifications made for the study. Section 3 presents the QTCM experiments, examines each of the three forcing terms of barotropic Rossby waves, and explores the effect of moist feedback in the teleconnection process. Section 4 presents the simple model experiments, narrowing down the role of each forcing term. Section 5 consists of a summary and discussion.

2.2 Models and Methodology

2.2.1 QTCM

The QTCM belongs in a class of tropical atmospheric models of intermediate complexity that occupies a niche between GCMs and simple models. In the QTCM, the derivation from the primitive equations is done systematically and the constraints placed on the baroclinic flow by the GCM convective parameterizations with quasi-equilibrium (QE) thermodynamic closures are exploited. Part of the QE convective closure can be used to carry forward analytically the model solution for the vertical structure in convective regions. Using the vertical structures based on these analytical solutions as the leading basis functions in a Galerkin projection of the primitive equations, self-consistent nonlinear terms can be retained in advection, moist convection, and vertical momentum transfer terms, among others. A more detailed model description can be found in Neelin and Zeng (2000). The model performance has been analyzed in Zeng et al. (2000) for climatology, and in Lin et al. (2000) and Lin and Neelin (2000, 2002) for intraseasonal variability. Moist teleconnection mechanisms within the tropics have been examined using this model in Su and Neelin (2002) and Neelin and Su (2005).

The present study uses the first generation QTCM (QTCM1) version 2.3 which retains a single basis function for the vertical structure of temperature. This is the simplest configuration but it has considerable success in capturing tropical phenomena, because the temperature structure matches the consequences of a quasi-equilibrium convective scheme, and the baroclinic velocity basis function is analytically compatible. This provides an appealing system for baroclinic-barotropic decomposition. One might anticipate that an additional degree of freedom in the boundary layer might alter some surface drag effects quantitatively. The numerical implementation of the QTCM1 here covers the domain from 78.75°S to 78.75°N and over all longitudes, with a horizontal resolution of 3.75° latitude and 5.625° longitude.

A brief review of the equation for the barotropic wind component in the QTCM is presented below to aid the analysis of the barotropic teleconnection process in the following sections. A summary of the QTCM1 equations are given for reference in the appendix. Using V_0 and V_1 as the basis functions for velocity, the projected barotropic vorticity equation in Neelin and Zeng (2000) is:

$$\partial_t \zeta_0 + curl_z[D_{V0}(\mathbf{v}_0, \mathbf{v}_1)] + \beta v_0 = -curl_z(\varepsilon_0 \mathbf{v}_0) - curl_z(\varepsilon_{10} \mathbf{v}_1) \tag{2.1}$$

where subscripts 0 and 1 denote barotropic and baroclinic components, respectively, and the operator containing nonlinear advection terms and horizontal diffusion $D_{v0}(\mathbf{v}_0, \mathbf{v}_1)$, is given by:

$$D_{V0}(\mathbf{v}_0, \mathbf{v}_1) = \mathbf{v}_0 \cdot \nabla \mathbf{v}_0 + \left\langle V_1^2 \right\rangle \mathbf{v}_1 \cdot \nabla \mathbf{v}_1 + \left\langle V_1^2 \right\rangle (\nabla \cdot \mathbf{v}_1) \mathbf{v}_1 - K_H \nabla^2 \mathbf{v}_0 \tag{2.2}$$

where the term in brackets denote vertical averages over the troposphere $\langle X \rangle = p_T^{-1} \int_{p_{rt}}^{p_{rs}} X dp$, where p_{rs} and p_{rt} denote a reference pressure at the surface and top of atmosphere. For the analysis of Rossby wave sources in the QTCM, we rearrange (2.1) to obtain:

$$\begin{aligned} &\partial_t \nabla^2 \psi_0{}' + curl_z(\mathbf{v}_0 \cdot \nabla \mathbf{v}_0)' - K_H \nabla^4 \psi_0{}' + \beta v_0{}' \\ &= -curl_z(\left\langle V_1^2 \right\rangle \mathbf{v_1} \cdot \nabla \mathbf{v_1})' - curl_z(\left\langle V_1^2 \right\rangle [\nabla \cdot \mathbf{v_1}] \mathbf{v_1})' - curl_z(\varepsilon_0 \mathbf{v_0} + \varepsilon_{10} \mathbf{v_1})' \end{aligned} \tag{2.3}$$

where ψ_0 is the barotropic streamfunction, and $()'$ denotes anomalies defined as the difference

between a climatological run and a run with an imposed heating anomaly. The stationary barotropic Rossby wave response [i.e., of the lhs of (2.3)] to a localized source is well known (e.g., Hoskins and Karoly, 1981; Simmons et al., 1983; Held and Kang, 1987), so we focus on the comparison of the forcing terms on the rhs of (2.3). The three forcing sources of the barotropic motion that involve the interactions with baroclinic motion are defined as follows: 1) the shear advection term $-curl_z(\langle V_1^2 \rangle \mathbf{v}_1 \cdot \nabla \mathbf{v}_1)'$, which represents advective interactions of the baroclinic wind component (with vertical shear); 2) the vertical advection term $-curl_z(\langle V_1^2 \rangle [\nabla \cdot \mathbf{v}_1]\mathbf{v}_1)'$, which represents the effect of vertical motion advecting the baroclinic wind component; 3) the surface drag term $-curl_z(\varepsilon_0 \mathbf{v}_0 + \varepsilon_{10}\mathbf{v}_1)'$, which derives from surface stress $-(g/p_T)\tau_s$ (where p_T is the pressure depth of the troposphere and g is gravitational acceleration, and a boundary condition has been used with zero stress at model top) and a bulk formula parameterization $\tau_s = \tau|_{p_s} = \rho_a C_D V_s \mathbf{v}_s$, where ρ_a is the near-surface air density, C_D is the drag coefficient, V_s is the near-surface wind speed, and $\mathbf{v}_s$ is the near-surface wind vector. These three forcing mechanisms of the barotropic motion involved in the baroclinic-barotropic interactions are further discussed in section 2.3.2 in the teleconnection experiments. We further note that linearizing the interaction terms in (2.3) yields: $-curl_z(\langle V_1^2 \rangle \bar{\mathbf{v}}_1 \cdot \nabla \mathbf{v}_1{}' + \langle V_1^2 \rangle \mathbf{v}_1{}' \cdot \nabla \bar{\mathbf{v}}_1) - curl_z[\langle V_1^2 \rangle (\nabla \cdot \mathbf{v}_1{}')\bar{\mathbf{v}}_1 + \langle V_1^2 \rangle (\nabla \cdot \bar{\mathbf{v}}_1)\mathbf{v}_1{}'] - curl_z(\varepsilon_0 \mathbf{v}_0{}' + \varepsilon_{10}\mathbf{v}_1{}')$. The linearized interaction terms make it clear that if there is no vertical shear or vertical velocity in the mean state ($\bar{\mathbf{v}}_1 = 0$) and no drag on the baroclinic mode ($\varepsilon_{10} = 0$), then the baroclinic mode can have any vertical velocity ($\nabla \cdot \mathbf{v}_1{}'$), but there will be no forcing of the barotropic mode. This appears quite different from the assumptions used in traditional Rossby wave source approaches based on a vorticity equation at upper levels, but it is similar in the sense that it diagnoses a vorticity source that drives the barotropic equation, in this case the equation for the full barotropic mode. We will refer to this as a "barotropic Rossby wave source" for clarity because it is the vorticity source term as it occurs projected on the full barotropic mode. We also note that while we have retained the whole surface stress term on the rhs above, arguably it is more consistent to move the barotropic component of this [i.e.,$-curl_z(\varepsilon_0 \mathbf{v}_0{}')$] to the lhs in (2.3) because it acts as a drag on the barotropic mode. In that case, the surface drag contribution to the barotropic Rossby wave source due to the baroclinic mode is simply $-curl_z(\varepsilon_{10}\mathbf{v}_1{}')$. We will show examples of both in diagnostics.

2.2.2 Simple model

The simple model we use in this study is based on that developed by Lee et al. (2009). This is a two-level model, in which equations are recast as baroclinic and barotropic components and are linearized about prescribed background wind fields. The model is designed to simulate both the local and remote stationary response of the atmosphere when forced with a localized heating. In this model, the baroclinic response to tropical heating anomalies is essentially the same as described by the Matsuno-Gill model (Matsuno, 1966; Gill, 1980) with damping used in Lee et al. (2009). This baroclinic response then excites a barotropic response by advective interactions with vertical background wind shear (i.e., through the shear advection mechanism), and the barotropic signals are in turn transmitted to high latitudes.

Our modification of the Lee et al. (2009) model allows for consideration of surface drag as another mechanism of baroclinic-barotropic interactions. This was done by eliminating, from the relative vorticity equations, the linear momentum damping $-r\nabla^2\psi$ both in the upper (250mb) and lower (750mb) levels, and adding in the lower level a term $-r_s\nabla^2\psi$, where the surface drag coefficient is $r_s = (g/p_T)\rho_a C_D V_s$. Thus, in the barotropic and baroclinic vorticity equations, the linear damping coefficients r_0 and r_1 become $r_0 = r_1 = r_s/2$. We set $r_s = (3.5\text{day})^{-1}$ for $p_T =$ 500mb, $C_D = 10^{-3}$, $V_s = 10\text{m s}^{-1}$. The simple model [as modified relative to Lee et al. (2009)] is thus given by the following modified barotropic and baroclinic vorticity equations:

$$\begin{aligned}&\tfrac{1}{a\cos\theta}\left[\tfrac{\partial}{\partial\lambda}(\bar{u}_0\nabla^2{\psi_0}' + {u_0}'\nabla^2\bar{\psi}_0) + \tfrac{\partial}{\partial\theta}(\cos\theta\bar{v}_0\nabla^2{\psi_0}' + \cos\theta{v_0}'\nabla^2\bar{\psi}_0)\right] + 2\Omega\tfrac{{v_0}'}{a}\\ &= -r_0\nabla^2{\psi_0}' + r_0\nabla^2{\psi_1}' + A_0\nabla^4{\psi_0}' + F_{\psi_0}\end{aligned} \tag{2.4}$$

$$\begin{aligned}&\tfrac{1}{a\cos\theta}\left[\tfrac{\partial}{\partial\lambda}(\bar{u}_1\nabla^2{\psi_1}' + {u_1}'\nabla^2\bar{\psi}_1) + \tfrac{\partial}{\partial\theta}(\cos\theta\bar{v}_1\nabla^2{\psi_1}' + \cos\theta{v_1}'\nabla^2\bar{\psi}_1)\right] + 2\Omega(\sin\theta\nabla^2\chi_1\tfrac{{v_1}'}{a})\\ &= -r_1\nabla^2{\psi_1}' + r_1\nabla^2{\psi_0}' + A_1\nabla^4{\psi_1}' + F_{\psi_1}\end{aligned} \tag{2.5}$$

where ψ denotes streamfunction, χ denotes velocity potential, and subscripts 0 and 1 denote barotropic and baroclinic mode respectively, variables are separated into the basic state and anomaly components denoted by bar and prime terms, and A_0 and A_1 are the momentum dif-

fusion coefficients for barotropic and baroclinic motions respectively. The differences from the model in Lee et al. (2009) are the two terms $r_0\nabla^2{\psi_1}'$ and $r_1\nabla^2{\psi_0}'$ that derive from the surface drag mechanism. The F_ψ terms represent the vorticity tendency terms due to the shear advection and vertical advection mechanisms of baroclinic-barotropic interactions. The complete form of F_{ψ_0} is:

$$\begin{aligned} F_{\psi_0} &= \tfrac{1}{a\cos\theta}\left[\tfrac{\partial}{\partial\lambda}(\bar{u}_1\nabla^2{\psi_1}' + {u_1}'\nabla^2\bar{\psi}_1) + \tfrac{\partial}{\partial\theta}(\cos\theta\bar{v}_1\nabla^2{\psi_1}' + \cos\theta{v_1}'\nabla^2\bar{\psi}_1)\right] \\ &= \tfrac{1}{a\cos\theta}\left\{\begin{array}{l} \nabla^2{\psi_1}'\left[\tfrac{\partial\bar{u}_1}{\partial\lambda} + \tfrac{\partial}{\partial\theta}(\cos\theta\bar{v}_1)\right] + \nabla^2\bar{\psi}_1\left[\tfrac{\partial{u_1}'}{\partial\lambda} + \tfrac{\partial}{\partial\theta}(\cos\theta{v_1}')\right] \\ + \left[\bar{u}_1\tfrac{\partial\nabla^2{\psi_1}'}{\partial\lambda} + \bar{v}_1\tfrac{\partial}{\partial\theta}(\cos\theta\nabla^2{\psi_1}')\right] + \left[{u_1}'\tfrac{\partial\nabla^2\bar{\psi}_1}{\partial\lambda} + {v_1}'\tfrac{\partial}{\partial\theta}(\cos\theta\nabla^2\bar{\psi}_1)\right] \end{array}\right\} \end{aligned} \tag{2.6}$$

The first term in the rhs of (2.6) represents the vertical advection of anomalous baroclinic vorticity via background vertical wind. The second term represents the vertical advection of background baroclinic vorticity via anomalous vertical wind. The third term represents the zonal and meridional advection of anomalous baroclinic vorticity via background zonal and meridional shear. The fourth term represents the zonal and meridional advection of background baroclinic vorticity via anomalous zonal and meridional shear.

The thermodynamic equation is given by:

$$\gamma\phi_1 + {c_g}^2\nabla^2\chi_1 = -Q \tag{2.7}$$

where γ is the thermal damping coefficient, ϕ_1 is the baroclinic geopotential, c_g is the internal gravity wave speed, χ_1 is the baroclinic divergence, and Q is the diabatic heating rate. Note that the simple model is explicitly steady state and linear and omits all moisture effects. A baroclinic divergence equation (not shown here) together with (2.4)-(2.7) are in a closed form and are the governing equations solved in the simple model.

In our simple model experiments, we are able to activate and deactivate each forcing mechanism—the surface drag, vertical advection and shear advection—and to compare the effects of each forcing with those in the QTCM results.

The numerical implementation of the three versions of the simple model covers the domain from 90°S to 90°N over all longitudes, with a horizontal resolution of 4.5° latitude and 4.5°

longitude.

2.2.3 Methodology

We concentrate on the period of June-August (JJA), during which the tropical heating and precipitation anomalies develop to their maximum strength in the Northern Hemisphere summer, including in the AWP region of interest here. In JJA, the subtropical jets are strong in the Southern Hemisphere (winter), which can favor the shear advection mechanism for interhemispheric teleconnections (Wang et al., 2010). Accordingly, in both the QTCM and simple model, the zonal mean of the barotropic and baroclinic wind fields are prescribed as the JJA zonal means. The time advance of the zonal mean fields in the QTCM is, therefore, bypassed. The prescribed velocities correspond to the streamfunction at the 250 and 750mb levels from the monthly National Centers for Environmental Prediction (NCEP)—National Center for Atmospheric Research (NCAR) reanalysis (Kalnay et al., 1996):

$$\bar{u}_0 = -\frac{\partial}{\partial y}\bar{\psi}_0^{NCEP} = -\frac{\partial}{\partial y}[(\bar{\psi}_{250}^{NCEP} + \bar{\psi}_{750}^{NCEP})/2] \tag{2.8}$$

$$\bar{u}_1 = -\frac{\partial}{\partial y}\bar{\psi}_1^{NCEP} = -\frac{\partial}{\partial y}[(\bar{\psi}_{250}^{NCEP} - \bar{\psi}_{750}^{NCEP})/2] \tag{2.9}$$

Further, in the QTCM we replace the zonal velocity that advects the temperature gradient by that corresponding to the zonal mean basic state velocity as in (2.8) and (2.9). This procedure removes the main source term for baroclinic instability, thus reducing weather variability. There are some trade-offs here. On the one hand, because of reduction in poleward fluxes, more moisture is available for precipitation in the subtropics, and interactions of the teleconnections with storm tracks are suppressed. On the other hand, the procedure has several advantages in view of our goals, including that (i) statistically significant signals are easy to detect in decadal runs, (ii) comparison to the simple model is facilitated, (iii) the basic state on which wave propagation occurs is strongly constrained towards observations, and (iv) interpretation in terms of stationary wave propagation is more straightforward. Thus, this should be viewed as an intermediate step between simple models and GCMS that would potentially include more complex effects such as interaction with baroclinic

transients.

2.3 QTCM Experiments and Results

2.3.1 Atlantic Warm Pool (AWP) teleconnection experiments set up

In this experiment, we prescribe a Gaussian-shaped baroclinic heating anomaly as in Lee et al. (2009). The anomaly amplitude is 169.2W/m^2 (which is equivalent to 6mm/day of precipitation) at the center (20°N, 70°W), and the zonal and meridional length scales are 5° latitude and 15° longitude (see Fig. 2.1a). The model is then run for 10 years using monthly climatological SSTs (Reynolds and Smith, 1994).

Figure 2.1b shows the precipitation response averaged over JJA for 10 years in response to the prescribed heating anomalies in this experiment. It can be seen that the latent heat associated with the precipitation anomalies enhance the local prescribed heating anomalies to a significant extent, and thus will enhance the teleconnection response in comparison to a model with dry dynamics. The shape of the heating is also slightly modified from the prescribed. We return to this moist feedback effect in section 2.3.3.

2.3.2 AWP teleconnections analysis

The JJA mean baroclinic and barotropic streamfunctions anomalies are shown in Figs. 2.2a and 2.2b. The baroclinic mode resembles the Gill-Matsuno-type response (Matsuno, 1966; Gill, 1980) and is equatorially trapped with most of the signal within equatorial deformation radius. An important aspect is that the off-equatorial heating projects sufficiently on the Kelvin mode (to the east of the heating) and the symmetric Rossby modes (to the west) that a substantial baroclinic signal crosses the equator. The barotropic mode shows an interesting pattern. Typically, a pure barotropic stationary Rossby wave propagating in a westerly region of the midlatitudes in an approximately barotropic basic state will approach a critical latitude where $\bar{u} = 0$ and thus will not propagate directly across the region of easterlies near equator. In our experiments, however, the barotropic signal has a significant component in the Southern Hemisphere. This is because the QTCM includes a full set of forcing sources of the barotropic motions through baroclinic-barotropic

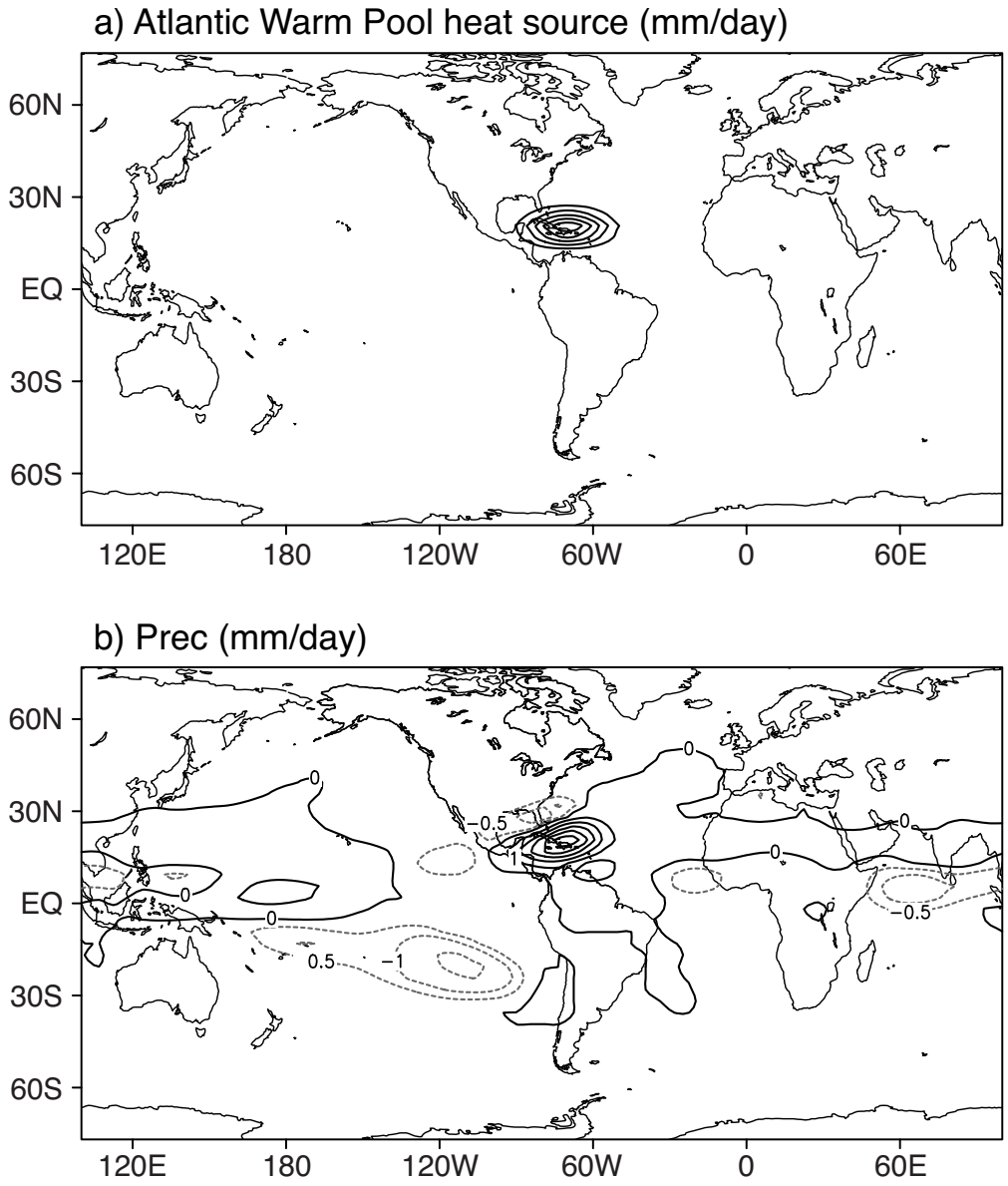

Figure 2.1: (a) The Gaussian-shaped baroclinic heating anomaly prescribed in the AWP region in QTCM. (b) Precipitation anomalies in QTCM AWP experiment (negative contour lines are dashed). The contour interval (CI) is 1mm/day (the 0.5mm/day precipitation contour is shown for easier recognition of the pattern).

interactions. As mentioned in section 2.2.1, in the model's barotropic component equation in QTCM, the three baroclinic forcing mechanisms–the shear advection, surface drag, and vertical advection–actively generate barotropic wave trains in the equatorial regions and within the Southern Hemisphere westerlies.

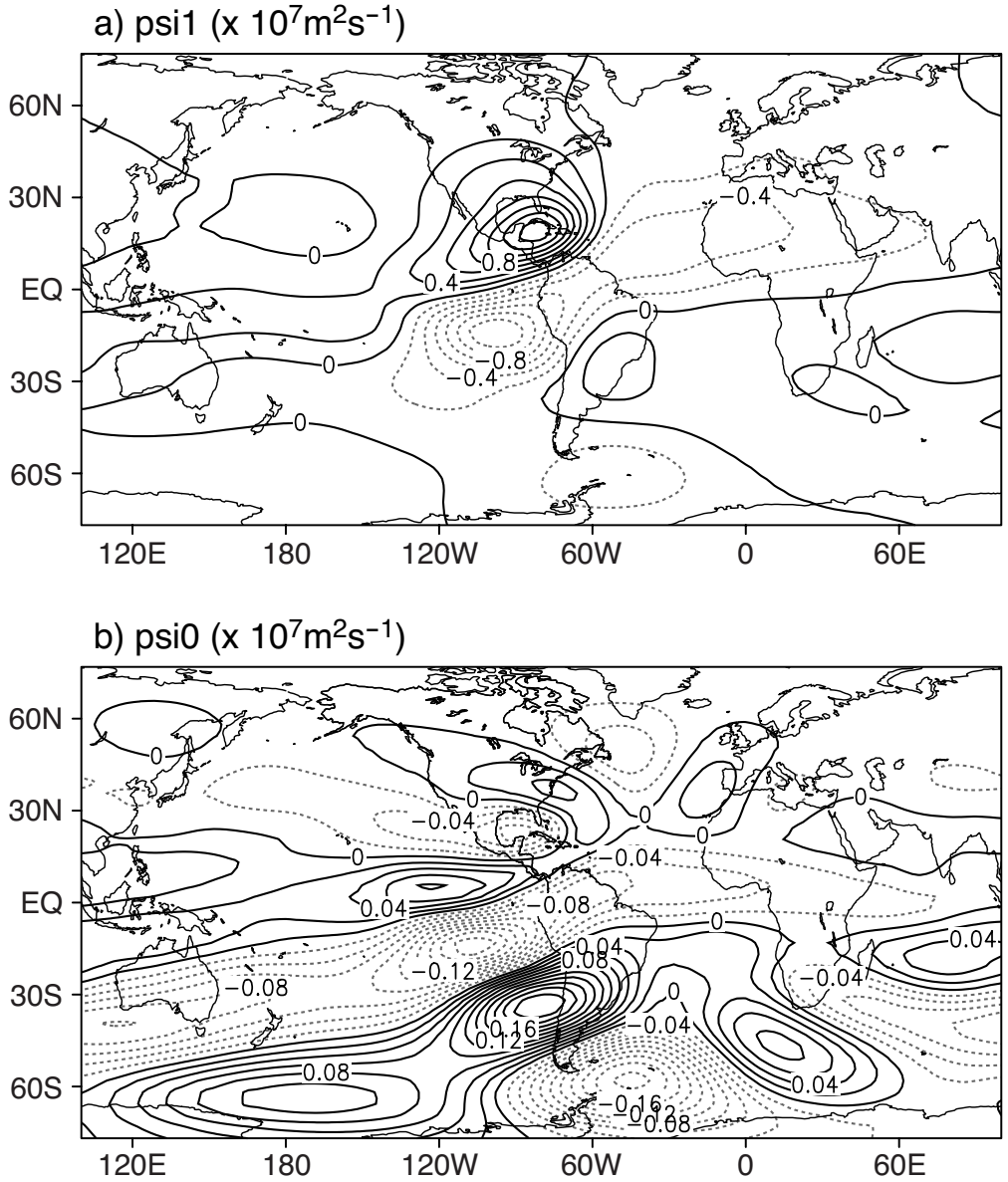

Figure 2.2: (a) Baroclinic and (b) barotropic streamfunction anomalies in the QTCM AWP experiment. Negative contours are dashed. The CI is 2 x 10^6m^2 s^{-1} in (a) and 2 x 10^5m^2 s^{-1} in (b).

To explore the relative importance of the three mechanisms of interest in the QTCM AWP experiment, in Figs. 2.3a, 2.3b, 2.3c we plot the amplitudes of the three terms in the rhs of (2.3),

and in Figs. 2.4a, 2.4b, 2.4c their inverse Laplacian (i.e., the equivalent barotropic streamfunction tendency terms). Shaded areas in Figs. 2.3 and 2.4 represent values that are statistically significant with a confidence level of 99% from a Student's t test. The shear advection term $-curl_z(\langle V_1^2 \rangle \mathbf{v}_1 \cdot \nabla \mathbf{v}_1)'$ shows a large dipole in the tropics (Figs. 2.3a and 2.4a), roughly coincident with where the baroclinic signal is strong. The southwest-northeast angle reflects the corresponding tilt seen in Fig. 2.2a close to the zero contour of ψ_1 where the strong gradient in ψ_1 indicates strong baroclinic wind anomalies. Thus the region of strong shear forcing reflects the heating-forced baroclinic anomalies, which, while equatorially trapped, are able to propagate into the Southern Hemisphere where they can excite barotropic waves.

The magnitude of the surface drag term $-curl_z(\varepsilon_0 \mathbf{v}_0 + \varepsilon_{10} \mathbf{v}_1)'$ in Fig. 2.3b is not locally as large as that of the shear advection term (Fig. 2.3a) and vertical advection term (Fig. 2.3c), but its inverse Laplacian (Fig. 2.4b) shows large values around the heat source with amplitudes comparable with the vertical advection term. The geographical spread of the surface drag forcing is broader in both hemispheres than the two other mechanisms. Note that Figs. 2.3b and 2.4b show the net effect of surface drag mechanism [i.e., the amplitude of the baroclinic forcing$-curl_z(\varepsilon_{10} \mathbf{v}_1{}')$ after compensation by linear damping$-curl_z(\varepsilon_0 \mathbf{v}_0{}')$]. Also note that the sign of the coefficient of transfer by surface stress between baroclinic and barotropic wind components ε_{10} is negative in order for all the turbulence terms to have the same form (refer to the appendix for more detail). For a rough estimate of this compensation, comparing the amplitudes of $-\varepsilon_{10}\psi_1$ [where $\varepsilon_{10} = (-28day)^{-1}$ and ψ_1 can be approximated from the values in Fig. 2.2a] and $-\varepsilon_0\psi_0$ [where $\varepsilon_0 = (5.6day)^{-1}$ and ψ_0 can be approximated from the values in Fig. 2.2b] indicates that the compensation effect of the linear damping can be as large as 50% of the baroclinic forcing. This estimate is confirmed by Fig. 2.3d, showing only the baroclinic forcing component of the surface drag$-curl_z(\varepsilon_{10} \mathbf{v}_1{}')$. As expected, this component is roughly twice as large locally as the total surface drag term (Fig. 2.3b). We can also see that the surface drag component has a significant contribution in the Southern Hemisphere. Thus the baroclinic forcing from the surface drag term can potentially exert a substantial impact on the generation and propagation of barotropic Rossby waves, especially in the Southern Hemisphere corresponding to the ψ_1 response there.

Finally, the vertical advection term$-curl_z(\langle V_1^2 \rangle [\nabla \cdot \mathbf{v}_1] \mathbf{v}_1)'$ (Figs. 2.3c and 2.4c) shows a

localized forcing around the heat source where the vertical velocity is large (also see Fig. 2.1b for the large local precipitation anomaly). Note that some degree of compensation can occur with the surface drag term in regions of upward vertical motion where the vertical velocity term contribution $-\left\langle V_1^2 \right\rangle (\nabla \cdot \bar{\mathbf{v}}_1) curl_z \mathbf{v}_1{}'$ has opposite sign but similar form to$-curl_z(\varepsilon_{10}\mathbf{v}_1{}')$. Far from the heat source, in certain regions of the Pacific and Indian Ocean, the vertical velocity term can still have fairly substantial contributions corresponding to the remote precipitation anomalies in those regions. The strong vertical advection forcing locally around the heat source (Fig. 2.3c) and the remote signals in the Southern Hemisphere imply that this mechanism has a substantial role in the interhemispheric teleconnections, and should not be neglected.

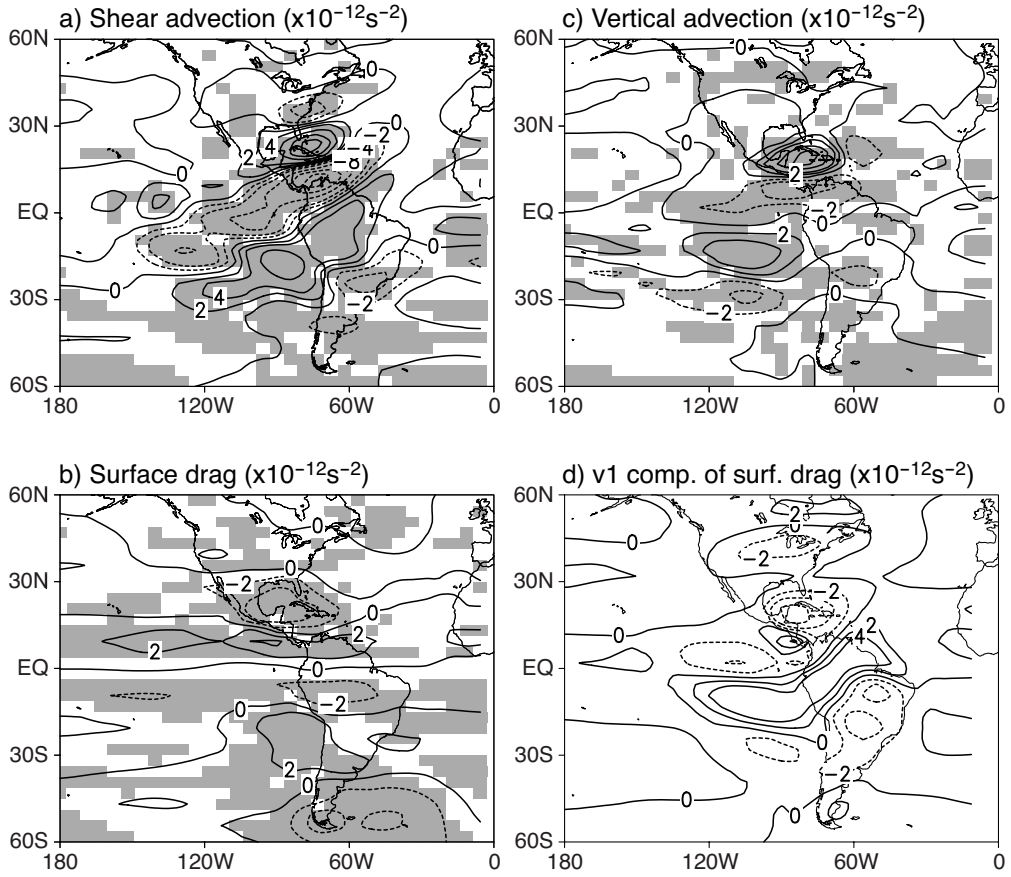

Figure 2.3: The three forcing sources in the QTCM AWP experiment: (a) shear advection, (b) surface drag, (c) vertical advection, and (d) the $\mathbf{v_1}$ component of the surface drag (see text for explanation). Negative contours are dashed. The CI is $2\text{x}10^{-12}$ s^{-2} within $\pm 4\text{x}10^{-12}$ s^{-2}, and is $4\text{x}10^{-12}$ s^{-2} outside of $\pm 4\text{x}10^{-12}$ s^{-2} in all four panels. Shaded areas represent values that are statistically significant with a confidence level of 99% from a Student's t test.

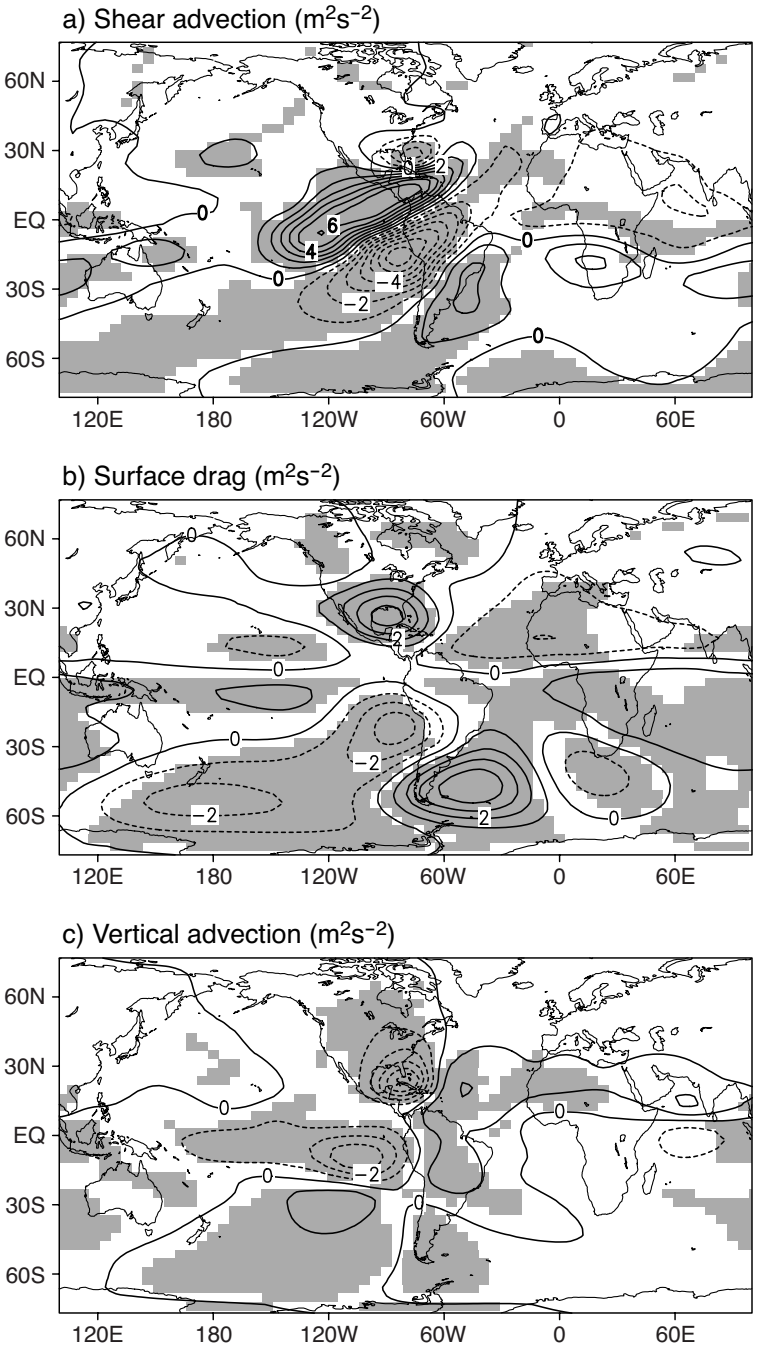

Figure 2.4: The inverse Laplacian of the three forcing sources in the QTCM AWP experiment: (a) shear advection, (b) surface drag, and (c) vertical advection. Negative contours are dashed. The CI is 1 $\mathrm{m}^2\ \mathrm{s}^{-1}$. Shaded areas represent values that are statistically significant with a confidence level of 99% from a Student's t test.

2.3.3 Moist feedback

The precipitation response in the QTCM AWP experiments is shown in Fig. 2.1b. There is clear evidence that moist processes enhance the teleconnection process. First, moist feedback enhances the prescribed anomalous heat source locally by approximately 6mm/day in this experiment, which is as large as the prescribed heat source. Second, the shape of the precipitation anomaly is stretched southwestward into eastern Pacific region. A similar feature is apparent in the GCM AWP experiments in Wang et al. (2007, 2008). This precipitation anomaly is the result of the Atlantic Warm Pool-induced subtropical Rossby waves propagating westward and interacting with the inter-tropical convergence zone (ITCZ) in the eastern Pacific. The impact of this convective heating anomaly in the eastern Pacific is further analyzed in section 2.3.4. Third, this elongated shape, and the compensating subsidence north of the precipitation anomaly are consistent with the mechanism described in Chou and Neelin (2003) as the result of the interaction between baroclinic Rossby wave dynamics and convective heating. The subsidence may modestly impact the teleconnection patterns north of the heating anomaly by reducing the baroclinic signal extent and by contributing to vertical advection. Finally, as the flow anomalies produced by the teleconnections interact with moist processes remotely (e.g., advecting the basic-state moisture gradient), they can induce remote precipitation anomalies that can contribute to the baroclinic-barotropic interaction. For instance, Fig. 2.1b shows precipitation anomalies in the equatorial western Pacific and in the subtropical southeastern Pacific. The latter corresponds to a significant contribution to the vertical advection forcing term in Figs. 2.3c and 2.4c in the Southern Hemisphere.

2.3.4 The impact of the response in the eastern Pacific ITCZ region

As mentioned in section 2.3.3, the moist feedback on the teleconnections leads to an elongation of the anomalous heat source in the AWP region into the eastern Pacific ITCZ region. This elongation is also seen in the GCM experiments of Wang et al. (2007, 2008). Here, we quantitatively investigate the influence of this additional heating in the ITCZ region on the AWP teleconnections into the Southern Hemisphere. We prescribe a similar Gaussian-shaped baroclinic heating anomaly with the same amplitude as in the one above the AWP, but with the center at 15°N, 95°W, and

scales of 3.0° latitude and 7.5° longitude. The model is then run for 10 years using monthly climatological SSTs (Reynolds and Smith, 1994).

Fig. 2.5 shows the barotropic streamfunction response to the heating prescribed in the eastern Pacific region. A comparison between this and Fig. 2.2b, reveals an overlap of the positive and negative phases of the response induced by the two different heating regions, and confirms that the induced eastern Pacific heating provides a positive feedback to the original AWP heating. We have also tested the sensitivity of results to the extension of the elongation, and found that the model response to a further elongation into the eastern Pacific as that in the GCM experiments of Wang et al. (2007, 2008) has virtually the same pattern (not shown).

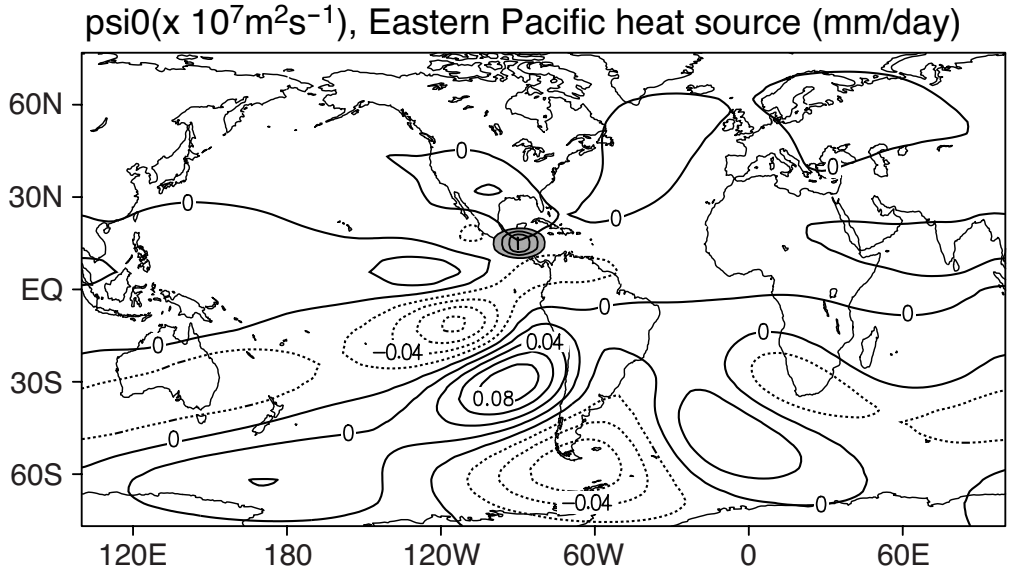

Figure 2.5: Barotropic streamfunction anomalies in the eastern Pacific experiment in QTCM. Negative contours are dashed. The CI is 2 x $10^5 m^2$ s^{-1}. The shaded area is the heating prescribed in the eastern Pacific, with an interval of 1mm/day.

2.3.5 Sensitivity of the teleconnection pattern to longitudinal location of heating anomaly

To explore the dependence of the teleconnection response to the heating location in longitude, we perform a supplementary experiment in which the heating source is placed in the central Pacific at a location 90° in longitude west of the AWP (see Fig. 2.6a). The precipitation anomalies in this experiment are shown in Fig. 2.6b, while the baroclinic and barotropic streamfunctions

response are shown in Figs. 2.7a and 2.7b, respectively. The zonally asymmetric basic state in the model can affect wave propagation, but some of the most obvious differences arise in the moist response to the source. The precipitation anomalies do not show elongation similar to that in the AWP experiment (Fig. 2.1b), which leads to smaller zonal wavelengths in the baroclinic and hence in the barotropic response (Fig. 2.7b). Based on the Wentzel-Kramers-Brillouin (WKB) theory for stationary barotropic Rossby wave propagation in latitudinally varying flow, the local meridional wave number $l(y)$ is given by $l(y) = \pm(\hat{\beta}\bar{u}_m^{-1} - k^2)^{1/2}$, where k is the zonal wavenumber and $\hat{\beta}$ and $\bar{u}_m$ are basic-state vorticity and zonal mean flow defined in Mercator coordinates equivalent to the form on a beta-plane with spherical effects incorporated (Hoskins and Karoly, 1981). The smaller zonal wavelengths (larger zonal wavenumber k) mean a lower turning latitude because the local meridional wavenumber for stationary barotropic Rossby waves goes to zero at smaller values of $\hat{\beta}\bar{u}_m^{-1}$. Thus, the wave arc in the Northern Hemisphere is more zonal. In the Southern Hemisphere, the barotropic responses in both the AWP and central Pacific experiments (Figs. 2.2b and 2.7b) are qualitatively similar, but the latter one has weaker magnitudes. This is partly due to the small baroclinic response in the Southern Hemisphere (Fig. 2.7a), as well as to the absence of the vertical advection forcing sources in the southern Pacific (Figs. 2.3c and 2.4c).

2.4 Simple Model experiments

In the simple model, an identical Gaussian-shaped heating anomaly is prescribed in the AWP region with a diabatic heating rate of 2.5 x 10^{-2} W kg^{-1}, which is equivalent to 2.15 K day^{-1} at 500mb. For the simple vertical structure of this model (linear within each layer), this would be roughly equivalent to 127.6 W m^{-2} using 500mb layer depth. This heating anomaly is the only heat source because there is no moist feedback in the model. Recall from section 2.2, that the model is linearized about the basic state from the JJA NCEP-NCAR reanalysis streamfunction averaged zonally around the globe. Other model parameters used in the present study are the same as those in Lee et al. (2009) with the following exceptions: the baroclinic and barotropic linear damping coefficient is set to $(3.5\text{day})^{-1}$ for compatibility with the QTCM, and the barotropic horizontal mixing coefficient is set to 2.5 x 10^5 m^2 s^{-1} following Wang et al. (2010). Altering these damping coefficients affects the rate at which the barotropic wave decays.

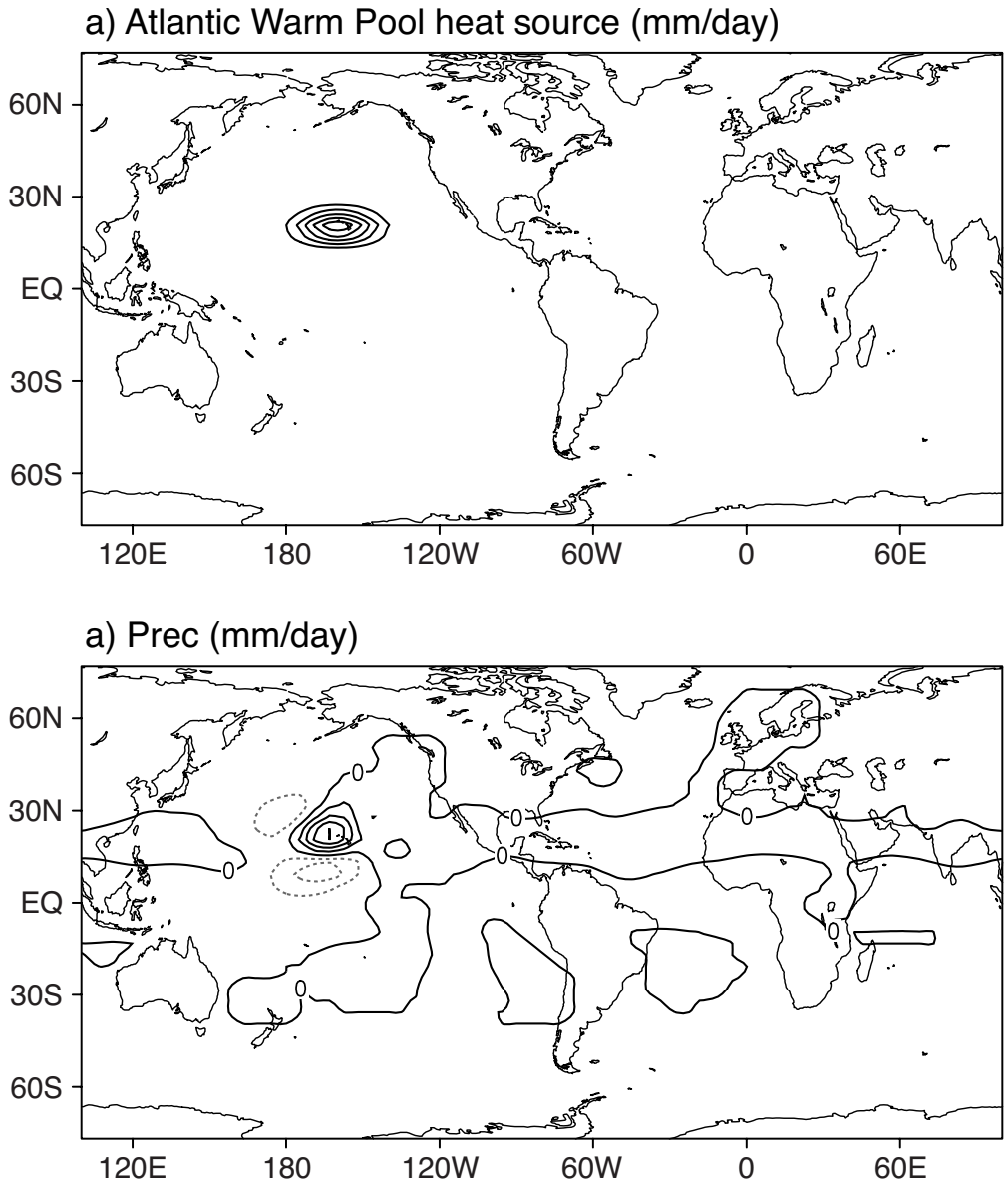

Figure 2.6: (a) As in Fig. 2.1a, but for the heat source shifted 90° in longitude to the central Pacific region. (b) Precipitation anomalies in the central Pacific experiment in QTCM. Negative contours are dashed. The CI is 1mm/day.

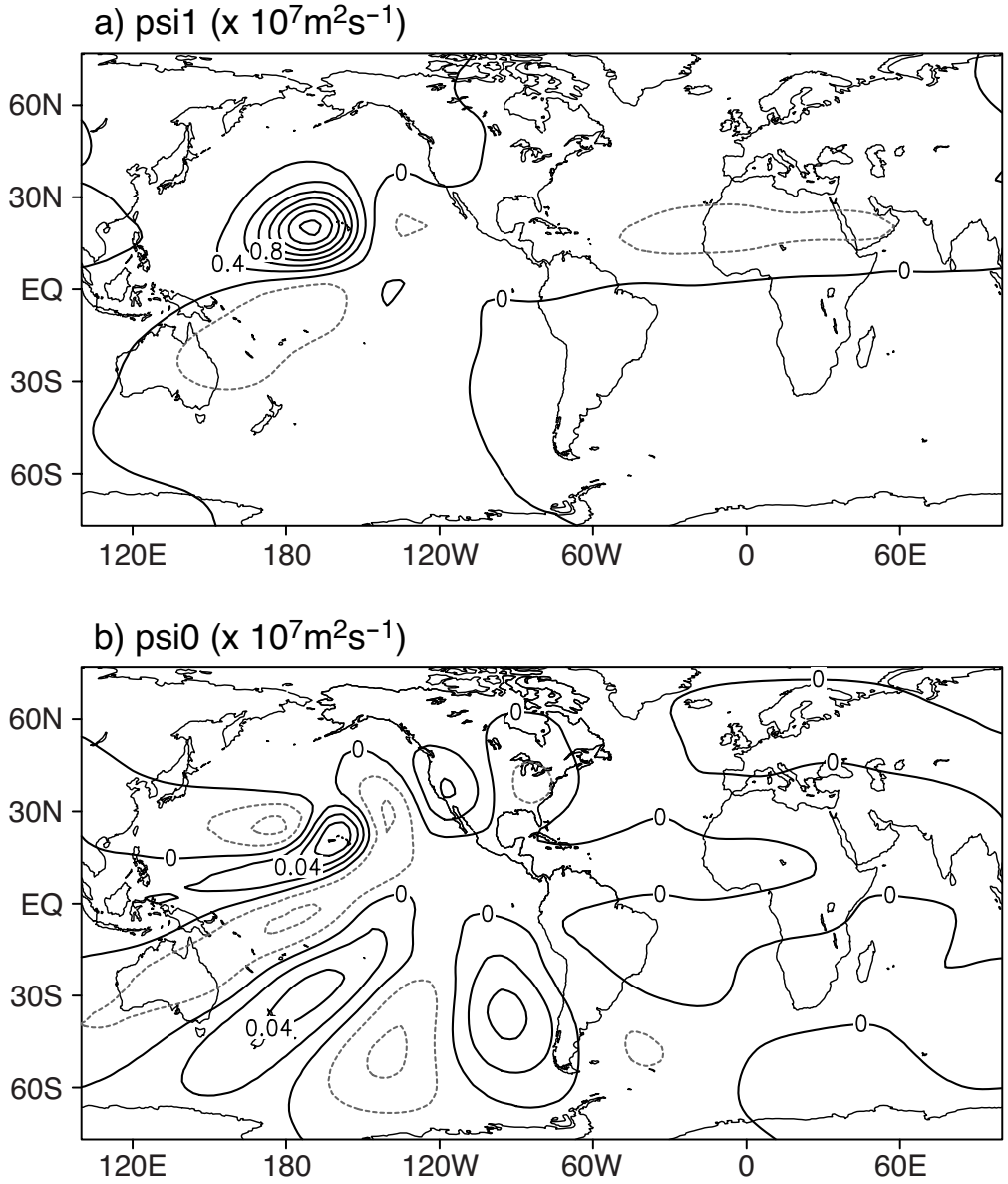

Figure 2.7: (a) Baroclinic and (b) barotropic streamfunction anomalies in the central Pacific experiment in QTCM. Negative contours are dashed. The CI is 2 x 10^6m^2 s^{-1} in (a) and 2 x 10^5m^2 s^{-1} in (b).

Figure 2.8a shows the response of the barotropic streamfunction in the model with the shear advection mechanism, and Fig. 2.8b shows the corresponding values with both shear advection and surface drag mechanisms included (note that the latitude coverage is adjusted to 78.75°S-78.75°N in order to compare with the QTCM results). Addition of the surface drag mechanism results in a strong amplification and extension of the barotropic response in the Southern Hemisphere. This supports the finding in the QTCM experiments that the surface drag mechanism is potentially very effective in forcing the barotropic response globally, especially in spreading the cross-equatorial barotropic signals.

Figure 2.8c shows the barotropic streamfunction response of the model experiment with both the shear advection and the vertical advection mechanisms. Comparing with Fig. 2.8a, as in the QTCM experiment, the vertical advection amplifies the barotropic response locally around the heating area and spreads the barotropic signals into the Southern Hemisphere, although the impact is moderate compared to the surface drag mechanism.

2.5 Summary and discussion

We have investigated the mechanisms that control the interhemispheric teleconnections from tropical heat sources. Our approach is based on the analysis of the response to idealized distributions of tropical heating sources in experiments in QTCM and in a simple steady-state, damped, linear stationary wave model. We concentrated primarily on the Atlantic Warm Pool region to prescribe the heating because it has been identified as significant in setting up interhemispheric influence in previous studies (e.g., Wang et al., 2010). The direct baroclinic response to this tropical heating is approximately a Gill-Matsuno-type response (Matsuno, 1966; Gill, 1980), which is equatorially trapped. The teleconnections to mid- and high latitudes are dominated by the barotropic mode. The baroclinic-to-barotropic pathway is complex, involving the basic-state shear with all its spatial dependence, as well as the basic-state vertical velocity and surface drag. In absence of basic-state shear and vertical velocity and of surface drag, baroclinic and barotropic components are decoupled. This makes the recent literature examining the role of these interaction terms as a driver for barotropic motions from heat forced baroclinic motions (e.g., Neelin and Zeng, 2000; Majda and Biello, 2003; Lee et al., 2009) appear very different from the earlier literature that

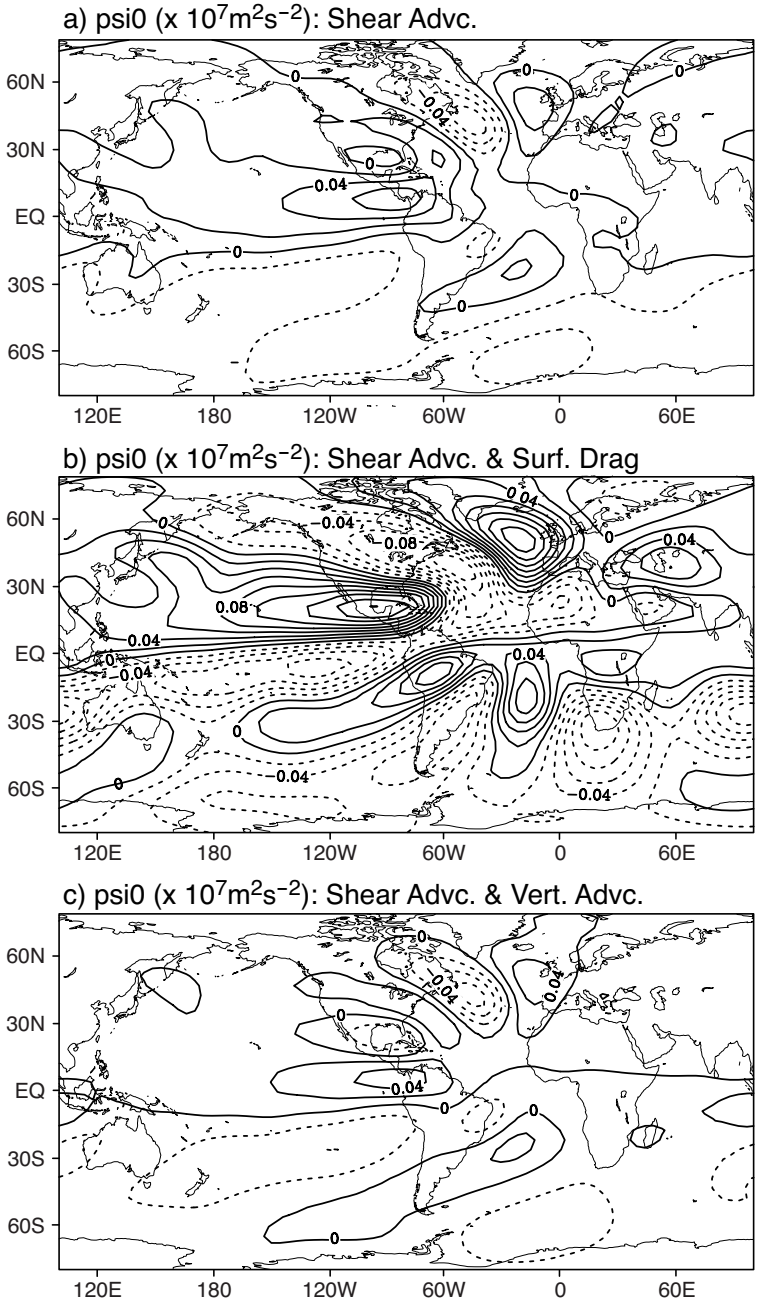

Figure 2.8: Barotropic streamfunctions anomalies in the simple model AWP experiment with (a) shear advection (b) shear advection and surface drag mechanisms, and (c) shear advection and vertical advection mechanisms. Negative contours are dashed. The CI is 2 x 10^5m^2 s^{-1}.

assumed upper-level divergence and related terms could be viewed as a driver (e.g., Sardeshmukh and Hoskins, 1988; Held and Kang, 1987), often summarized as a vorticity source term (the Rossby wave source) for a single-level barotropic equation. Here, we diagnose the interaction terms as a consistent vorticity source for the barotropic mode in a primitive equation model that has an explicit vertical mode decomposition. In addition to explicit computation of the interaction terms as in earlier theoretical studies, the study retains a complex three-dimensional basic state and moist processes for a quantitative examination.

The interaction-term framework results in some very substantial differences in the way one views the teleconnections generated by anomalous heating. First, it should be noted that upper-level divergence in the baroclinic mode does not necessarily drive a response in the barotropic mode, as is commonly assumed, unless appropriate conditions such as basic-state shear occur in the regions of descent. Furthermore, for interhemispheric teleconnections or tropical-to-midlatitude teleconnections, the first leg of the teleconnection occurs in the baroclinic mode. Equatorially trapped baroclinic waves can be responsible for most of the propagation within regions where low-frequency barotropic modes are evanescent, including across the equator. Diagnosis of interaction terms as a forcing in the barotropic equation in the QTCM then allows us to identify the relative importance of each mechanism in exciting the barotropic mode: the shear advection mechanism, the surface drag mechanism, and the vertical advection mechanism. In these results, the Rossby wave source in the barotropic equation due to shear advection roughly coincides with the baroclinic signal in the tropics and subtropics, and thus can be effective in contributing to the Southern Hemisphere response to an Atlantic Warm Pool heat source. The barotropic Rossby wave source due to surface drag is more broadly spatially spread, essentially reflecting the contribution of the baroclinic mode to low-level wind, and has large enough magnitude to provide a substantial forcing mechanism for interhemispheric teleconnections. Last, the barotropic Rossby wave source due to vertical advection is significant in locations where the climatological vertical velocity and vertical shear are both large. These mechanisms were further examined by modifying the simple model to include the surface drag and vertical advection one by one, and by comparing their effects with the shear advection mechanism. The results from the simple model provide support to the interpretation of QTCM results.

The QTCM results also allowed for an assessment of effects that moist feedbacks can have in such interhemispheric teleconnections. Moist processes strengthen the initial heating locally. In the Atlantic Warm Pool experiment, the region of anomalous heating is extended westward by the induced precipitation anomalies in the eastern Pacific ITCZ region. This amplifies the original teleconnection response, as shown by an experiment in which these anomalies are applied separately. Such an effect depends on the regional basic state: it does not occur for a similar initial anomaly applied in the central Pacific. Additional moist feedbacks can occur remotely. In the Atlantic Warm Pool experiment, induced precipitation anomalies are obtained in both the equatorial western Pacific and the subtropical eastern Pacific. The latter contribute to the vertical advection forcing of barotropic motions in the Southern Hemisphere. The total moist feedback on the teleconnection process is thus able to alter significantly the teleconnection response to tropical heating.

Appendix

QTCM equations

QTCM is a nonlinear tropical circulation model that makes use of constraints from a particular QE convective scheme, the Betts-Miller scheme, but does not assume that convective QE has to hold. To achieve this, temperature, velocity and moisture are expanded in terms of a truncated series of basis functions in the vertical:

$$T = T_r(p) + \sum_{k=1}^{K} a_k(p) T_k(x, y, t) \tag{A.1}$$

$$\mathbf{v} = \sum_{k=0}^{L} V_k(p) \mathbf{v}_k(x, y, t) \tag{A.2}$$

$$q = q_r(p) + \sum_{k=1}^{K} b_k(p) q_k(x, y, t) \tag{A.3}$$

The model simply takes analytical solutions that hold approximately under QE conditions and

employs them as leading basis functions to represent the vertical structure of the flow.

For the standard version of QTCM1, a single deep convective mode is retained in the vertical thermodynamic structure [i.e.,$T = T_r(p) + a_1(p)T_1(x, y, t)$] with two components [barotropic $V_0(p)$ and baroclinic $V_1(p)$] in the vertical structure of velocity. Discretization of the moisture equation is largely independent. The model simply chooses a truncation for the moisture equation to have a similar level of complexity as for the temperature equation.

Using V_0 and V_1 as the basis functions, the momentum equations are projected onto these (i.e., taking the inner product of the momentum equation with V_0 and V_1, respectively) to obtain the prognostic equations for barotropic wind component and baroclinic wind component:

$$\partial_t \zeta_0 + curl_z[D_{V0}(\mathbf{v_0},\mathbf{v_1})] + \beta v_0 = -curl_z(\varepsilon_0 \mathbf{v_0}) - curl_z(\varepsilon_{10}\mathbf{v_1}) \tag{A.4}$$

and

$$\partial_t \mathbf{v}_1 + D_{V1}(\mathbf{v_0},\mathbf{v_1}) + f\mathbf{k} \times \mathbf{v}_1 = -\kappa \nabla T_1 - \varepsilon_1 \mathbf{v}_1 - \varepsilon_{01}\mathbf{v}_0 \tag{A.5}$$

where κ is the ratio of the gas constant for air over the heat capacity at constant pressure, and the advection-diffusion operators are given by:

$$D_{V0}(\mathbf{v_0},\mathbf{v_1}) = \mathbf{v_0} \cdot \nabla \mathbf{v_0} + \left\langle V_1^2 \right\rangle \mathbf{v_1} \cdot \nabla \mathbf{v_1} + \left\langle V_1^2 \right\rangle (\nabla \cdot \mathbf{v_1})\mathbf{v_1} - K_H \nabla^2 \mathbf{v_0} \tag{A.6}$$

and

$$D_{V1}(\mathbf{v_0},\mathbf{v_1}) = \mathbf{v_0}\cdot\nabla\mathbf{v}_1 + \frac{\left\langle V_1^3 \right\rangle}{\left\langle V_1^2 \right\rangle}\mathbf{v_1}\cdot\nabla\mathbf{v_1} + \mathbf{v}_1\cdot\nabla\mathbf{v_0} - (\langle V_1\Omega_1\partial_p V_1\rangle \,/\, \left\langle V_1^2 \right\rangle)(\nabla\cdot\mathbf{v_1})\mathbf{v_1} - K_H\nabla^2\mathbf{v}_1 \tag{A.7}$$

Vertical averages over the troposphere are defined as:

$$\hat{X} = \langle X \rangle = p_T^{-1} \int_{p_{rt}}^{p_{rs}} X dp \tag{A.8}$$

and $\Omega_1(p)$ represents the vertical structure of vertical velocity from the baroclinic wind. Because

vertical velocity is diagnostic in the primitive equations, solving the continuity equation gives:

$$\omega_1(x, y, p, t) = -\Omega_1(p)\nabla \cdot \mathbf{v_1}(\mathbf{x}, \mathbf{y}, \mathbf{t}) \tag{A.9}$$

and

$$\Omega_1(p) = \int_p^{p_s} V_1(p)dp \tag{A.10}$$

Two of the terms arising from vertical transfer of momentum to surface stress by parameterized subgrid-scale turbulence in the barotropic equation are defined as:

$$\varepsilon_0 = (g/p_T)\rho_a C_D V_s \tag{A.11}$$

and

$$\varepsilon_{10} = \left\langle V_1^2 \right\rangle \varepsilon_{01} = (g/p_T)\rho_a C_D V_s V_{1s} \tag{A.12}$$

where V_s is calculated as $\sqrt{u_s^2 + v_s^2 + V_{s\,\min}^2}$, and V_{1s} is value of the baroclinic basis function V_1 at surface. The surface drag coefficient C_D changes according to land surface type. The sign of ε_0 and ε_{10} are set as opposite in the model for the two surface drag terms to have the same form.

Vertically integrating the temperature and moisture equations from the standard nonlinear primitive equations, with vertical velocity and velocity truncated at V_1 yields:

$$\hat{a}_1(\partial_t + D_{T1})T_1 + M_{S1}\nabla \cdot \mathbf{v}_1 = \langle Q_c \rangle + (g/p_T) \times (-R_t^{\uparrow} - R_s^{\downarrow} + R_s^{\uparrow} + S_t - S_s + H) \tag{A.13}$$

and

$$\hat{b}_1(\partial_t + D_{q1})q_1 + M_{q1}\nabla \cdot \mathbf{v}_1 = \langle Q_q \rangle + (g/p_T)E \tag{A.14}$$

where the advection-diffusion operators are:

$$D_{T1} = \mathbf{v}_0 \cdot \nabla + \hat{a}_1^{-1} \langle a_1 V_1 \rangle \mathbf{v}_1 \cdot \nabla - K_H \nabla^2 \tag{A.15}$$

and

$$D_{q1} = \mathbf{v}_0 \cdot \nabla + \hat{b}_1^{-1} \langle b_1 V_1 \rangle \mathbf{v}_1 \cdot \nabla - K_H \nabla^2 \tag{A.16}$$

respectively, and the dry static stability$M_{S1}$and the gross moisture stratification M_{q1} are given by:

$$M_{S1} = p_T^{-1} \int_{p_{rt}}^{p_{rs}} \Omega_1(-\partial_p s) dp \tag{A.17}$$

and

$$M_{q1} = p_T^{-1} \int_{p_{rt}}^{p_{rs}} \Omega_1(-\partial_p q) dp \tag{A.18}$$

respectively, where $s = T + \phi$ is the dry static energy, with ϕ being the geopotential. The moist convective parameterization projects the Betts?Miller scheme onto the basis functions of temperature and moisture, resulting in:

$$\langle Q_c \rangle = - \langle Q_q \rangle = {\varepsilon_c}^* (q_1 - T_1) \tag{A.19}$$

where ${\varepsilon_c}^* \equiv \hat{a_1}\hat{b_1}(\hat{a_1} + \hat{b_1})^{-1}\varepsilon_c$ and $\varepsilon_c = {\tau_c}^{-1}\mathcal{H}(C_1)$, with τ_c being the convective adjustment time, $\mathcal{H}(C_1)$ a Heaviside function that represents the dependence of convection on conditional instability in the column, and C_1 a measure of CAPE for this model. Detailed treatment and parameterization of other terms on the rhs of the temperature and moisture equations can be found in Neelin and Zeng (2000), including sensible heat H, evaporation E, and longwave and shortwave fluxes at top of atmosphere and surface, R_t, R_s, S_t and S_s, respectively.

Chapter 3

El Niño/Southern Oscillation Sea Level Pressure Anomalies in the Western Pacific: Why are they there?

Abstract

Although sea level pressure (SLP) anomalies in the western Pacific have long been recognized as an integral part of the classic Southern Oscillation pattern associated with El Niño/Southern Oscillation (ENSO), there is an unresolved question regarding the dynamics that maintain these anomalies. Traditional studies of the ENSO response in the tropics assume a single deep baroclinic mode associated with the tropospheric temperature anomalies. However, the SLP anomalies in the western Pacific are spatially separated from the baroclinic signal in the NCEP-NCAR reanalysis, CMIP5 models, and an intermediate complexity model [a Quasi-equilibrium Tropical Circulation Model (QTCM)]. Separation of ENSO SLP anomalies in the tropical Pacific into baroclinic and barotropic components indicates that the barotropic component contributes throughout the tropics and constitutes the primary contribution in the western Pacific. To demonstrate the roles of baroclinic and barotropic modes in ENSO teleconnections within the tropics, a series of QTCM experiments is performed, where anomalies in the interactions between baroclinic and barotropic modes are suppressed over increasingly wider latitudinal bands in the tropical Pacific. If this suppression is done in the 15°N-15°S band, the pressure signals in the western Pacific are only partly removed, whereas if it is done in the 30°N-30°S band, the anomalies in the western Pacific are almost entirely removed. This suggests the following pathway: interactions with SST anomalies create the baroclinic response in the central and eastern Pacific, but baroclinic-barotropic interactions, arising substantially in the subtropical Pacific, generate a barotropic response that yields the SLP

anomalies in the western Pacific.

3.1 Introduction

El Niño/Southern Oscillation (ENSO) is associated with sea level pressure (SLP) anomalies that have long been recognized to form an oscillation pattern with poles in the western equatorial and southeastern Pacific (e.g., Walker, 1923; Berlage, 1957; Wallace et al., 1998). ENSO is also associated with tropospheric temperature anomalies that spread from the central and eastern Pacific and that in many ways resemble basic equatorial wave dynamics (Kiladis and Diaz, 1989; Wallace et al., 1998; Chiang and Sobel, 2002; Su and Neelin, 2002; Kumar and Hoerling, 2003). Some major aspects of ENSO dynamics can be understood through conceptual models based on a single deep baroclinic mode that is separable from the barotropic mode in the absence of baroclinic advection and vertical turbulent momentum transport (Matsuno, 1966; Webster, 1972; Gill, 1980). Such highly damped shallow-water models often give a plausible first approximation to the low-level wind response in the immediate vicinity of ENSO convective heating anomalies.

As we will show in the analysis in section 3.3, motivated by results from Wallace et al. (1998), the SLP anomalies in the western tropical Pacific are spatially separated from the baroclinic signal associated with the tropospheric temperature anomalies over the central and eastern Pacific. This raises a puzzle: if there are no significant ENSO-associated tropospheric temperature anomalies in the western Pacific, then the SLP anomaly cannot be due to baroclinic response that region. In other words, a conceptual model including only baroclinic mode cannot explain the western Pacific portion of the canonical ENSO SLP anomaly.

Teleconnections from the ENSO heating region into midlatitudes are largely barotropic (Horel and Wallace, 1981; Hoskins and Karoly, 1981; Simmons, 1982; Branstator, 1983; Simmons et al., 1983; Held and Kang, 1987) because the barotropic mode can reach high turning latitudes. Lee et al. (2009) have analyzed the interaction of baroclinic and barotropic components in the response to ENSO-like heating, as well as the importance of vertical background wind shear in exciting the barotropic response in midlatitudes. In intermediate complexity models in which both barotropic and baroclinic components are included, such as the QTCM used in part of this study (Neelin and Zeng, 2000; Zeng et al., 2000, hereafter NZ00), the barotropic component forms an

important part of the solution in climatology and ENSO variations. It is thus natural to ask whether the resolution to the above-mentioned puzzle might lie in the barotropic component of the ENSO response within the tropics, which appears so far not to have been extensively examined.

In the present study we show that in reanalysis data the western Pacific SLP response is part of a widespread barotropic contribution to the ENSO signal, whose spatial pattern differs substantially from the baroclinic signal. We then turn to model analysis and mechanism suppression experiments to argue that within the tropics, barotropic teleconnections excited by the baroclinic-barotropic interactions are responsible for the ENSO atmospheric response in SLP over the tropical western Pacific. Our hypothesis is the following: as baroclinic Rossby waves propagate west from the central and eastern equatorial Pacific, they excite barotropic wave trains through barotropic-baroclinic interactions. These wave trains can then propagate west to generate the SLP anomalies in the western Pacific, where it is observed that the baroclinic mode propagation does not reach. The barotropic mode can be forced by three barotropic-baroclinic interaction terms: 1) shear advection (Wang and Xie, 1996; Majda and Biello, 2003; Biello and Majda, 2004b), 2) surface drag (NZ00, Biello and Majda, 2004a), and 3) vertical advection (Bacmeister and Suarez, 2002). Recently, Ji et al. (2014) provided a detailed analysis of the effects these three terms have in interhemispheric teleconnections from tropical heat sources.

To demonstrate the respective roles of baroclinic and barotropic modes in ENSO teleconnections within the tropics, we first analyze the teleconnection patterns in the NCEP reanalysis and in several simulations done with general circulation models (GCMs) participating in phase 5 of the Coupled Model Intercomparison Project (CMIP5). Then to analyze the dynamics that maintain the SLP anomalies in the western Pacific associated with ENSO, we perform a set of diagnostic experiments using the QTCM, where the impact of the baroclinic-barotropic interaction terms on the SLP anomalies in the western Pacific can be artificially suppressed.

The remainder of the text is organized as follows: Section 2 gives a brief introduction of the datasets, model and methodology used in this study. Section 3 presents the analysis of baroclinic and barotropic modes in ENSO tropical teleconnections, based on data from the NCEP-NCAR reanalysis and CMIP5 simulations. Section 4 presents the results of several diagnostic experiments with the QTCM that demonstrate the dynamical pathway involved in ENSO tropical

teleconnections. Section 5 consists of a summary and discussion.

3.2 Datasets, model and methodology

3.2.1 Datasets

We use monthly diagnostic surface temperature from NOAA NCEP-NCAR Climate Data Assimilation System 1 (CDAS-1; Kalnay et al., 1996) to compute the Niño-3.4 SST index (Trenberth, 1997). Meteorological variables including sea level pressure, air temperature, sea surface temperature, and precipitation are taken from NCEP-NCAR reanalysis (Kalnay et al., 1996) and AMIP runs using prescribed SST anomalies for the period 1980-2008 of several models participating in CMIP5 (Taylor et al., 2012). For presentation, we only show results from four atmospheric general circulation models (AGCMs): CCSM4, CanAM4, GISS, and GFDL HIRAM-C360.

3.2.2 Conditions of baroclinic and barotropic mode separation

In this subsection we summarize conditions of separation of baroclinic and barotropic modes, and the methods and approximations involved in computing barotropic and baroclinic components of SLP in both reanalysis data and AGCM outputs.

The hydrostatic equation in pressure coordinates, $\partial_p \phi = -RT/p$, can be expressed in vertical integral form as:

$$\phi = \int_p^{p_r} RT d\ln p + \phi_r, \tag{3.1}$$

where ϕ is the geopotential at pressure level p, T is temperature, R is the gas constant for air, p_r is a reference pressure, and ϕ_r is the geopotential on that pressure surface. The momentum equation of the primitive equations combined with the hydrostatic equation can be written as:

$$\begin{aligned} &(\partial_t + \mathbf{v}\cdot\nabla + \omega\partial_p - K_H\nabla^2)\mathbf{v} + f\mathbf{k}\times\mathbf{v} + g\partial_p\tau \\ &= -\nabla\textstyle\int_p^{p_r} RT d\ln p - \nabla\phi_r, \end{aligned} \tag{3.2}$$

where $\mathbf{v}$ is horizontal velocity, ω is vertical velocity in pressure coordinates, K_H is the horizontal

diffusion coefficient, f is the Coriolis parameter, τ is vertical flux of horizontal momentum, and g is gravitational acceleration. Separation of the baroclinic and barotropic modes occurs under the following conditions: neglecting advection by baroclinic velocity (horizontal and vertical components) and neglecting the contribution of baroclinic wind in the surface drag on the barotropic mode. Under these circumstances the solution of Eq. (3.2) for velocity must simply match the vertical structures of the barotropic and baroclinic pressure gradient terms. The barotropic mode has constant vertical structure, since by definition it has no contribution from temperature yielding vertical variations in Eq. (3.2). These conditions are typically not met in subtropical to midlatitude conditions (e.g., Held et al., 1985), but it has been common to assume separation for simple tropical models such as Gill (1980). We argue here that the baroclinic-barotropic interactions cannot be neglected for important aspects of the tropical solutions. In diagnosing this, it is useful to compute components of the flow associated with the barotropic and baroclinic contributions. We underline, however, that these should not be viewed as perfectly separated modes — the interaction terms will be introduced in the next section for the case where a deep baroclinic component and the barotropic component are the leading contributors to the solution.

Because the barotropic pressure gradient has no vertical variation and the velocity component matches this vertical structure, a vertical average can be used to diagnose the barotropic contribution (projections on this decomposition are further discussed in the next section). The vertical average over the troposphere is $\hat{X} = \langle X \rangle = p_T^{-1} \int_{p_{rt}}^{p_{rs}} X dp$, where p_{rs} and p_{rt} are pressure at the near-surface and tropopause reference levels, respectively (here, 1000 and 150 hPa, respectively), and $p_T = p_{rs} - p_{rt}$. The barotropic component of the geopotential can be defined as $\phi_0 = \langle \phi \rangle$ for all levels. The barotropic (subscript 0) and baroclinic (subscript 1) components of the near-surface (1000 hPa) geopotential are thus defined by:

$$\phi_{rs0} = \langle \phi \rangle \,, \quad \text{and} \quad \phi_{rs1} = \phi_{rs} - \phi_{rs0}, \tag{3.3}$$

that is, $\phi_{rs} = \phi_{rs0} + \phi_{rs1}$. Working in pressure coordinates, this near-surface geopotential contains the key dynamical information, but since sea level pressure is the traditional diagnostic, we present figures here in terms of sea level pressure. Furthermore we are interested in departures from long-term time averages $()'$. Assuming that density ρ_s is constant between the surface and the

near-surface reference level, and using Eq. (3.3) with ϕ obtained directly from the reanalysis and model outputs, the baroclinic and barotropic components of the surface pressure perturbations are then:

$$p_s{}' \approx \rho_s \phi'_{rs0} + \rho_s \phi'_{rs1}. \tag{3.4}$$

A second way to do the decomposition is to compute ϕ from temperature via Eq. (3.1), and then calculate:

$$p_{s1}{}' = \rho_s(\phi_s{}' - \langle \phi' \rangle), \quad \text{and} \quad p_{s0}{}' = p_s{}' - p_{s1}{}', \tag{3.5}$$

where surface pressure p_s is obtained directly from the reanalysis and model outputs. The first choice [Eq. (3.4)] benefits from all computations having been done at the model native levels, while the second method [Eq. (3.5)] has the advantage of permitting computation of temperature perturbations through different layers (in particular, boundary layer versus free troposphere). Results from both computations are compared in Figs. S3.1 and S3.2 (see the supplemental material), further discussed below, and are in good agreement for all major features. The calculations in Eq. (3.5) are used in reanalysis and model figures in the main text.

3.2.3 Baroclinic and barotropic mode interactions in the QTCM

The QTCM belongs to a class of tropical atmospheric models of intermediate complexity that occupies a niche between GCMs and simple models. The model takes analytical solutions that hold approximately under quasi-equilibrium (QE) conditions and employs them as leading basis functions to represent the vertical structure of the flow. The primitive equations are then projected onto these simplified vertical structures, with self-consistent nonlinear terms retained in advection, moist convection, and vertical momentum transfer terms, among others. A more detailed model description can be found in NZ00.

The QTCM has been used to analyze the moist dynamics of ENSO teleconnections in a number of contexts (Su et al., 2001, 2003, 2005; Neelin and Su, 2005; Lintner and Chiang, 2007). The present study uses the first generation QTCM (QTCM1), version 2.3, which retains a single

basis function for the vertical structure of temperature, with two components [barotropic V_0 and baroclinic $V_1(p)$] in the vertical structure of velocity. This is the simplest configuration but it has considerable success in capturing tropical phenomena, because the temperature structure matches the consequences of a quasi-equilibrium convective scheme and the baroclinic velocity basis function is analytically compatible. Thus, the QTCM provides an appealing tool to analyze the contributions of baroclinic and barotropic modes to the ENSO tropical teleconnections. We note here that the subscript 1 in this section refers to the single deep baroclinic mode in the QTCM, which is a little different from the notation in the previous section, where subscript 1 refers to the baroclinic contribution that can have any vertical structure.

In the QTCM, the momentum Eq. (3.2) is projected onto the barotropic and baroclinic wind components $\mathbf{v}_0(x,y,t)$ and $\mathbf{v}_1(x,y,t)$, respectively. For the barotropic component:

$$\begin{aligned} &\partial_t \mathbf{v_0}' + D_{V0}(\mathbf{v_0},\mathbf{v_1})' + f\mathbf{k}\times\mathbf{v_0}' + (g/p_T)\tau_s{}' \\ &= -\nabla\phi_{s0}', \end{aligned} \tag{3.6}$$

with

$$D_{V0}(\mathbf{v_0},\mathbf{v_1})' = (\mathbf{v}_0\cdot\nabla\mathbf{v}_0)' + (\langle V_1^2\rangle\,\mathbf{v_1}\cdot\nabla\mathbf{v_1})' + [\langle V_1^2\rangle\,(\nabla\cdot\mathbf{v_1})\mathbf{v_1}]' - K_H\nabla^2\mathbf{v_0}', \tag{3.7}$$

where $V_1(p)$ is the vertical structure of the baroclinic component. The baroclinic wind component is governed by:

$$\begin{aligned} &\partial_t \mathbf{v_1}' + D_{V1}(\mathbf{v_0},\mathbf{v_1})' + f\mathbf{k}\times\mathbf{v_1}' + g\langle V_1^2\rangle^{-1}\langle V_1\partial_p\tau\rangle' \\ &= -\kappa\nabla T_1', \end{aligned} \tag{3.8}$$

where $D_{V1}(\mathbf{v_0},\mathbf{v_1})'$ is the advection-diffusion operator similar to Eq. (3.7) but for the baroclinic wind component. The geopotential gradient term $\kappa\nabla T_1{}'$ appears simple because $V_1(p)$ has been chosen to match the hydrostatic integral of the vertical structure of temperature, $a_1(p)$, with $\kappa = R/c_p$. The temperature coefficient, $T_1(x,y,t)$, is governed by the temperature equation for deep baroclinic structure:

$$\langle a_1\rangle\,(\partial_t + D_{T1})T_1 + M_{S1}\nabla\cdot\mathbf{v_1} = \langle Q_c\rangle + \langle Q_R\rangle\,, \tag{3.9}$$

where D_{T1} is the advection-diffusion operator for temperature, M_{S1} is the dry static stability for a vertical velocity profile derived from $V_1(p)$, and $\langle Q_c \rangle$ and $\langle Q_R \rangle$ are the vertical average convective and radiative plus sensible heating of the column, respectively. The convective heating is given by the convective parameterization that depends on temperature and moisture, with the moisture equation vertically projected on a single basis function (see NZ00 for details and other definitions). The driving by SST appears in the surface radiative and sensible heat fluxes that contribute to $\langle Q_R \rangle$ and in evaporation, as in a standard primitive equation model. The SST thus directly forces a prognostic baroclinic response in temperature, moisture and baroclinic wind. The barotropic response is forced by the baroclinic response through the interaction terms in Eq. (3.6), including surface drag and the baroclinic advection terms given by Eq. (3.7).

In diagnosing near-surface geopotential perturbation, the baroclinic contribution ${\phi_{s1}}'$ is obtained analytically from the vertical structure of temperature using the hydrostatic equation (as in NZ00):

$$ {\phi_{s1}}' = -R \left\langle \int_p^{p_s} a_1(p) d\ln p \right\rangle {T_1}', \tag{3.10} $$

and the barotropic contribution ${\phi_{s0}}'$ is calculated from Eq. (3.6). The total surface pressure ${p_s}'$ is then diagnosed with ${p_s}' = \rho_s {\phi_{s1}}' + \rho_s {\phi_{s0}}'$ as in Eq. (3.4).

Taking the curl_z of Eq. (3.6), the equation for the barotropic streamfunction ψ_0 is:

$$ \begin{aligned} &\partial_t \nabla^2 {\psi_0}' + curl_z(\mathbf{v}_0 \cdot \nabla \mathbf{v}_0)' - K_H \nabla^4 {\psi_0}' + \beta {v_0}' \\ &= -curl_z(\langle V_1^2 \rangle \, \mathbf{v_1} \cdot \nabla \mathbf{v_1})' - curl_z[\langle V_1^2 \rangle \, (\nabla \cdot \mathbf{v_1}) \mathbf{v_1}]' - curl_z(\varepsilon_0 \mathbf{v_0} + \varepsilon_{10} \mathbf{v_1})', \end{aligned} \tag{3.11} $$

where β is the meridional derivative of the Coriolis parameter, $(g/p_T){\tau_s}'$ is parameterized with $(\varepsilon_0 \mathbf{v_0} + \varepsilon_{10} \mathbf{v_1})'$, and where ε_0 and ε_{10} are momentum transfer rates from projection of turbulent stress terms as in NZ00. The terms on the right-hand side of Eq. (3.11) act as an effective Rossby wave source (RWS), which acts to excite the barotropic mode in a manner akin to well-known studies of barotropic teleconnections (Hoskins and Karoly, 1981; Held and Kang, 1987; Sardeshmukh and Hoskins, 1988). We remark, first, that this is not quite the same as the Rossby wave source that

would be defined by assuming an upper-level forcing applied to the barotropic mode, but rather results from a representation of the modal breakdown over the full depth of the troposphere (NZ00; Majda and Biello, 2003). Under certain circumstances, in particular if one could assume horizontally constant vertical shear in the geostrophic approximation, an alternate vertical mode decomposition can be constructed in which the barotropic mode properties are modified to create an external or equivalent barotropic mode with some baroclinic component included (Held et al., 1985). The interaction term approach here treats the same process in a manner that is easier to use in a spatially varying basic state. Second, the third term on the right-hand side is shown in a form where it is proportional to surface stress, which can be simpler for diagnosis and interpretation. However it might alternately be separated into a forcing term $-curl_z(\varepsilon_{10}\mathbf{v}_1)'$, with the $-curl_z(\varepsilon_0\mathbf{v}_0)'$ portion on the left-hand side. Interpreting the respective terms in the effective Rossby wave source in Eq. (3.11), the sources of baroclinic-barotropic interaction are: 1) $-curl_z(\langle V_1^2\rangle\,\mathbf{v_1}\cdot\nabla\mathbf{v_1})'$, representing interactions of vertical shear in horizontal advection terms; 2) $-curl_z[\langle V_1^2\rangle\,(\nabla\cdot\mathbf{v_1})\mathbf{v_1}]'$, representing vertical motion advecting the baroclinic wind component; and 3) $-curl_z(\varepsilon_0\mathbf{v}_0+\varepsilon_{10}\mathbf{v}_1)'$, representing interactions via surface stress in the boundary layer. Ji et al. (2014) analyzed the effects of each mechanism on forcing barotropic mode and associated teleconnection pathways from a tropical heat source.

We perform several diagnosis experiments with the QTCM to analyze the pathway for the atmospheric response in the tropical western Pacific associated with ENSO. In these experiments, the interannual variations in the baroclinic-barotropic interaction terms are suppressed by replacing these terms with their monthly mean values from a 100-yr climatological model run. To gain insight on the geographical extent of the region where the interactions act in the tropical teleconnections, interannual variations are suppressed over increasingly wider latitudinal bands in the tropical Pacific.

3.3 Baroclinic and barotropic modes in ENSO tropical teleconnections

In this section we examine the meteorological anomalies associated with ENSO. These are defined by regression of each quantity onto the Niño-3.4 SST index. We start with the monthly means for the winter season [December-February (DJF)] in the NCEP-NCAR reanalysis. The

results, shown in the panels of Fig. 3,1, are in good agreement with previous observational results, notably from Wallace et al. (1998), a study that helped inspire the investigation here.

In Fig. 3.1a, the SST anomalies show positive values in the central and eastern equatorial Pacific. Figure 3.1b shows positive precipitation anomalies around the central equatorial Pacific with negative anomalies around them and maximum values slightly to the west of the largest SST anomalies. The anomalies in vertical mean tropospheric temperature (Fig. 3.1c) show positive values over a broad region of the tropical central and eastern Pacific. The structure of these temperature anomalies is consistent with a baroclinic Rossby wave straddling the equator to the west and a Kelvin wave around the equator to the east of the precipitation anomalies in Fig. 3.1b, which correspond to regions of deep convective heating anomalies. The magnitude of the tropospheric temperature anomalies drops off sharply from around the date line toward the western Pacific. The lack of baroclinic mode propagation toward the west is at least in part due to the slow phase speed of baroclinic Rossby wave packets, although it may also be affected by more complex factors, such as the slower speed of waves interacting strongly with convection. In either case, it is clear that the deep baroclinic anomalies do not reach the western Pacific. The SLP anomalies (Fig. 3.1d) are reminiscent of the classic Southern Oscillation pattern: strong negative and positive anomalies in the eastern and western Pacific, respectively. Thus, in the western Pacific the SLP anomalies are spatially separated from the baroclinic signal associated with the temperature anomalies.

Next, we break down the SLP anomalies in Fig. 3.1d into their baroclinic and barotropic components. The baroclinic component (Fig. 3.2a) has strong magnitudes in the eastern Pacific in the same region where tropospheric temperature anomalies are strong (Fig. 3.1c), as expected from the hydrostatic relationship. The barotropic component (Fig. 3.2b), on the other hand, shows a broad band of anomalies across the entire tropics with a clear local maximum in the western Pacific, where the values are comparable to those of the total SLP anomalies in Fig. 3.1d. Thus, the positive SLP anomalies in the western Pacific are due to the barotropic contribution, since the baroclinic contribution has the opposite sign and is small

The robustness of the results in Figs. 3.1 and 3.2 is examined in several figures in the supplemental material. Similar results are obtained for regression of monthly anomalies over the full

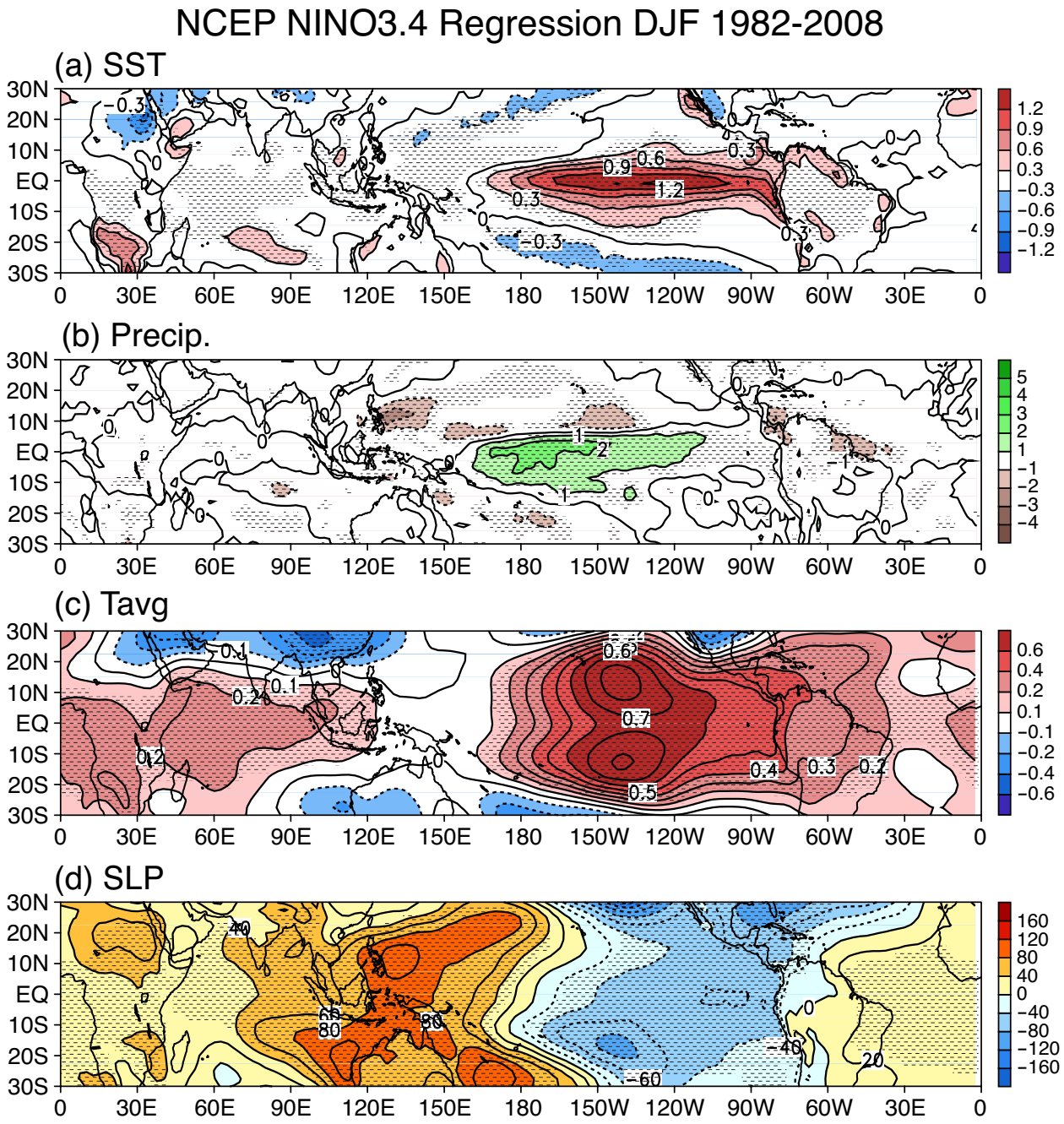

Figure 3.1: (a) SST (K $^{\circ}C^{-1}$), (b) precipitation (mm $day^{-1}{}^{\circ}C^{-1}$), (c) tropospheric temperature (K $^{\circ}C^{-1}$), and (d) SLP (Pa $^{\circ}C^{-1}$) from NCEP-NCAR reanalysis DJF regression onto Niño3.4, with a two-tailed t test applied to the regression values and stippled at 99% confidence.

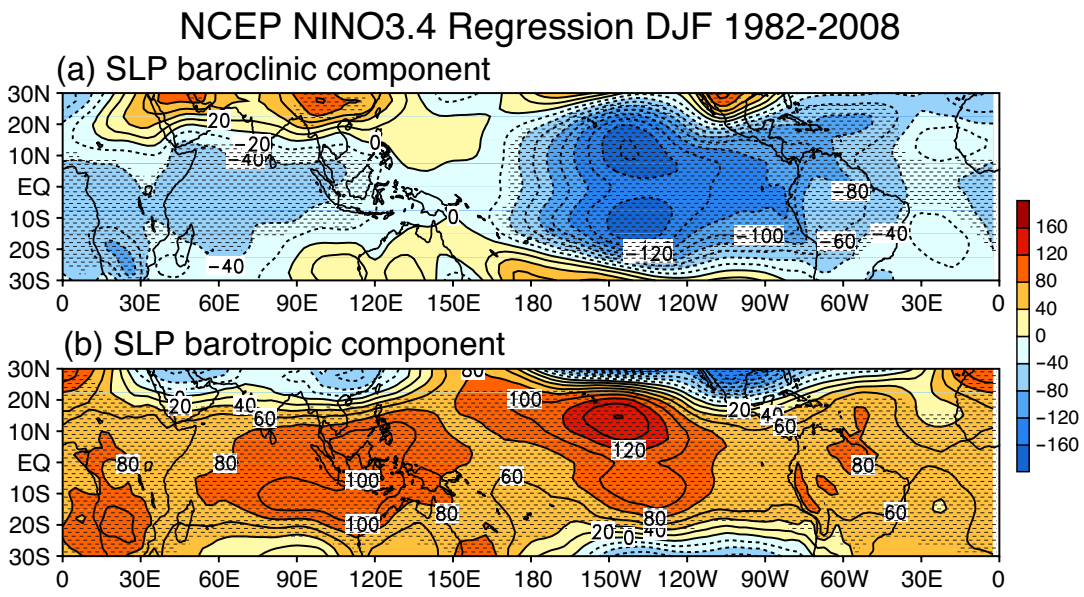

Figure 3.2: (a) SLP baroclinic component (Pa $^{\circ}C^{-1}$) and (b) SLP barotropic component (Pa $^{\circ}C^{-1}$) from NCEP-NCAR reanalysis DJF regression onto Niño3.4, with a two-tailed t test applied to the regression values and stippled at 99% confidence.

annual cycle (Fig. S3.1 in the supplemental material) and using Eq. (3.4) instead of Eq. (3.5) to decompose the SLP anomalies into baroclinic and barotropic components (Fig. S3.2 in the supplemental material). The conclusion in Fig. 3.2 that the barotropic contribution is not negligible even in the deep tropics also holds when viewed in terms of the associated surface wind contributions (Figs. S3.3 and S3.4 in the supplemental material). In the subtropics, the barotropic wind contribution considerably cancels the baroclinic contribution to the surface wind, as one would expect when surface drag is effective at damping the near-surface baroclinic wind component and spinning up a barotropic wind component. Finally, the baroclinic contribution to SLP anomalies in Fig. 3.2a comes primarily from the free troposphere rather than the boundary layer (Fig. S3.5 in the supplemental material). In either case, baroclinic contributions to SLP anomalies in the western Pacific are very weak.

In the following, we examine the anomalies in SLP and tropospheric temperature associated with ENSO in the AGCM simulations described in section 3.2 using the monthly mean fields for the winter season. We show in Fig. 3.3 the SLP and the tropospheric temperature anomalies based on models participating in the CMIP5. Thirty models are examined but four typical models are shown, which are consistent at large scales with the corresponding patterns in the NCEP-NCAR

reanalysis (Fig. 3.1). The large SLP anomalies and weak tropospheric temperature anomalies in the western Pacific are also present in the AGCMs of other CMIP5 models (not shown). When model SLP anomalies are decomposed into baroclinic and barotropic components (Fig. S3.6 in the supplemental material), the barotropic contribution dominates in the western Pacific, where the baroclinic contribution is small as in the NCEP-NCAR reanalysis (Fig. 3.2). Examining the model SLP patterns in Figs. 3.3a, 3.3c, 3.3e, and 3.3g in more detail, some variation may be noted in the western Pacific, suggesting that while the overall mechanism is common among the models, there may be some sensitivity in the precise spatial pattern and amplitude.

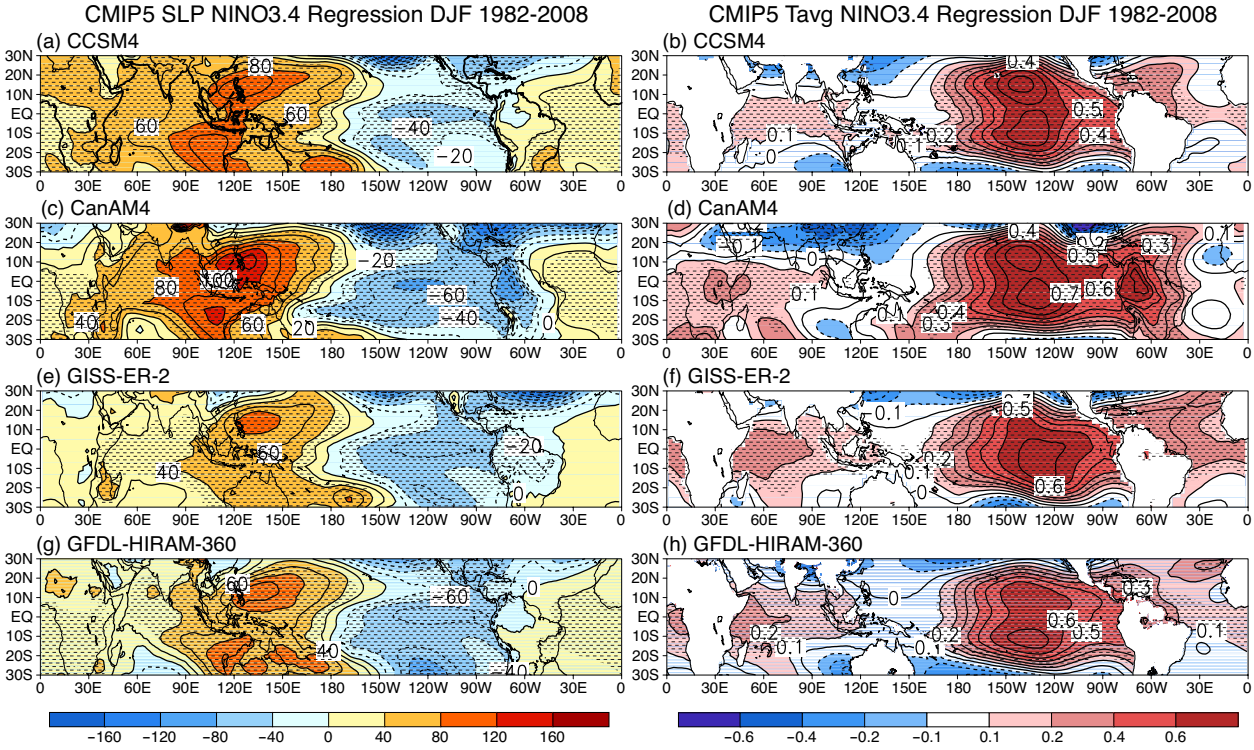

Figure 3.3: (left) SLP (Pa $^{\circ}C^{-1}$), and (right) tropospheric temperature (K $^{\circ}C^{-1}$) from selected AGCM runs participating in CMIP5 DJF regression onto Niño3.4, with a two-tailed t test applied to the regression values and stippled at 99% confidence.

In section 3.4, the dynamical mechanisms at work in the ENSO tropical teleconnection process are investigated using QTCM. First, it is necessary to confirm the extent to which the QTCM has a similar response to ENSO as in the NCEP-NCAR reanalysis and CMIP5 models. Figure 3.4 shows the wintertime meteorological anomalies associated with ENSO based on the 26 winters (DJF) in a 27-yr (1982-2008) QTCM run with observed SSTs. A comparison between

panels in Fig. 3.4 with those obtained using the NCEP-NCAR reanalysis in Figs. 3.1 and 3.2 reveals similarities of pattern, although simulated amplitudes are weaker. This is possibly due to the simplified vertical structure of temperature in the QTCM, which tends to cause the tropospheric temperature anomalies to be more strongly damped toward SST anomalies. For the purpose of this study, the similarities of pattern between the QTCM and reanalysis data are sufficient to motivate analysis of mechanisms in a model where the baroclinic-barotropic interaction terms can be explicitly altered.

3.4 Diagnosis experiment with the QTCM

In this section, we use the QTCM to gain insight into the dynamical mechanisms at work for the ENSO tropical teleconnection process. The question to be addressed is how the barotropic teleconnection patterns are forced in the western Pacific by the effective barotropic Rossby wave source due to the baroclinic-barotropic interactions. This is examined by conducting mechanism-suppression experiments in which anomalies in the baroclinic-barotropic interaction terms are artificially suppressed over specified regions. The results in this section are based on pairs of 100-yr QTCM simulations: one with monthly composites of El Niño SST anomalies added to monthly mean climatology (El Niño run) and the other with monthly mean climatological SSTs (climatological run). The El Niño run monthly SST anomalies are composited from July through the following June of five large El Niño events (1957/58, 1965/66, 1972/73, 1982/83, and 1997/98). The 100-yr simulation length is used to obtain statistically significant results, including in the western Pacific when the signal is artificially reduced. The barotropic-baroclinic interaction terms for the QTCM barotropic Eq. (3.11) are saved from the climatological run, and are specified as a seasonally varying source term in the specified target region of the suppression experiments. Each pair of El Niño and climatological runs is conducted with the same climatological barotropic-baroclinic interaction terms specified in the target region. Differences between each pair are thus due to the response to SST anomalies in the absence of barotropic-baroclinic interaction term anomalies within the target region.

Figure 3.5 shows the December-February mean SST anomalies, precipitation anomalies, tropospheric average temperature anomalies, SLP anomalies, and the baroclinic and barotropic

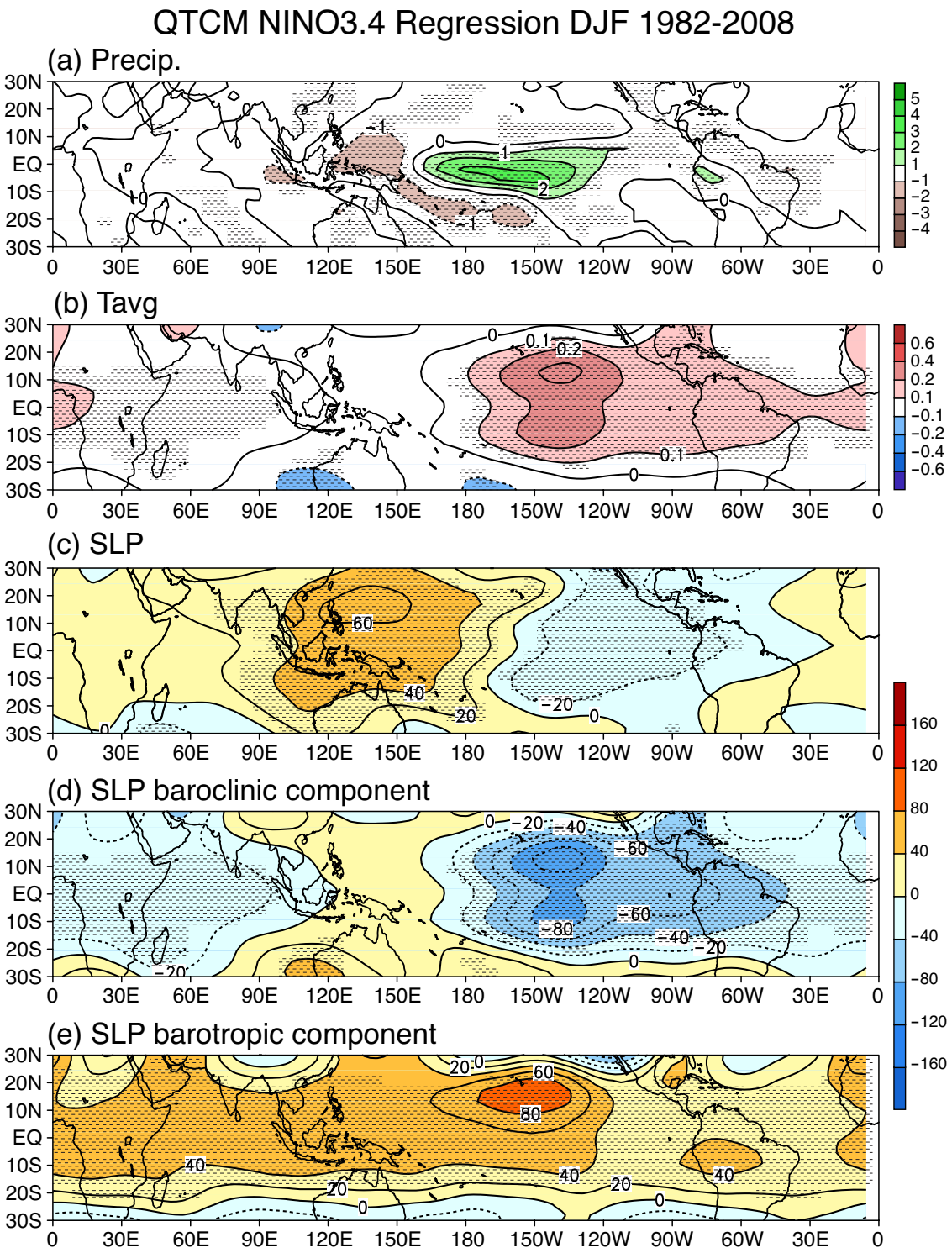

Figure 3.4: (a) Precipitation (mmday-1 °C-1), (b) tropospheric temperature (K °C-1), (c) SLP (Pa °C-1), (d) SLP baroclinic component (Pa °C-1), and (e) SLP barotropic component (Pa °C-1) from a 26-year (1982-2008) QTCM run with real-time SSTs DJF regression onto Niño3.4, with a two-tailed t test applied to the regression values and stippled at 99% confidence.

SLP anomalies (differences) between the El Niño run and the climatological run with full Rossby wave source (i.e., no suppression). Each panel shows a similar pattern to the one obtained by regressing each variable onto Niño-3.4 SST shown in Figs. 3.1 and 3.2 for NCEP reanalysis data and Fig. 3.4 from a 27-yr (1982-2008) QTCM run with observed SSTs. Note that the regression plots in Fig. 3.4 show values per degree of SST anomalies associated with ENSO, whereas the fields in Fig. 3.5 are associated with SST anomalies on the order of 2-3 K (Fig. 3.5a). Thus, values in Fig. 3.5 are all 2-3 times larger than those in Fig. 3.4. The breakdown of the SLP anomalies (Fig. 3.5d) into the baroclinic (Fig. 3.5e) and barotropic (Fig. 3.5f) components again indicates that the positive SLP anomalies in the western Pacific, especially the maximum around 180°, 20°N, are due to the barotropic contribution.

Figure 3.6 displays the December-February mean SLP differences between the El Niño run and the climatological run. The SLP anomalies in Fig. 3.5d are repeated in Fig. 3.6a. Figures 3.6b-d portray the impact of suppressing the Rossby wave source anomalies in the region from 150°E to 100°W for successively wider latitudinal bands around the equator. Comparisons among Figs. 3.6b-d reveal that the SLP anomalies in the western Pacific are gradually weaker with wider bands of suppression. This weakening indicates that the baroclinic-barotropic interactions in the Pacific subtropics are important in addition to those in the tropics to the SLP anomalies in the western Pacific.

Figure 3.7 presents the total Rossby wave source (Fig. 3.7a) as well as its three components (shear advection, surface drag, and vertical advection) between the two 100-yr simulations, that is, the Rossby wave source that we suppressed in the QTCM experiments in Fig. 3.6. The surface drag (Fig. 3.7c) and vertical advection (Fig. 3.7d) terms each have nonnegligible contributions in the equatorial central Pacific. Note that Fig. 3.7c shows the baroclinic portion $-curl_z(\varepsilon_{10}\mathbf{v}_1)'$ as the forcing component in the surface drag, since the barotropic portion $-curl_z(\varepsilon_0\mathbf{v}_0)'$ acts as damping on the barotropic mode, while in the QTCM experiment we suppress the surface stress term as a whole. The shear advection term (Fig. 3.7b) tends to have the largest contribution, especially in the subtropics. This horizontal advection term arises substantially from the baroclinic wind anomalies interacting with basic-state vertical shear. The importance of the horizontal shear advection term in the subtropics is consistent with the need to suppress the Rossby wave source through the latitude

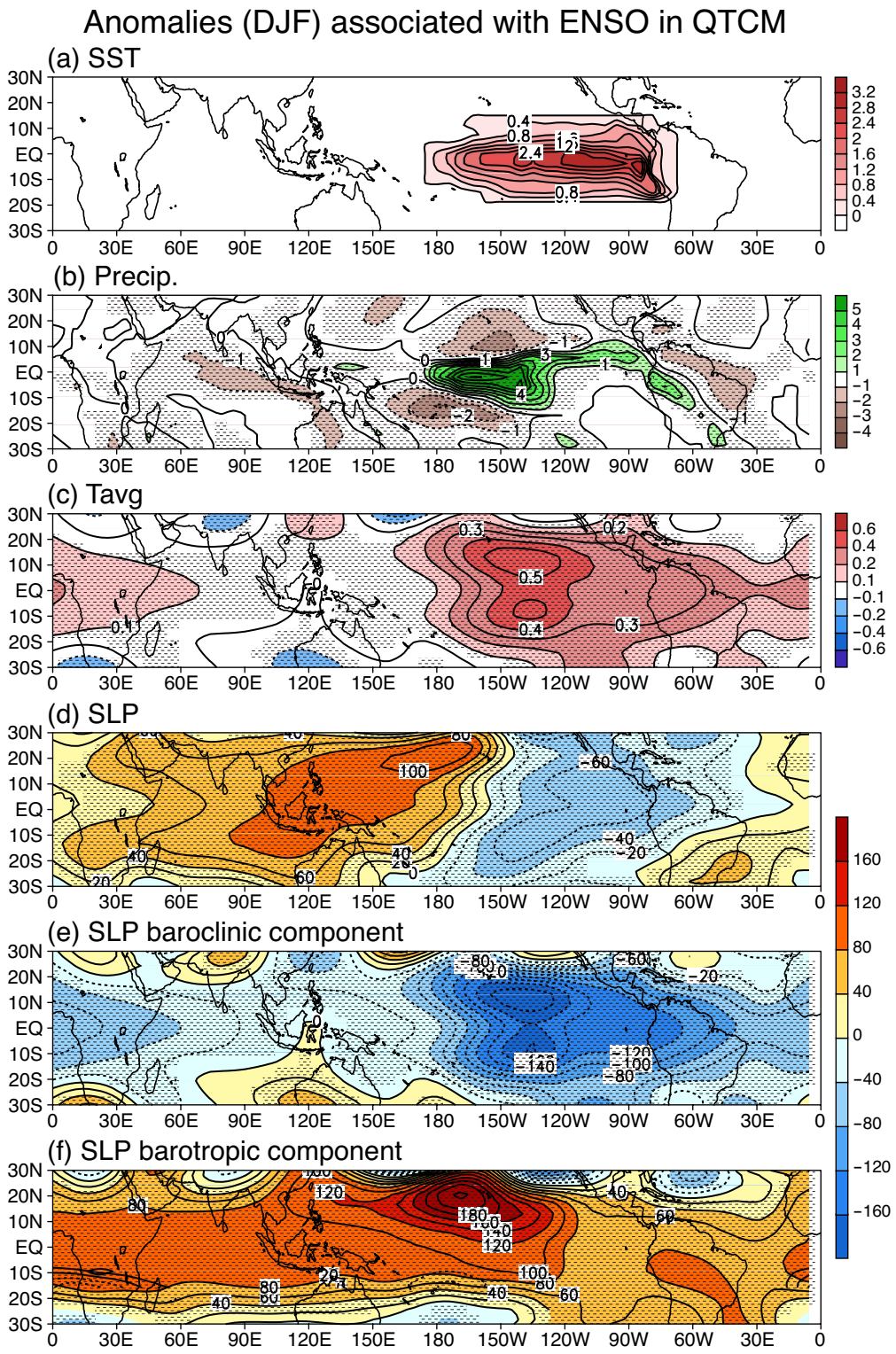

Figure 3.5: (a) SST anomaly (°C), (b) precipitation (mm day^{-1}) anomaly, (c) tropospheric temperature (K) anomaly, (d) SLP anomaly (Pa), (e) SLP anomaly baroclinic component (Pa), and (f) SLP anomaly barotropic component (Pa) associated with ENSO from the QTCM experiment with full barotropic Rossby wave source (i.e., no suppression), stippled where a t test yields grid points significant at or above the 99% confidence level.

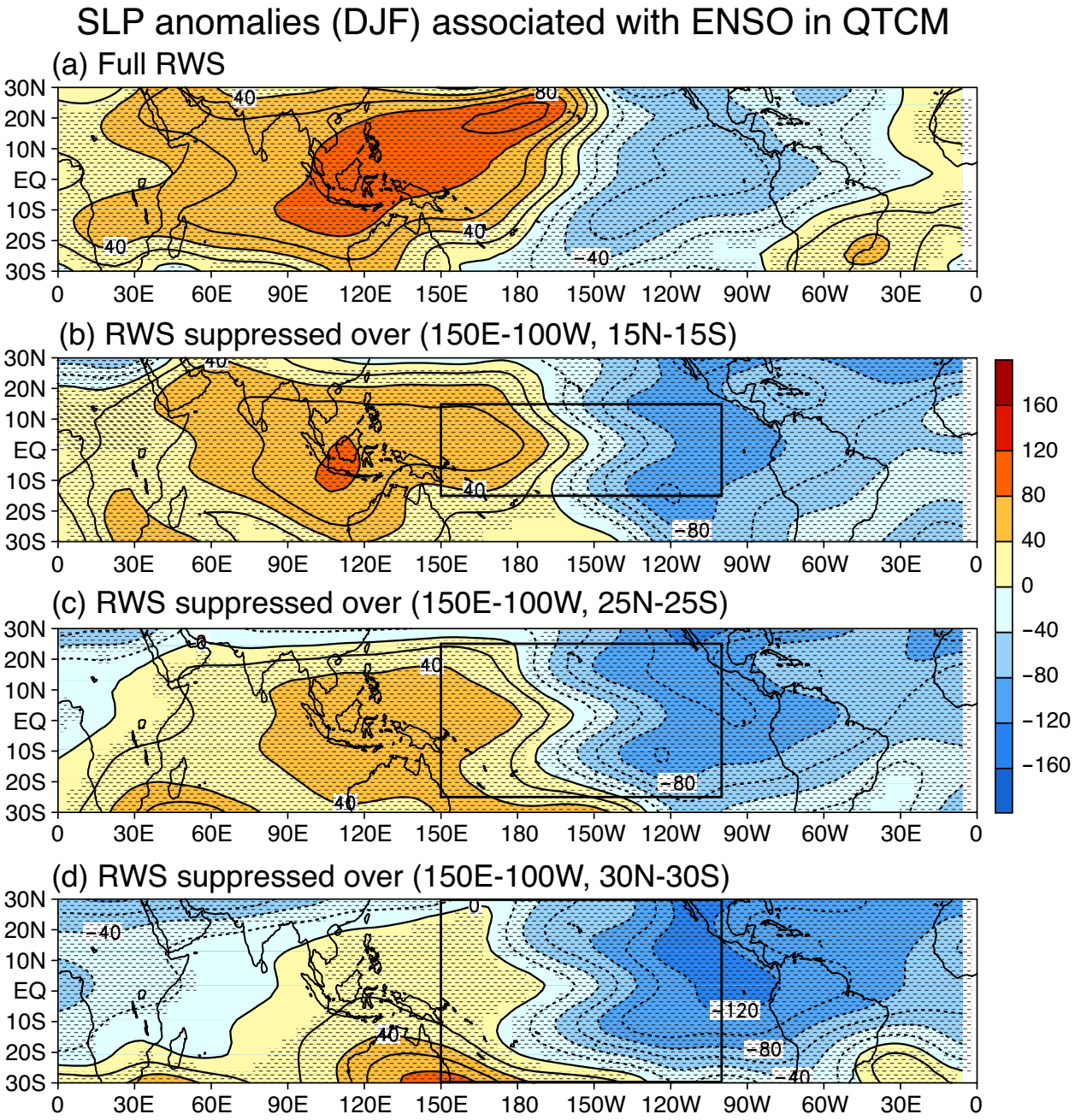

Figure 3.6: SLP anomaly (Pa) associated with ENSO from QTCM experiments with (a) full barotropic Rossby wave source (RWS); (b) RWS suppressed over 15°N-15°S, 150°E-100°W; (c) RWS suppressed over 25°N-25°S, 150°E-100°W; and (d) RWS suppressed over 30°N-30°S, 150°E-100°W, stippled where a t test yields grid points significant at or above the 99% confidence level. Box indicates the region of RWS suppression.

band that includes the subtropics in the suppression experiments to reduce barotropic signal in the western Pacific. The strong subtropical horizontal shear contribution results when the ENSO baroclinic anomaly spreads in latitude over roughly an equatorial radius of deformation, as was seen in the temperature anomalies of Fig. 3.1c, and encounters the regions of strong climatological shear in the subtropics.

3.5 Conclusions

We have investigated the mechanisms that generate the SLP anomalies in the western Pacific, which have long been known as part of the classic Southern Oscillation pattern associated with ENSO. Contrary to the traditional view that assumes a single deep baroclinic mode for ENSO response in the tropics, the SLP anomalies in the western Pacific occur in a region where there is little baroclinic signal associated with the tropospheric temperature anomalies in NCEP-NCAR reanalysis, CMIP5 models, and QTCM. Separation of the SLP into its baroclinic and barotropic components indicates that the baroclinic mode SLP contributions extend over the central and eastern equatorial Pacific, coincident with the temperature anomalies, and in a spatial pattern consistent with first baroclinic mode wave dynamics. On the other hand, SLP anomalies in the western Pacific arise primarily from barotropic mode contributions and thus must be associated with a slightly more complex dynamical pathway.

The following pathway is found in QTCM diagnostic experiments: interactions with SST anomalies create the baroclinic mode signal in the central and eastern Pacific, but baroclinic-barotropic interactions, arising substantially in the subtropical Pacific, create a barotropic response. This barotropic contribution is widespread in the tropics, but it is particularly important in yielding the SLP anomaly pattern in the western Pacific where the baroclinic contribution is small. In a set of QTCM experiments, we suppress anomalies in baroclinic-barotropic interaction terms over increasingly wider latitudinal bands in the tropical Pacific, to diagnose their effects on the SLP anomalies in the western Pacific associated with ENSO. In the 15°N-15°S experiment, the pressure signals in the western Pacific are only partly suppressed, whereas in the 30°N-30°S suppression experiment, the anomalies in the western Pacific are almost entirely removed. We note that the suppression experiment does not necessarily imply that the westward teleconnection is

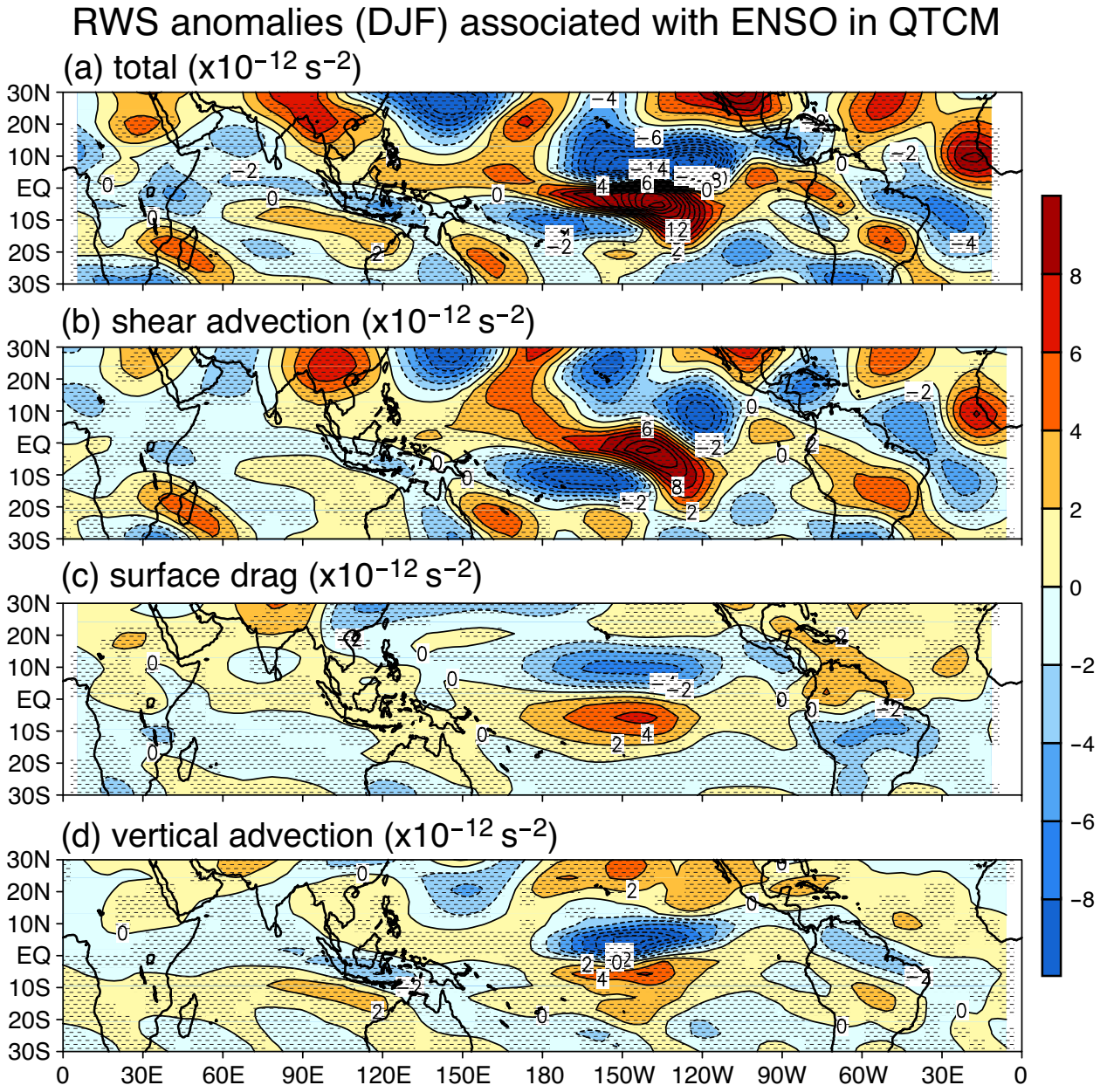

Figure 3.7: QTCM barotropic Rossby wave source anomalies associated with ENSO. (a) Total, (b) shear advection term, (c) surface drag baroclinic component, and (d) vertical advection term, stippled where a t test yields grid points significant at or above the 99% confidence level. See text for a description of each term.

purely barotropic. However, it does demonstrate that anomalies of an effective barotropic Rossby wave source due to the baroclinic-barotropic interaction terms are key to maintaining the largely barotropic signal in the western Pacific that yields the classical SLP patterns in this region. Furthermore, it demonstrates the importance of the subtropical contribution to this effective Rossby wave source. This arises substantially from the vertical shear term that occurs as the ENSO baroclinic anomalies, spread by wave dynamics into the subtropics, interact with basic-state vertical shear approaching the subtropical jet.

Chapter 3 supplementary material

Here we examine the robustness of essential features presented in the main text with a number of alternate or extended diagnostics. Figure S3.1 shows anomalies in SLP and its baroclinic and barotropic components, as well as the tropospheric temperature, similar to Figs. 3.1 and 3.2 of the main text, but computed by regressing the monthly mean fields onto Niño 3.4 through the full annual cycle for the 26-year (1982-2008) period from the NCEP-NCAR reanalysis. Similar patterns are obtained, albeit with weaker magnitudes in this annual case as for the DJF case in the main text. This suggests that the spatial discrepancy between regions of larger SLP anomalies and tropospheric temperature anomalies associated with ENSO in the tropical Pacific is robust throughout the year, despite the seasonal asymmetries of the subtropical circulation and associated baroclinic and barotropic interactions in the subtropics.

Figure S3.2 shows the calculations of SLP, SLP baroclinic component, and SLP barotropic component with Eq. (3.4) in the main text using NCEP-NCAR reanalysis geopotential height. Compared with Fig. S3.1 panels (d) (e) and (f), using Eq. (3.5) of the main text, respectively, the two methods for decomposition of SLP anomalies are in good agreement for all major features.

It is also useful to have an estimate of how the teleconnection pattern translates into surface wind. Figures S3.3a and S3.4a show the regression of NCEP-NCAR reanalysis surface zonal wind and vector surface wind onto Niño3.4, respectively (through the full annual cycle, as in Fig. S3.1). Figures S3.3b and S3.4b show the reconstructed winds from the NCEP 1000hPa geopotential field using simple damping assumptions (Stevens et al., 2002). The reconstruction compares to the actual surface winds sufficiently well over oceans to motivate reconstructing separately the baroclinic and barotropic components from the respective geopotential contributions. In Figures S3.3c, d, the baroclinic zonal wind contribution near the equator in the tropical Pacific is substantially larger

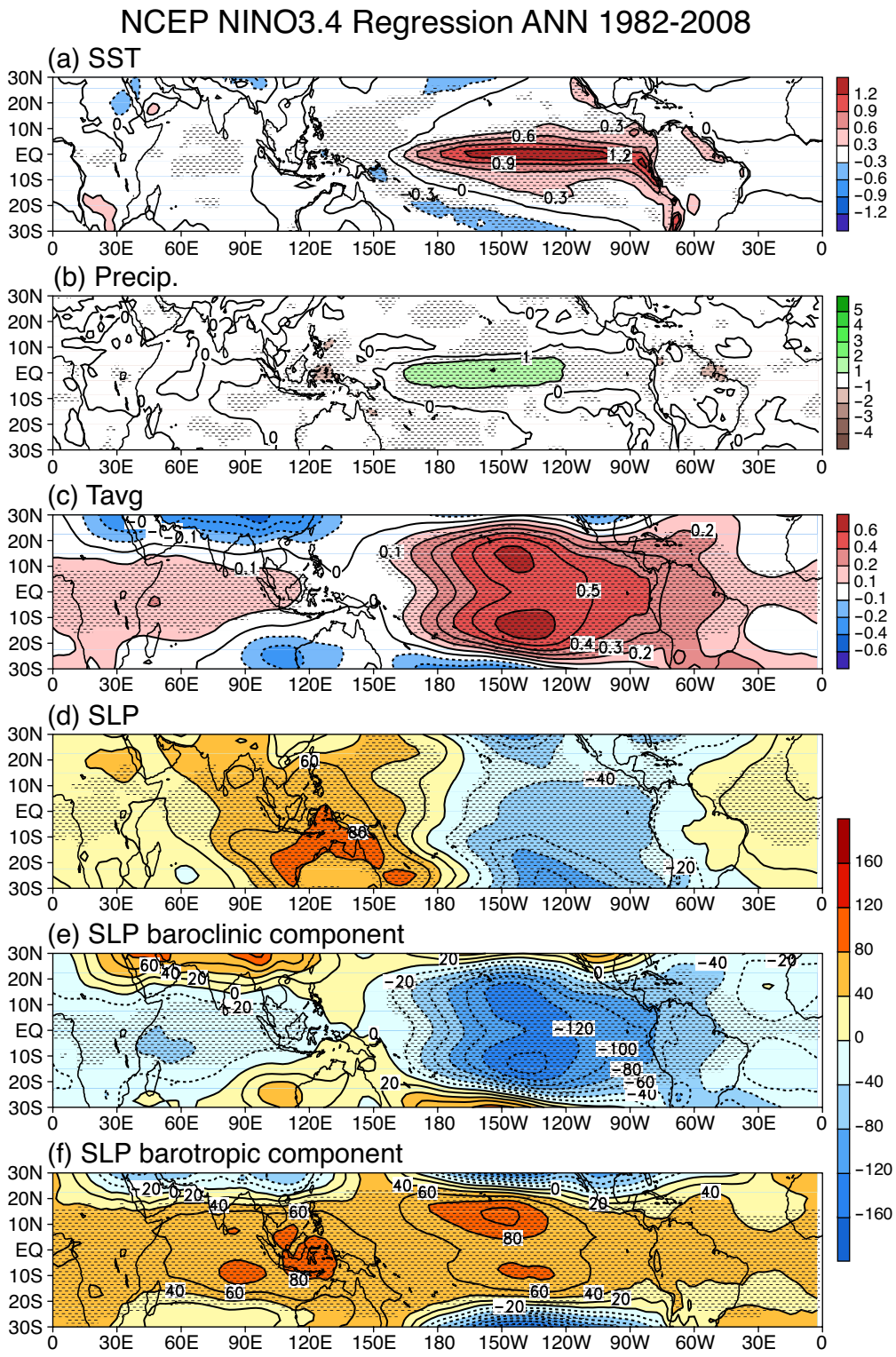

Figure S3.1: (a) SST (K $^{\circ}C^{-1}$), (b) precipitation (mm day$^{-1}{}^{\circ}C^{-1}$), (c) tropospheric temperature (K $^{\circ}C^{-1}$), (d) SLP (Pa $^{\circ}C^{-1}$), (e) SLP baroclinic component (Pa $^{\circ}C^{-1}$), and (f) SLP barotropic component (Pa $^{\circ}C^{-1}$) from NCEP-NCAR reanalysis regression of monthly anomalies onto Niño3.4 over the full annual cycle (referred to as the *annual* case), with a two-tailed t test applied to the regression values and stippled at 99% confidence.

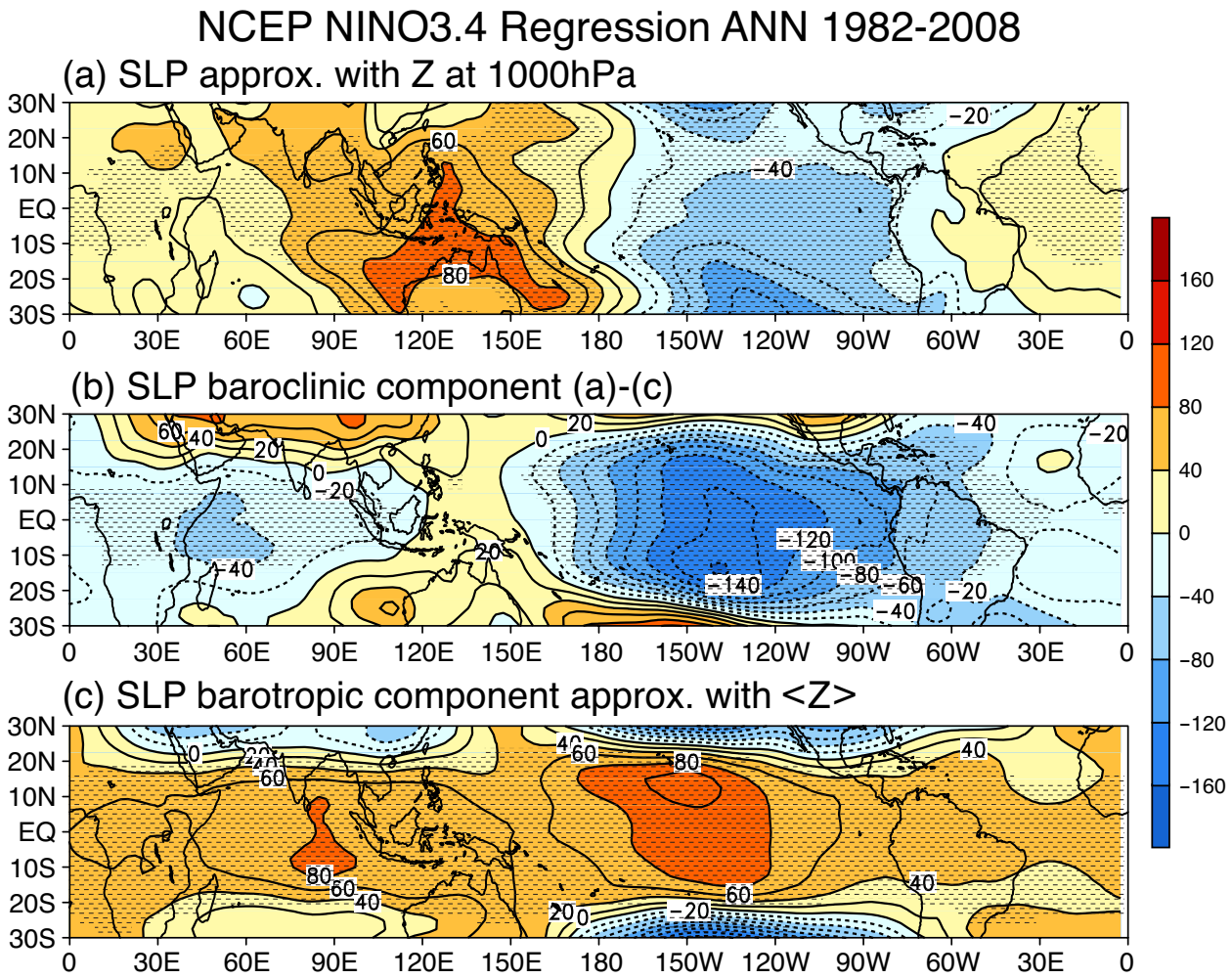

Figure S3.2: (a) SLP (Pa $^{\circ}C^{-1}$), (b) SLP baroclinic component (Pa $^{\circ}C^{-1}$), and (c) SLP barotropic component (Pa $^{\circ}C^{-1}$), calculated with Eq. (3.4) of the main text, from NCEP-NCAR reanalysis geopotential height (Z) *annual case* regression onto Niño3.4, with a two-tailed t test applied to the regression values and stippled at 99% confidence.

than the barotropic contribution, so an approximation that would include only the baroclinic mode would have qualitatively useful features. However, the barotropic contribution is not negligible even in the deep tropics. Furthermore, in the subtropics, the barotropic contribution considerably cancels the baroclinic contribution to the surface wind, as one would expect when surface drag is effective at damping the near surface baroclinic wind component and spinning up a barotropic wind component.

In Figure S3.5, we further decompose the baroclinic component of SLP (Fig. S3.1e) into its free troposphere (900-150hPa) contribution (Fig. S3.5b) and boundary layer (1000-900hPa) contribution (Fig. S3.5d). The corresponding decomposition of the tropospheric temperature anomalies in Fig. S3.1c, i.e., the vertical average over free troposphere and boundary layer, respectively, is also shown in Figs. S3.5a and S3.5c. The tropospheric temperature anomalies in the free troposphere and the boundary layer have similar magnitudes but very different patterns, with the latter resembling the SST anomalies in Fig. S3.1a. However, the baroclinic contribution to SLP anomalies from the free tropospheric temperature is much larger than that of the boundary layer due to the greater depth of the free troposphere. Notice that in either case, the contributions to SLP anomalies in the western Pacific are very weak.

Figure S3.6 shows the winter season (December, January and February) mean tropospheric temperature anomalies, SLP anomalies and the baroclinic and barotropic SLP anomalies associated with ENSO using the example of the GFDL HiRAM-C360 model. Overall, the results obtained with the GFDL HiRAM-C360 (Fig. S3.6) are similar to those from the NCEP-NCAR reanalysis (Figs. 3.1 and 3.2 of the main text) in large-scale patterns and magnitudes. In particular, the positive SLP anomalies in the western Pacific are due to the barotropic contribution since the baroclinic contribution has the opposite sign and is small. Details of the spatial pattern within the western Pacific differ slightly, but overall the barotropic contribution is substantial and spreads widely through the tropical band in the model simulation as in reanalysis.

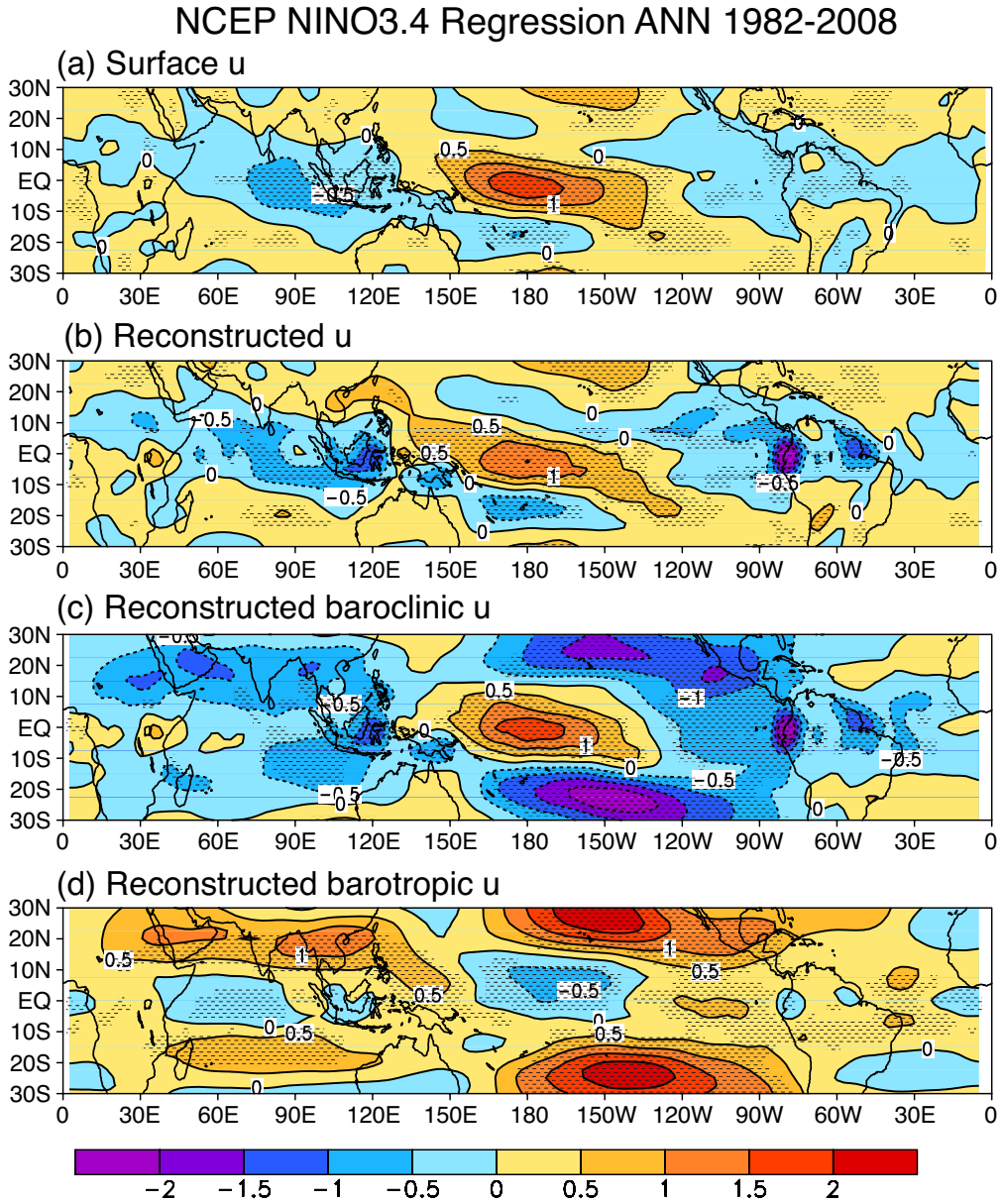

Figure S3.3: (a) Zonal wind, (b) zonal wind reconstructed from geopotential height at 1000hPa, (c) zonal wind baroclinic component reconstructed from baroclinic geopotential height at 1000hPa, (d) zonal wind barotropic component reconstructed from barotropic geopotential height at 1000hPa from NCEP-NCAR reanalysis *annual case* regression onto Niño3.4, with a two-tailed t test applied to the regression values and stippled at 99% confidence. The reconstructed wind is a solution to the equations $-\varepsilon u + fv = -\partial_x \phi$ and $-\varepsilon v - fu = -\partial_y \phi$ forced by the specified 1000hPa geopotential, where an assumed bulk damping due to surface stress is used, with a value $\varepsilon = (1day)^{-1}$. The units are m s^{-1}.

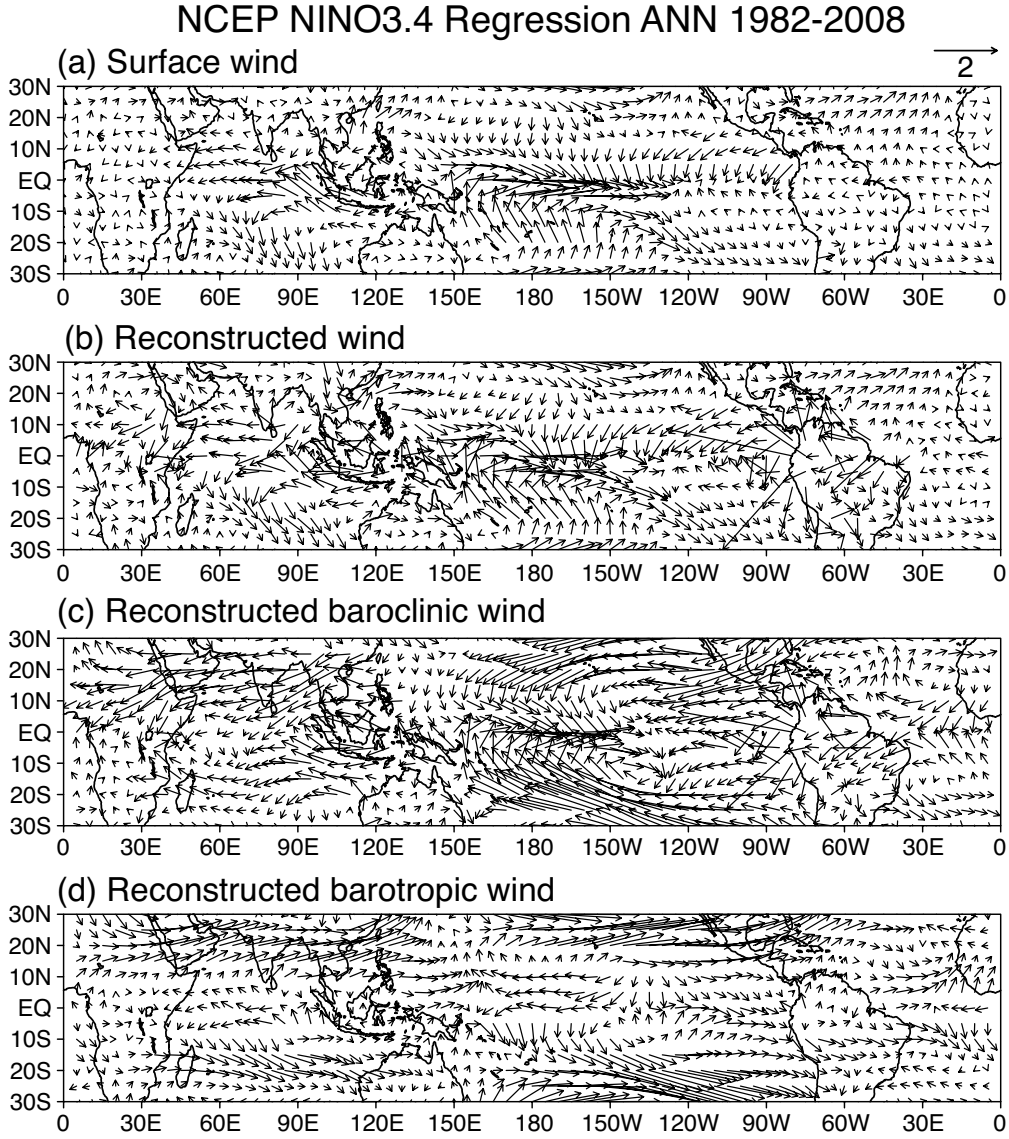

Figure S3.4: (a) Surface wind, (b) surface wind reconstructed from geopotential height at 1000hPa, (c) surface wind baroclinic component reconstructed from baroclinic geopotential height at 1000hPa, (d) surface wind barotropic component reconstructed from barotropic geopotential height at 1000hPa from NCEP-NCAR reanalysis *annual case* regression onto Niño3.4. The units are m s^{-1}.

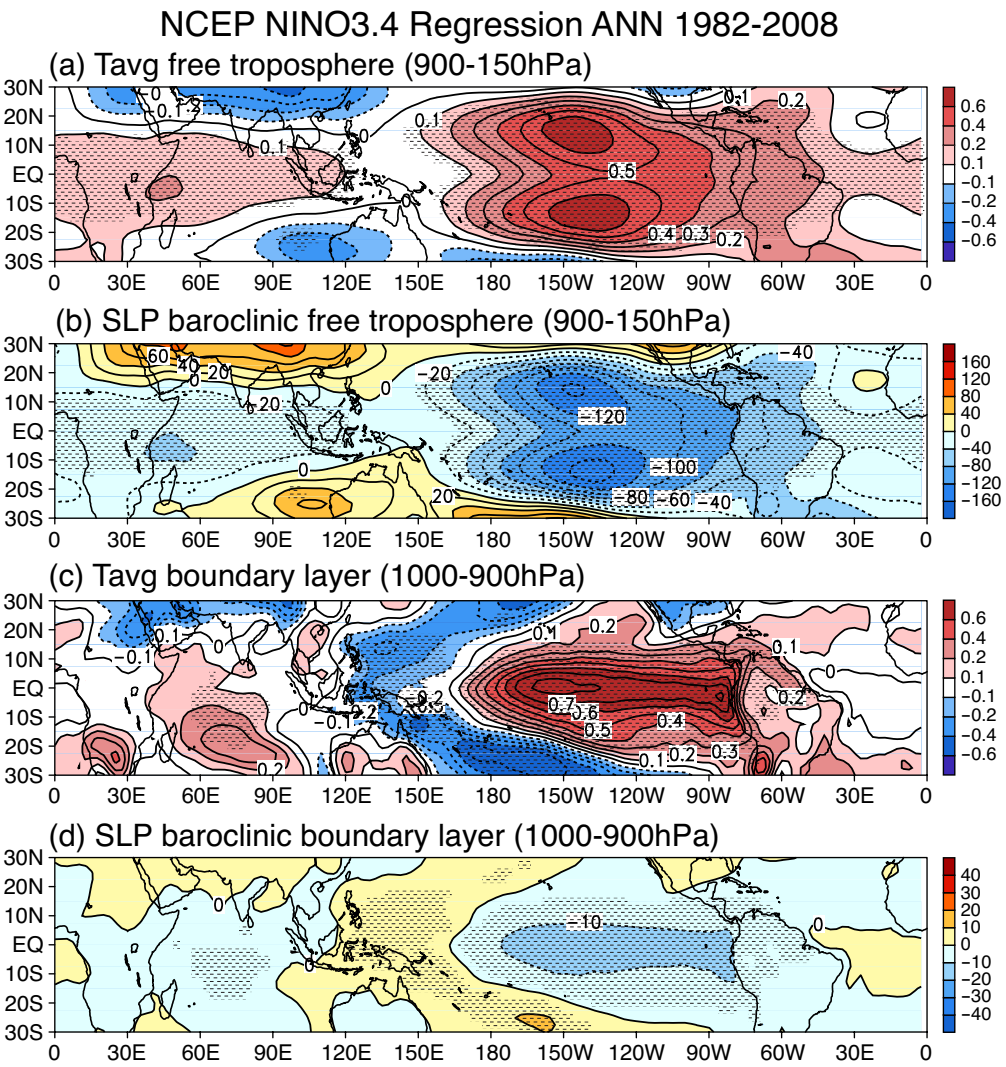

Figure S3.5: (a) Tropospheric temperature average over free troposphere (900-150hPa) (K $^{\circ}C^{-1}$), (b) SLP baroclinic free troposphere (900-150hPa) component (Pa $^{\circ}C^{-1}$), (c) tropospheric temperature average over boundary layer (1000-900hPa) (K $^{\circ}C^{-1}$), and (d) SLP baroclinic boundary layer (1000-900hPa) component (Pa $^{\circ}C^{-1}$), from NCEP-NCAR reanalysis *annual case* regression onto Niño3.4, with a two-tailed t test applied to the regression values and stippled at 99% confidence.

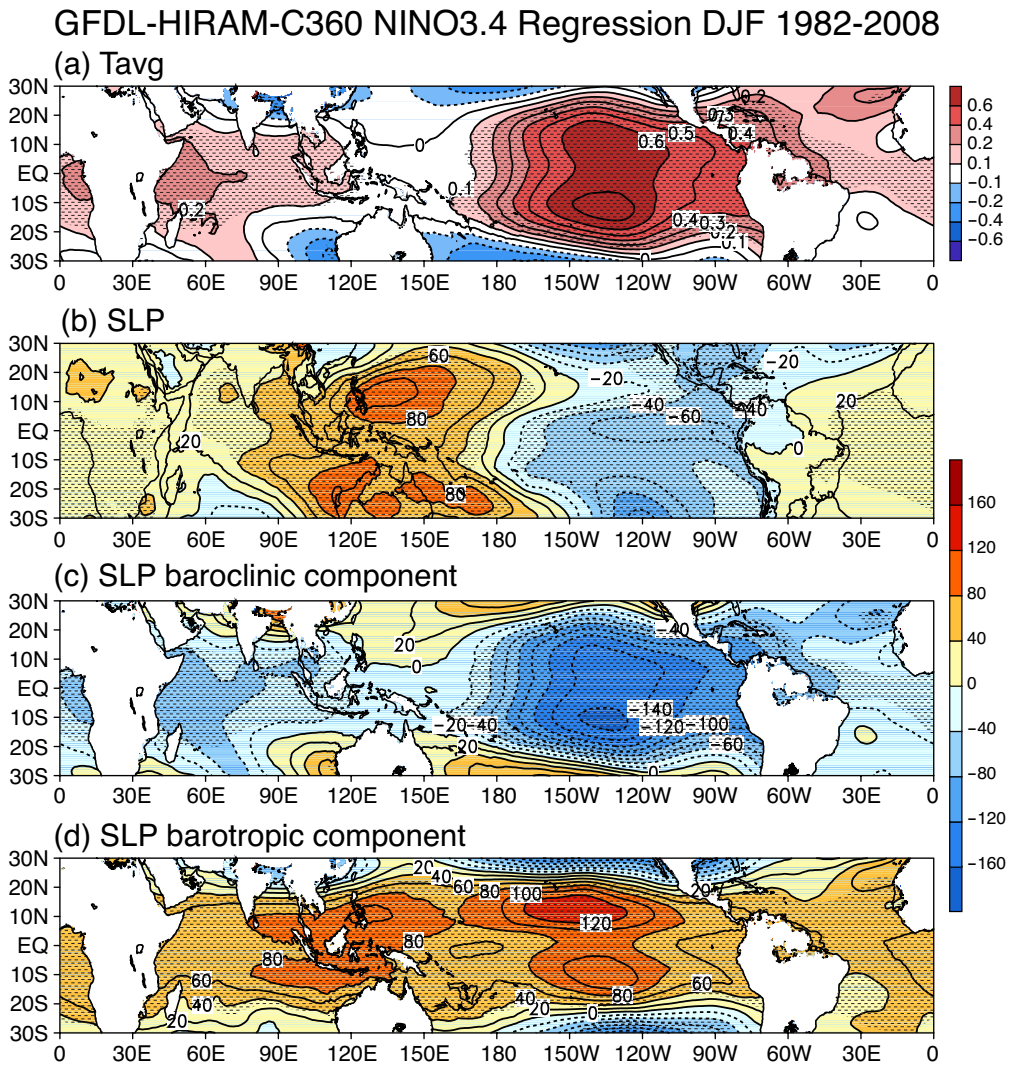

Figure S3.6: (a) Tropospheric temperature (K $^{\circ}C^{-1}$), (b) SLP (Pa $^{\circ}C^{-1}$), (c) SLP baroclinic component (Pa $^{\circ}C^{-1}$), and (d) SLP barotropic component (Pa $^{\circ}C^{-1}$) from GFDL HiRAM-C360 run with prescribed SSTs DJF regression onto Niño3.4, with a two-tailed t test applied to the regression values and stippled at 99% confidence. Note in (a), (c), and (d), land points for which temperature does not extend to 1000hPa are masked; SLP interpolation in (b) is as provided by the modeling center.

Chapter 4

Baroclinic-to-barotropic pathway in El Niño/Southern Oscillation teleconnections from the viewpoint of an effective Rossby wave source

Abstract

The baroclinic-to-barotropic pathway in ENSO teleconnections is examined from the viewpoint of an effective Rossby wave source that results from decomposition into barotropic and baroclinic components. Diagnoses using the NCEP-NCAR reanalysis are supplemented by analysis of the response of a tropical atmospheric model of intermediate complexity to the NCEP-NCAR effective Rossby wave source. Among the three barotropic Rossby wave source contributions (shear advection, vertical advection and surface drag), the leading contribution is from shear advection, and more specifically, the mean baroclinic zonal wind advecting the anomalous baroclinic zonal wind. Vertical advection is the smallest term, while surface drag tends to cancel and reinforce the shear advection in different regions through damping on baroclinic mode, which spins up a barotropic response. There are also non-trivial impacts of transients in the barotropic wind response to ENSO. Both tropical and subtropical baroclinic vorticity advection contribute to the barotropic component of the Pacific subtropical jet near coast of North America, where the resulting barotropic wind contribution approximately doubles the zonal jet anomaly at upper levels, relative to the baroclinic anomalies alone. In this view, the effective Rossby wave source in the subtropics simply arises from the basic-state baroclinic flow acting on the well-known baroclinic ENSO flow pattern that spreads from the deep tropics into the subtropics over a scale of equatorial radius of deformation. This is inseparably connected to the leading deep tropical Rossby wave source that arises from eastern Pacific climatological baroclinic winds advecting the tropical

portion of the same ENSO flow pattern.

4.1 Introduction

Teleconnections from the ENSO heating region into midlatitudes are largely barotropic (Horel and Wallace, 1981; Hoskins and Karoly, 1981; Simmons, 1982; Branstator, 1983; Simmons et al., 1983; Held and Kang, 1987) because barotropic modes can propagate to high turning latitudes. However, the tropical heat source associated with ENSO does not directly force a barotropic response. In the central and eastern Pacific, ENSO is associated with tropospheric temperature anomalies that can be well described by baroclinic equatorial wave dynamics, with response to heating tending to approximately resemble a baroclinic Rossby wave straddling the equator and a Kelvin wave at the equator (Kiladis and Diaz, 1989; Wallace et al., 1998; Chiang and Sobel, 2002; Su and Neelin, 2002; Kumar and Hoerling, 2003). Interactions between baroclinic and barotropic modes then force the barotropic Rossby wave trains that dominate the ENSO teleconnections in the North Pacific and North America.

In view of the vertical structure of teleconnections into midlatitudes, pure barotropic models have been widely used for their study (e.g., Hoskins and Karoly, 1981; Simmons, 1982; Simmons et al., 1983; Held and Kang, 1987). Applications of this methodology, however, typically have prescribed a vorticity source or "Rossby wave source" (Sardeshmukh and Hoskins, 1988). The prescribed source can be based, for instance, on the specification of baroclinic divergence at upper levels or on baroclinic transient motions diagnosed from a GCM simulation (Held and Kang, 1987). Many components of a fixed source in this approach come from dynamical processes whose scales, spatial form, and so on depend on the interaction of the baroclinic mode with the basic state in ways that can be interesting to elucidate.

The motivation of our work is to investigate the complex baroclinic-to-barotropic pathway in the tropics to midlatitudes teleconnection process through baroclinic-barotropic interactions. In the equation for the barotropic component of the flow, these interactions are formally similar to a Rossby wave source, but their structure can be quantitatively and conceptually quite different than those based on upper-level divergent flow. For instance, if there is no vertical shear and no damping on the baroclinic mode associated with surface stress, then upper level divergence in the

baroclinic mode does not produce any linear forcing of the barotropic mode. At the same time, by explicitly modeling the gravest baroclinic mode, the teleconnection pathway can be followed as the two modes interact.

Multilevel linear, steady-state wave models with both baroclinic and barotropic components (Hoskins and Karoly, 1981; Ting and Held, 1990; DeWeaver and Nigam, 2004) can capture at least some aspects of the tropical/baroclinic - midlatitude/barotropic transition. Held et al. (1985) show how a geostrophic barotropic mode is modified to an external mode in presence of shear, as further discussed in section 2b. Lee et al. (2009) use a simple two-level model to analyze the interaction of baroclinic and barotropic components in response to ENSO-like heating, as well as the importance of vertical background wind shear in exciting the barotropic response in midlatitudes. Majda and Biello (2003) emphasize the central role of baroclinic mean shear for sufficiently rapid nonlinear exchange of energy between the tropics and midlatitudes. Biello and Majda (2004a) explain how the dissipative mechanisms arising from radiative cooling and atmospheric boundary layer drag, creates barotropic/baroclinic spinup/spindown in the teleconnection process. Interactions with baroclinic transient eddies (Held et al., 1989; Hoerling and Ting, 1994) also alter the teleconnection pattern in a manner that is not easily captured by stationary wave models.

Our focus in the present study is on the forcing of the midlatitude barotropic response to ENSO by three barotropic-baroclinic interaction processes: (1) shear advection (Wang and Xie, 1996; Neelin and Zeng, 2000; Majda and Biello, 2003; Biello and Majda, 2004b; Lee et al., 2009), (2) surface drag (Neelin and Zeng, 2000; Biello and Majda, 2004a), and (3) vertical advection (Neelin and Zeng, 2000; Bacmeister and Suarez, 2002). Recently, Ji et al. (2014) analyzed in detail the roles that these three terms play in interhemispheric teleconnections from tropical heat sources. Moreover, Ji et al. (2015) examined the effects of these three terms in generating the sea level pressure anomalies in the western Pacific during El Niño, which are integral part of the Southern Oscillation pattern. We examine the ENSO composites of baroclinic-barotropic interaction terms [the effective "Rossby wave source" (RWS)] calculated from NCEP-NCAR reanalysis and then use the same quasi-equilibrium tropical circulation model (QTCM, see model description in section 4.2.3) as in previous studies to perform a set of diagnostic experiments, where the NCEP RWS are prescribed in the barotropic vorticity equation of the QTCM. The barotropic teleconnection responses in these

experiments are then compared to ENSO composites of the NCEP-NCAR reanalysis winds.

The remainder of the text is organized as follows. Section 4.2 gives a brief introduction of the datasets, model and methodology used in this study. Section 4.3 presents ENSO composite anomalies of tropospheric temperature, and of the baroclinic and barotropic components of wind, based on data from the NCEP-NCAR reanalysis. Section 4.4 presents the results of QTCM experiments in response to ENSO composite anomalies of the effective "Rossby wave source" — the baroclinic-barotropic interaction terms — computed using NCEP-NCAR reanalysis, and further analysis of the dominant component of Rossby wave source. Section 4.5 consists of a summary and discussion.

4.2 Datasets, Model and Methodology

4.2.1 Datasets

We use monthly air temperature, zonal and meridional winds from NCEP-NCAR reanalysis (Kalnay et al., 1996), which covers the period from 1948 to the present date. Using this dataset we created composite plots corresponding to 6 El Niño events (1982-1983, 1986-1987, 1991-1992, 1997-1998, 2002-2003, and 2009-2010).

4.2.2 The effective barotropic Rossby wave source

The hydrostatic equation in pressure coordinates, $\partial_p \phi = -RT/p$, can be expressed in vertical integral form as:

$$\phi = \int_p^{p_r} RT d\ln p + \phi_r \tag{4.1}$$

where ϕ is the geopotential at pressure level p, T is temperature, R is the gas constant for air, p_r is a reference pressure, and ϕ_r is the geopotential on that pressure surface. The momentum equation of the primitive equations combined with the hydrostatic equation can be written as:

$$
\begin{aligned}
&(\partial_t + \mathbf{v}\cdot\nabla + \omega\partial_p - K_H\nabla^2)\mathbf{v} + f\mathbf{k}\times\mathbf{v} + g\partial_p\tau \\
&= -\nabla\textstyle\int_p^{p_r} RTd\ln p - \nabla\phi_r
\end{aligned}
\tag{4.2}
$$

where $\mathbf{v}$ is horizontal velocity, ω is vertical velocity in pressure coordinates, K_H is the horizontal diffusion coefficient, f is the Coriolis parameter, τ is vertical flux of horizontal momentum, and g is gravitational acceleration.

The barotropic component of Eq. (4.2) is defined as a vertical average in the troposphere, $\langle X\rangle = p_T^{-1}\int_{p_{rt}}^{p_{rs}} X dp$, where p_{rs} and p_{rt} are pressure at the near-surface and tropopause reference levels, respectively (here, 1000 and 200 hPa, respectively), and $p_T = p_{rs} - p_{rt}$, and is denoted with subscript "0":

$$
\begin{aligned}
&\partial_t\mathbf{v_0} + \mathbf{v_0}\cdot\nabla\mathbf{v_0} - K_H\nabla^2\mathbf{v_0} + f\mathbf{k}\times\mathbf{v_0} + \nabla\phi_0 \\
&= -\langle\mathbf{v_1}\cdot\nabla\mathbf{v_1}\rangle - \langle(\nabla\cdot\mathbf{v_1})\mathbf{v_1}\rangle - (g/p_T)\tau_s
\end{aligned}
\tag{4.3}
$$

where the subscript "1" denotes the baroclinic components (i.e., the deviation from the vertical mean), and is a function of p. For simplicity, in the applications here where we are examining usefulness for ENSO anomalies, the effect of topography in the vertical integrals is omitted.

Taking $curl_z$ of Eq. (4.3), the anomaly equation for the barotropic stream function ψ_0 is, denoting anomalies relative to long-term mean climatology by prime:

$$
\begin{aligned}
&\partial_t\nabla^2{\psi_0}' + curl_z(\mathbf{v}_0\cdot\nabla\mathbf{v}_0)' - K_H\nabla^4{\psi_0}' + \beta{v_0}' + curl_z(\varepsilon_0\mathbf{v}_0)' \\
&= -\langle curl_z(\mathbf{v}_1\cdot\nabla\mathbf{v}_1)'\rangle - \langle curl_z[(\nabla\cdot\mathbf{v}_1)\mathbf{v}_1]'\rangle - curl_z(\varepsilon_1\mathbf{v}_{1s})'
\end{aligned}
\tag{4.4}
$$

where β is the meridional derivative of the Coriolis parameter, $(g/p_T)\tau_s$ is parameterized by $(\varepsilon_0\mathbf{v}_0 + \varepsilon_1\mathbf{v}_{1s})$, with $\varepsilon_0 = \varepsilon_1 = (g/p_T)\rho_a C_D V_s$, and where ρ_a is the near-surface air density, C_D is the drag coefficient, V_s is the near-surface wind speed. Note that all terms that involve the barotropic component of the flow have been placed on the lhs of Eq. (4.4). The terms on the rhs of Eq. (4.4) act as an effective Rossby wave source, which acts to excite the barotropic mode in a manner akin to well-known studies of barotropic teleconnections reviewed in the Introduction section of this chapter (Hoskins and Karoly, 1981; Held and Kang, 1987; Sardeshmukh and Hoskins, 1988). We emphasize that this is noticeably different than the Rossby wave source that would be defined by assuming an

upper-level forcing applied to the barotropic mode, because it results from a representation of the modal breakdown over the full depth of the troposphere (Neelin and Zeng, 2000; Majda and Biello, 2003). If one considers a linearization of Eq. (4.4) about a basic state with no baroclinic mean wind or surface damping, the barotropic mode is a free solution, separated from baroclinic modes. Held et al. (1985) show that in presence of horizontally constant shear, a solution can be obtained for an external mode that is closely related to the barotropic mode but with some baroclinic contributions. These contributions vanish as the basic state shear goes to zero. A barotropic vorticity equation with an assumed Rossby wave source containing an upper-level divergence term does not capture this dependence on shear. In the approximation here, the vertical velocity interaction with shear is seen as one term in the effective Rossby wave source.

Interpreting the individual terms on the rhs of Eq. (4.4), the contributions of baroclinic-barotropic interaction in such an effective Rossby wave source are: (1) $-\langle curl_z(\mathbf{v}_1 \cdot \nabla \mathbf{v}_1)' \rangle$, representing the horizontal advection processes; (2) $-\langle curl_z[(\nabla \cdot \mathbf{v}_1)\mathbf{v}_1]' \rangle$, representing vertical advection processes; (3) $-curl_z(\varepsilon_1 \mathbf{v}_{1s})'$, representing surface drag processes. Ji et al. (2014) analyzed the effects of each mechanism on forcing barotropic mode and associated teleconnection pathways from a tropical heat source. Ji et al. (2015) further examined the effects of each mechanism on the sea level pressure anomalies in the western Pacific during El Niño/Southern Oscillation events.

4.2.3 QTCM

The QTCM belongs to a class of tropical atmospheric models of intermediate complexity that occupies a niche between GCMs and simple models. The model takes analytical solutions that hold approximately under quasi-equilibrium (QE) conditions and employs them as leading basis functions to represent the vertical structure of the flow. The primitive equations are then projected onto these simplified vertical structures, with self-consistent nonlinear terms retained in advection, moist convection, and vertical momentum transfer terms, among others. A more detailed model description can be found in Neelin and Zeng (2000). The QTCM has been used to analyze the moist dynamics of ENSO teleconnections in a number of contexts (Su et al., 2001, 2003, 2005; Neelin and Su, 2005; Lintner and Chiang, 2007).

The present study uses the first generation QTCM (QTCM1), version 2.3. This version

retains a single basis function for the vertical structure of temperature, with two components in the vertical structure of velocity: barotropic V_0 and baroclinic V_1, where the subscript 0 refers to the barotropic mode that is vertically independent to horizontal temperature variations, which has the same form as Eq. (4.4); and the subscript 1 refers to a single deep baroclinic mode corresponding to the vertical structure of temperature in the QTCM. Note the slight difference with the notation used in the previous section, where the subscript 1 referred to the baroclinic contribution that can have any vertical structure.

We perform several experiments with the QTCM to analyze the pathway of atmospheric teleconnections in the Pacific from tropical ENSO heating to the mid- and high latitudes. In these experiments, the ENSO December-February (DJF) composite anomalies of monthly baroclinic-barotropic interaction terms are used to substitute the ENSO SST anomalies. Then the barotropic teleconnections in response to those interaction terms are compared to the teleconnection patterns calculated as the ENSO composite anomalies in NCEP-NCAR reanalysis. These experiments provide a way of interpreting the large-scale barotropic wave response to ENSO forced by those baroclinic-barotropic interactions. Although we keep the barotropic-to-baroclinic feedback in the QTCM, the results here should be reproduced using a pure barotropic model. The caveats are that as waves propagate far from the source, the accurate simulation of background zonal wind becomes essential. The QTCM uses its own background field, which is shown below (Fig. 4.1) to have good agreement with that from NCEP-NCAR reanalysis. While we should not completely trust the far field response, the wave response close to the source in this self-consistent baroclinic-barotropic decomposition model should compare reasonably well with that from NCEP-NCAR reanalysis and other models prescribing the reanalysis background winds.

Figure 4.1 shows the DJF mean climatology of barotropic zonal wind and baroclinic zonal wind at 200mb from NCEP-NCAR reanalysis and a 100yr QTCM run with climatological SSTs. Recall that the barotropic component is independent of p, and is represented as the vertical mean in NCEP-NCAR reanalysis. The baroclinic component is calculated as the departures from vertical mean at each level. We choose to present 200mb baroclinic wind because this level is important for steering storms that impact the California coast during ENSO, and is also a typical level selected for representing the basic state flow in previous studies using simpler barotropic models. The most

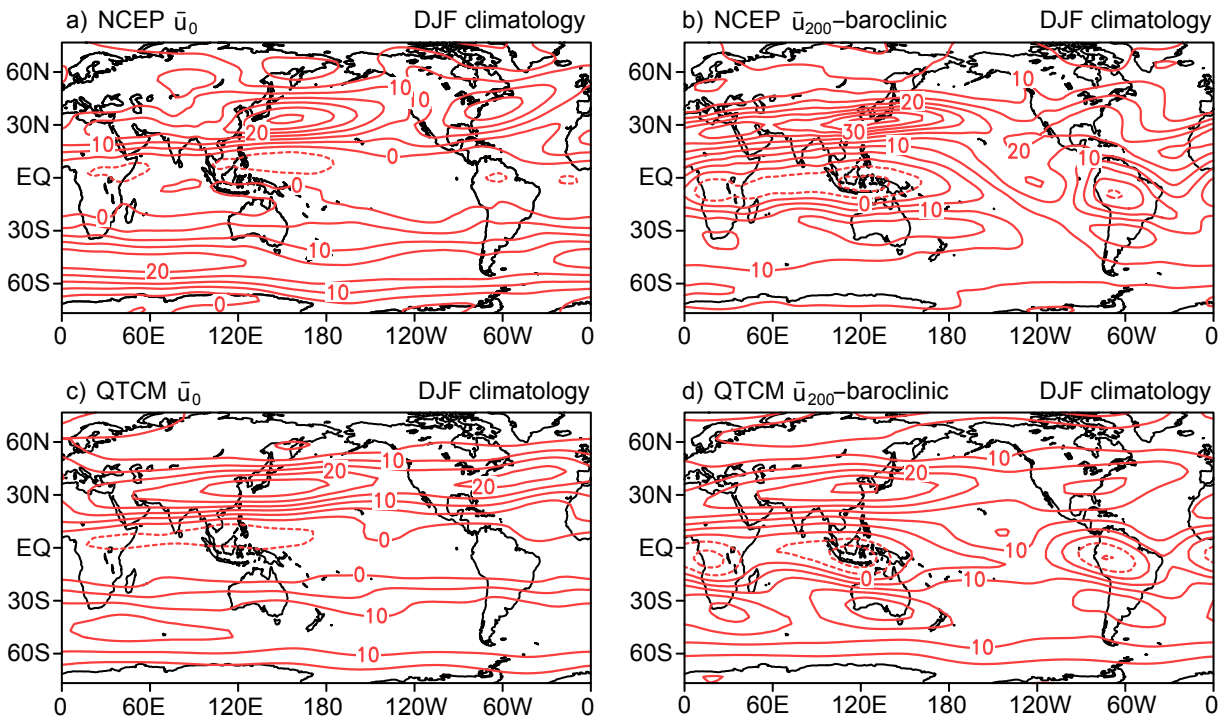

Figure 4.1: DJF climatology of (a) NCEP barotropic zonal wind ($\bar{u}_0$), (b) NCEP baroclinic zonal wind at 200mb ($\bar{u}_{200}$-baroclinic), (c) $\bar{u}_0$ from a 100yr QTCM run with climatological SSTs, and (d) QTCM $\bar{u}_{200}$-baroclinic. The units are m s $^{-1}$.

noticeable feature in Fig. 4.1 is that the barotropic and baroclinic components reinforce each other in the subtropical jet region in the Northern Pacific. The background winds generally agree well between the reanalysis and model simulation, in regards to the jet location in western Pacific, the extended westerlies in the tropics, as well as the westerlies in the subtropical North Atlantic, which is broader in the NCEP-NCAR reanalysis compared to the model simulations.

4.3 ENSO composites in the NCEP-NCAR reanalysis

Figure 4.2 shows ENSO DJF composite anomalies of the tropospheric temperature and baroclinic vector wind at 200mb from NCEP-NCAR reanalysis. The most prominent structure of these temperature anomalies is consistent with a baroclinic Rossby wave straddling the equator in the eastern Pacific and a Kelvin wave-like structure extending to the east. There are also statistically significant temperature anomalies in the North Pacific and North America region. The

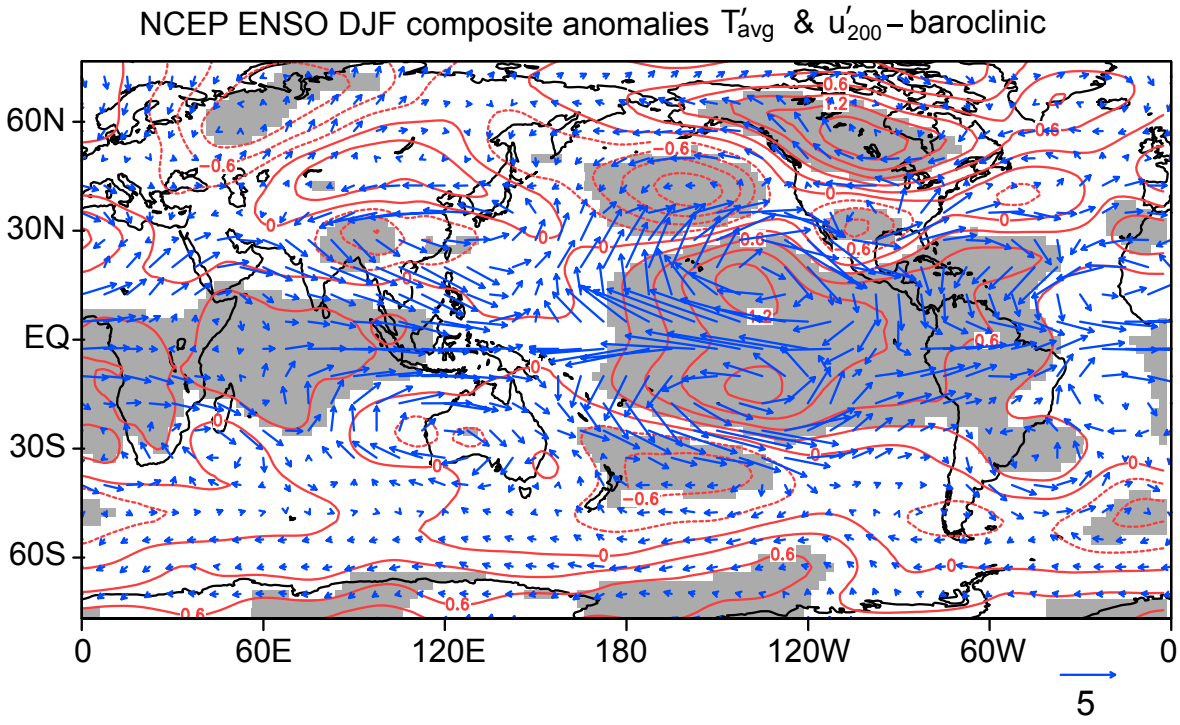

Figure 4.2: NCEP ENSO DJF composite anomalies of vertically averaged tropospheric temperature (T'_{avg}) and 200mb baroclinic wind (u'_{200}-baroclinic). The units are K for temperature, and m s^{-1} for winds.

baroclinic wind anomalies at 200mb are roughly consistent with geostrophic thermal wind balance in the subtropics and midlatitudes. The baroclinic shear advecting the baroclinic wind anomalies in both tropics and subtropics force the barotropic response in ENSO teleconnections, which we will discuss in further detail in Fig. 4.4.

Figure 4.3 shows ENSO DJF composite anomalies of upper-level (200mb) and lower-level (1000mb) zonal winds and their baroclinic components from NCEP-NCAR reanalysis. The upper-level easterlies on the equator in 200mb zonal wind, together with the lower level westerlies in 1000mb zonal wind, indicate a dominant baroclinic structure in the deep tropics. In the subtropical Pacific, the wind anomalies associated with ENSO have a substantial barotropic component, indicated by anomalous westerlies throughout the troposphere in 200mb and 1000mb winds. In the subtropics and midlatitudes, at 1000mb, the barotropic contribution (Fig. 4.4) considerably cancels the baroclinic contribution (Fig. 4.3d) to the surface wind, as one would expect when surface drag

is effective at reducing the near-surface wind, and spinning up a strong barotropic component.

Figure 4.4 shows ENSO DJF composite anomalies of barotropic zonal wind from NCEP-NCAR reanalysis. The barotropic component is substantial in the subtropics where the subtropical jet extends between 20°N-30°N off the U.S coast, with a magnitude similar to the baroclinic component (Fig. 4.3b). The barotropic contribution in the tropics is also not negligible.

4.4 The effective RWS and QTCM experiments

Figure 4.5 shows ENSO DJF composite anomalies of the effective RWS (Fig. 4.5a) [i.e., the rhs of Eq. (4.4)], and each of the three components: shear advection (Fig. 4.5b), vertical advection (Fig. 4.5c), and surface drag (Fig. 4.5d) from NCEP-NCAR reanalysis. Figure 4.5e shows the residual calculated by subtracting the effective RWS from $curl_z(\mathbf{v}_0 \cdot \nabla \mathbf{v}_0) + \beta v_0$, and Fig. 4.5f is sum of the effective RWS and the residual. Because the curl is taken in the effective RWS terms, many small-scale features are present due to the spatial derivative. However, the barotropic wind (or stream function) response will appear primarily on scales of the stationary Rossby wavelength, roughly a few thousand kilometers (estimated using $2\pi\sqrt{\frac{u_0}{\beta}}$ with u_0 around 30 m s^{-1}, and β on the order of 10^{-11} m^{-1} s^{-1}). To better visualize the response, it is useful to have a model result forced by these RWS terms, for which we use the QTCM. The box indicates the Pacific region where the forcing is applied in the QTCM experiments, values outside the region is set to zero.

We next present results of the model experiments. These results are from pairs of 100-year QTCM simulations: one is the control or climatological run and the other is performed with ENSO DJF composite anomalies of each forcing source in Fig. 4.5 added to the rhs of the barotropic vorticity equation (RWS run). Both runs use monthly-mean climatological SSTs. Differences between each pair are thus due to the response to each forcing anomalies within the Pacific region. The 100-year simulation length is used to obtain statistically significant results.

Figure 4.6 shows the QTCM DJF barotropic wind anomalies in response to each forcing source in Fig. 4.5. The barotropic wind response to the effective RWS show qualitatively good agreement with the DJF composite anomalies of barotropic wind from NCEP-NCAR reanalysis in Fig. 4.4, in the tropical central Pacific, the subtropical northern Pacific and the North America region. The contributions from each of the three baroclinic-barotropic interaction terms are not

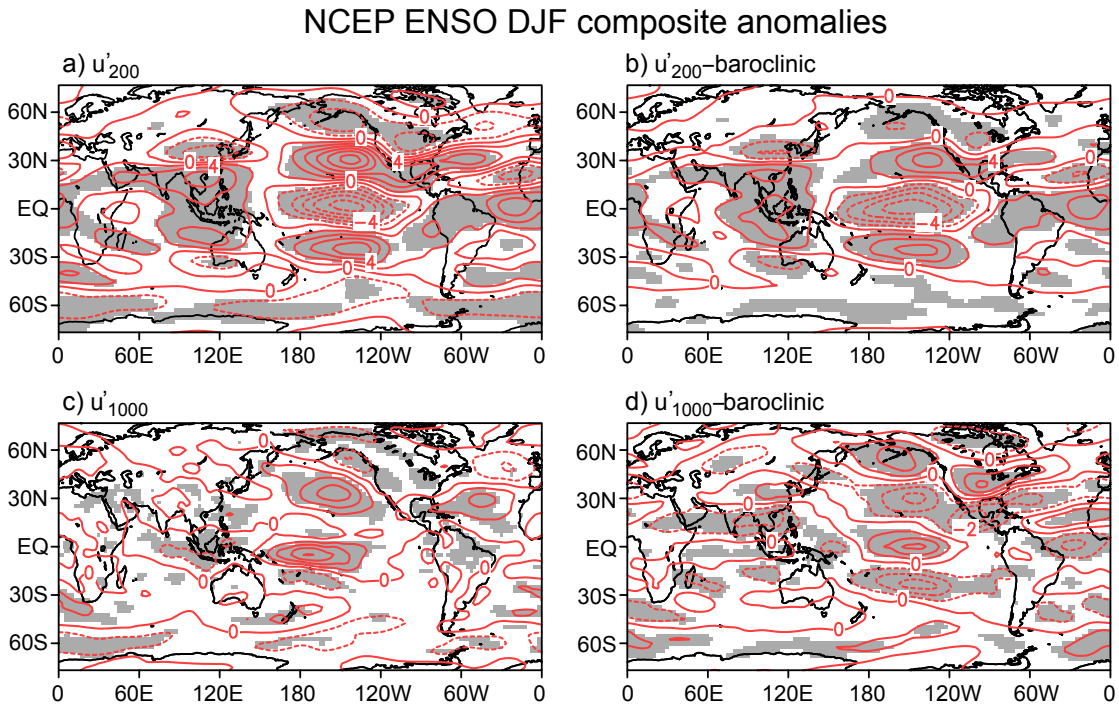

Figure 4.3: NCEP ENSO DJF composite anomalies of (a) zonal wind at 200mb (u'_{200}, contour interval is 2 m s^{-1}), (b) u'_{200} baroclinic component (contour interval is 2 m s^{-1}), (c) zonal wind at 1000mb (u'_{1000}, contour interval is 1 m s^{-1}), and (d) u'_{1000} baroclinic component (contour interval is 1 m s^{-1}).

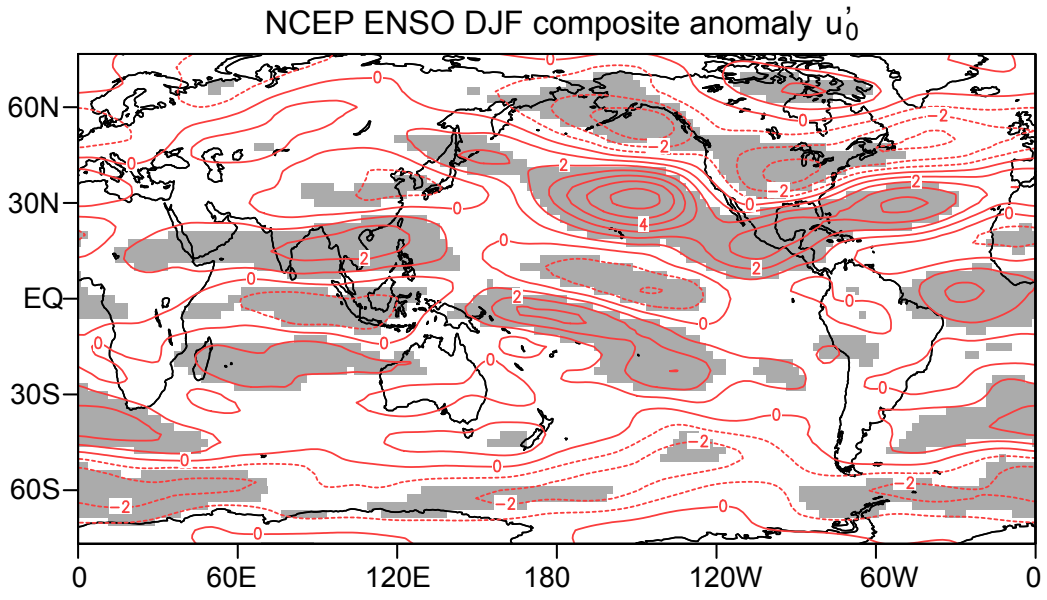

Figure 4.4: NCEP ENSO DJF composite anomaly of barotropic component of zonal wind ($u_0{}'$, contour interval is 1 m s^{-1}).

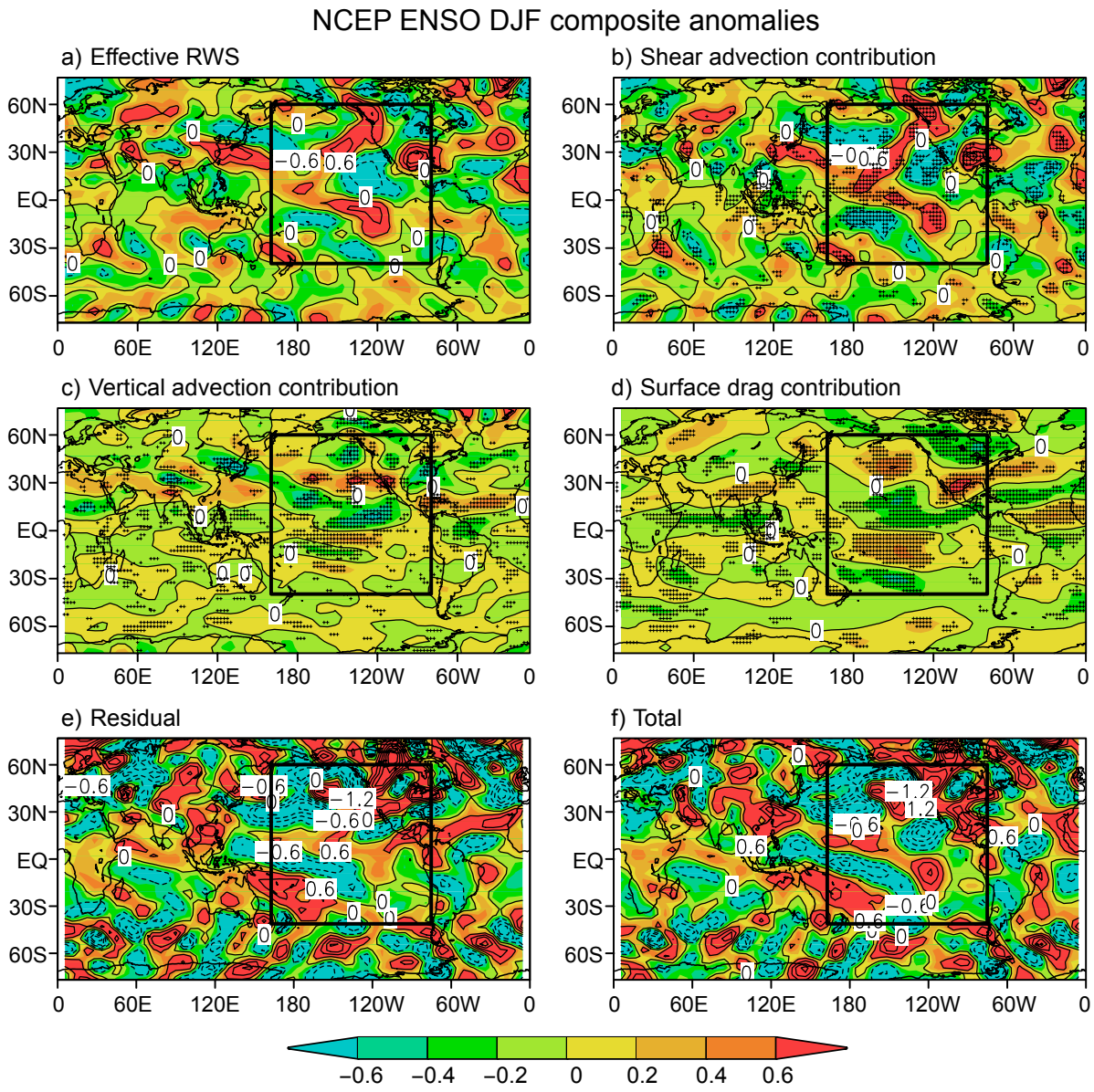

Figure 4.5: NCEP ENSO DJF composite anomalies of (a) the effective RWS, (b) shear advection contribution, (c) vertical advection contribution, (d) surface drag contribution, (e) the residual, and (f) the effective RWS plus the residual (total). The box indicates the Pacific region where the forcing is applied in the QTCM experiments, values outside the region is set to zero. The units are (x10^{-11} s^{-2}).

negligible, and they cancel and reinforce each other in different regions. That being said, the vertical advection contribution is noticeably smaller among the three, even in the tropics. This is in contrast to traditional assumptions that upper-level divergence is an important forcing term. The shear advection contribution is larger among the three, modified by the other two sources, especially by surface drag in the western Pacific. In the region off California coast, where the subtropical jet extends further east in ENSO, the three interaction terms reinforce each other. For the case of residual forcing shown in Fig. 4.6e, there is a substantial response off the U.S. coast. And lastly, in Fig. 4.6f, we show the barotropic wind response to the sum of the effective RWS and the residual. In this case, the response off U.S. coast is qualitatively similar to the case forced by the effective RWS in Fig. 4.6a, with a larger amplitude. While we have to be cautious about the residual calculation, it is presumed to be due to nonlinear effects of departures from the monthly averages due to high-frequency storm transients. Reinforcement of the ENSO subtropical to mid-latitude anomalies by changes in storm statistics has previously been noted (Held et al., 1989; Hoerling and Ting, 1994). The jet anomalies in the subtropics can be interpreted as a substantial contribution from the monthly RWS, reinforced by associated changes in transients.

To identify the dominant component of shear advection forcing, we linearize the shear advection term $-\langle curl_z(\mathbf{v}_1 \cdot \nabla \mathbf{v}_1)' \rangle$ approximately as: $\frac{\partial}{\partial y}\left\langle \bar{u}_1 \frac{\partial {u_1}'}{\partial x} + \bar{v}_1 \frac{\partial {u_1}'}{\partial y} \right\rangle + \frac{\partial}{\partial y}\left\langle {u_1}' \frac{\partial \bar{u}_1}{\partial x} + {v_1}' \frac{\partial \bar{u}_1}{\partial y} \right\rangle - \frac{\partial}{\partial x}\left\langle \bar{u}_1 \frac{\partial {v_1}'}{\partial x} + \bar{v}_1 \frac{\partial {v_1}'}{\partial y} \right\rangle - \frac{\partial}{\partial x}\left\langle {u_1}' \frac{\partial \bar{v}_1}{\partial x} + {v_1}' \frac{\partial \bar{v}_1}{\partial y} \right\rangle$. Examining each of the four components, we find the largest component is the first term $\frac{\partial}{\partial y}\left\langle \bar{u}_1 \frac{\partial {u_1}'}{\partial x} + \bar{v}_1 \frac{\partial {u_1}'}{\partial y} \right\rangle$, which is shown in Fig. 4.7a. Figure 4.7b shows the same term as in 4.7a, but without the curl, as it appears in ${u_0}'$ equation, i.e., $\partial_t {u_0}' = -\left\langle \bar{u}_1 \frac{\partial {u_1}'}{\partial x} + \bar{v}_1 \frac{\partial {u_1}'}{\partial y} \right\rangle + ...$ Without the curl, the same term shows slightly larger spatial scales and shifted maximum and minimum locations. Figures 4.7c and 4.7d show $\left\langle \bar{u}_1 \frac{\partial {u_1}'}{\partial x} \right\rangle$ and $\left\langle \bar{v}_1 \frac{\partial {u_1}'}{\partial y} \right\rangle$ respectively. The mean baroclinic zonal wind advecting the anomalous baroclinic zonal wind $\left\langle \bar{u}_1 \frac{\partial {u_1}'}{\partial x} \right\rangle$ is the larger of the two, the pattern of which coincides well with barotropic wind response to shear advection in Fig. 4.6b. In the subtropics, baroclinic $\bar{u}_1$ at 200mb (Fig. 4.1b) advecting positive $\frac{\partial {u_1}'}{\partial x}$ (Fig. 4.2) results in the large positive area in the subtropical jet region in Fig. 4.7c. Similarly, the negative area east of the positive area close to the U.S. coast is due to the negative $\frac{\partial {u_1}'}{\partial x}$ (Fig. 4.2) in that region. The large positive region in tropical eastern Pacific is because of the modest $\bar{u}_1$ at 200mb (Fig. 4.1b) advecting strong positive gradient $\frac{\partial {u_1}'}{\partial x}$ (Fig. 4.2).

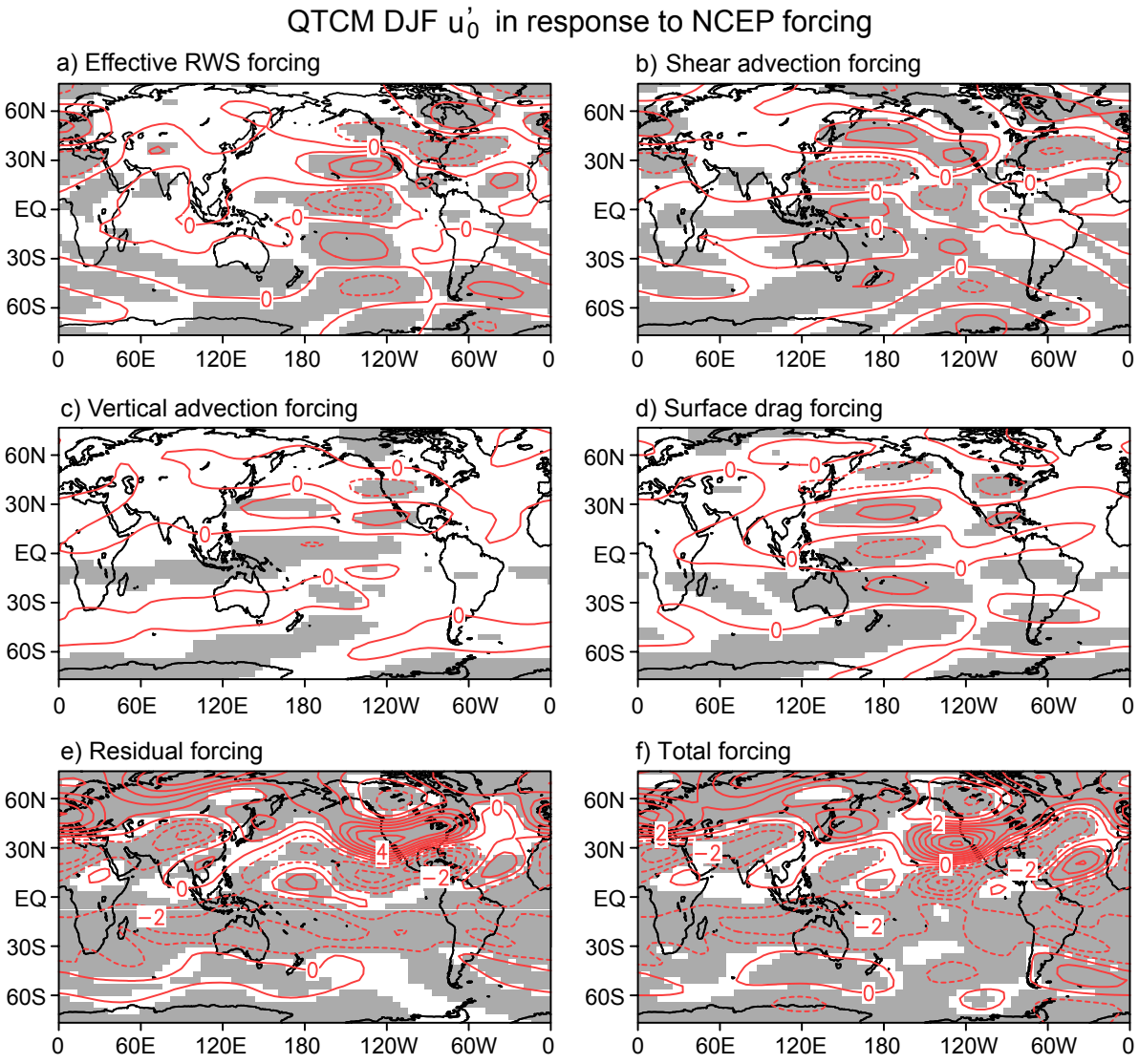

Figure 4.6: QTCM DJF barotropic wind anomalies (u_0') forced with (a) the effective RWS forcing, (b) shear advection forcing, (c) vertical advection forcing, (d) surface drag forcing, (e) the residual forcing, and (f) total forcing (the effective RWS plus the residual forcing) in Fig. 4.5. The units are m s^{-1}.

For the meridional case in Fig. 4.7d, the two negative regions are the results from modest $\bar{v}_1$ (not shown) advecting large gradient $\frac{\partial u_1'}{\partial y}$ (Fig. 4.2). The same analysis applies at lower levels with sign reversed for both mean and anomalies, which gives the forcing in the same direction.

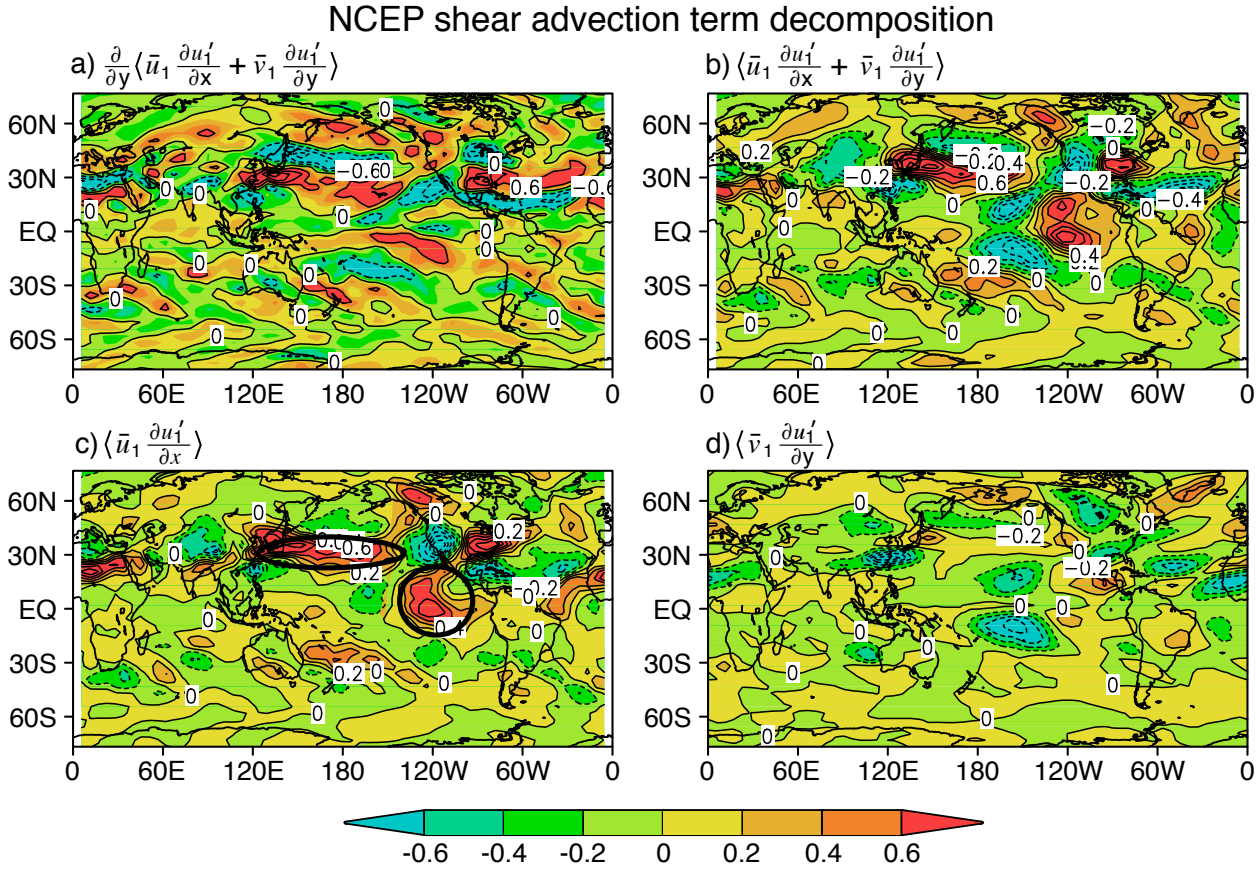

Figure 4.7: Shear advection term decomposition: (a) the largest term in shear advection: $\frac{\partial}{\partial y}\left\langle \bar{u}_1 \frac{\partial u_1'}{\partial x} + \bar{v}_1 \frac{\partial u_1'}{\partial y} \right\rangle$, (b) the largest term in shear advection without curl: $\left\langle \bar{u}_1 \frac{\partial u_1'}{\partial x} + \bar{v}_1 \frac{\partial u_1'}{\partial y} \right\rangle$, (c) the u component: $\left\langle \bar{u}_1 \frac{\partial u_1'}{\partial x} \right\rangle$, and (d) the v component: $\left\langle \bar{v}_1 \frac{\partial u_1'}{\partial y} \right\rangle$. Black ovals in panel c highlight regions of strong $\left\langle \bar{u}_1 \frac{\partial u_1'}{\partial x} \right\rangle$ shear advection discussed in the text.

If we assume that the response to the effective RWS is linear, we can explore how large the contribution is from each region. We perform two experiments with the effective RWS in two narrower boxes: one is in tropics (15°N-15°S, 160°E-80°W); the other is in subtropics (15°N-40°N, 160°E-100°W). We find that off the U.S. coast, roughly half of the jet response is due to forcing in the subtropics locally, and half is due to forcing in the tropics (figures not shown). From the previous analysis on shear advection decomposition, it is easy to see that while such experiments

are easy to do, and may help to understand the relative contribution of different parts of the Rossby wave source, the separation into tropics and subtropics is artificial. The barotropic teleconnections in the subtropical jet region result from the basic state baroclinic wind advection acting on the baroclinic response to ENSO seen in the flow pattern in Fig. 4.2, which spreads by baroclinic wave dynamics from the deep tropics into subtropics on the scale of equatorial radius of deformation.

4.5 Conclusions

To understand the complex baroclinic-to-barotropic pathway in the tropical to midlatitude ENSO teleconnection process, it can be useful to examine an approach that considers a systematic modal breakdown of baroclinic and barotropic modes. In this view, the barotropic mode is forced by the baroclinic-barotropic interaction terms, which yield the effective Rossby wave source. These RWS interaction terms are diagnosed from the NCEP-NCAR reanalysis data to create ENSO anomalies. Different from the classic studies that assume that a diagnosed upper-level vorticity source forces a barotropic mode, the effective RWS in our approach represents the forcing on the barotropic component evaluated through the atmospheric column (here 200mb to the surface). Under these approximations, baroclinic and barotropic components of ENSO wind anomalies are examined as composites from the NCEP-NCAR reanalysis. The barotropic component is substantial even in the tropical Pacific, implying that a purely baroclinic mode representation of ENSO would be incomplete even within the forcing region. In the subtropical Pacific off the U.S. west coast, which can be important for ENSO impacts on North America, the baroclinic contribution remains substantial, but the barotropic mode contribution doubles the subtropical jet response to ENSO.

Composite ENSO anomalies of the effective RWS as vorticity source contributions that appear on the rhs of barotropic vorticity equation can be interpreted directly, but it can also be useful to see the associated wind solutions. For this, the QTCM, a model with an explicit baroclinic barotropic mode breakdown, is used to diagnose the response. In these QTCM experiments, the barotropic vorticity equation of the model is forced by the composite ENSO anomaly effective RWS diagnosed from the NCEP-NCAR reanalysis. The resulting zonal wind anomalies (compared to the wind in a control run) are qualitatively in good agreement with those of the ENSO composite

barotropic wind response from the NCEP reanalysis, including in the subtropics off the U.S. coast. Although there are non-trivial impacts of transients in the barotropic wind response to ENSO, qualitatively, the barotropic response near coast of North America is mainly due to the effective Rossby wave source term as diagnosed from monthly means. Among the three barotropic Rossby wave source contributions (shear advection, vertical advection and surface drag), vertical advection contributions arise from anomalous vertical velocity in regions where there is climatological baroclinic shear, but these terms tend to be smaller than the others. This is in contrast to traditional assumptions that upper-level divergence is an important forcing term. The surface drag contribution alternately tends to cancel or reinforce the shear advection in different regions through damping on baroclinic mode which spins up a barotropic response. The dominant contributions are from the shear advection. Further decomposition of the shear advection term shows that the mean baroclinic zonal wind advecting the anomalous baroclinic zonal wind is the most import component. Shear advection in both the tropics and subtropics contribute to the subtropical response, but both are an integral part of basic state advection of the baroclinic ENSO flow pattern. In this view, the effective Rossby wave source in the subtropics simply arises from the basic state baroclinic flow acting on the well-known baroclinic ENSO flow pattern that spreads from the deep tropics into the subtropics over a scale of equatorial radius of deformation. This is inseparably connected to the leading deep tropical Rossby wave source that arises from Eastern Pacific basic state baroclinic winds advecting the tropical portion of the same ENSO flow pattern.

Bibliography

Bacmeister, J. T., and M. J. Suarez, 2002: Wind stress simulations and the equatorial momentum budget in an AGCM. *Journal of the Atmospheric Sciences*, **59 (21)**, 3051–3073.

Barnston, A. G., A. Leetmaa, V. E. Kousky, R. E. Livezey, E. O'Lenic, H. Van den Dool, A. J. Wagner, and D. A. Unger, 1999: NCEP forecasts of the El Niño of 1997—98 and its U.S. impacts. *Bulletin of the American Meteorological Society*, **80 (9)**, 1829–1852.

Berlage, H. P., 1957: *Fluctuations of the General Atmospheric Circulation of More Than One Year, Their Nature and Prognostic Value*, Vol. 69. Koninkijk Nedeerlands Meteorologisch Instituut Mededelingen en Verhandelingen.

Biello, J. A., and A. J. Majda, 2004a: Boundary layer dissipation and the nonlinear interaction of equatorial baroclinic and barotropic rossby waves. *Geophysical & Astrophysical Fluid Dynamics*, **98 (2)**, 85–127.

Biello, J. A., and A. J. Majda, 2004b: The effect of meridional and vertical shear on the interaction of equatorial baroclinic and barotropic rossby waves. *Studies in Applied Mathematics*, **112 (4)**, 341–390.

Branstator, G., 1983: Horizontal energy propagation in a barotropic atmosphere with meridional and zonal structure. *Journal of the Atmospheric Sciences*, **40 (7)**, 1689–1708.

Chiang, J. C. H., and A. H. Sobel, 2002: Tropical tropospheric temperature variations caused by ENSO and their influence on the remote tropical climate. *Journal of Climate*, **15 (18)**, 2616–2631.

Chou, C., and J. D. Neelin, 2003: Mechanisms limiting the northward extent of the northern summer monsoons over north america, asia, and africa. *Journal of Climate*, **16 (3)**, 406–425.

DeWeaver, E., and S. Nigam, 2004: On the forcing of ENSO teleconnections by anomalous heating and cooling. *Journal of Climate*, **17 (16)**, 3225–3235.

Gill, A. E., 1980: Some simple solutions for heat-induced tropical circulation. *Quarterly Journal of the Royal Meteorological Society*, **106 (449)**, 447–462.

Goddard, L., and N. E. Graham, 1999: Importance of the Indian Ocean for simulating rainfall anomalies over eastern and southern Africa. *Journal of Geophysical Research: Atmospheres*, **104 (D16)**, 19 099–19 116.

Held, I. M., and I.-S. Kang, 1987: Barotropic models of the extratropical response to El Niño. *Journal of the Atmospheric Sciences*, **44 (23)**, 3576–3586.

Held, I. M., S. W. Lyons, and S. Nigam, 1989: Transients and the extratropical response to El Niño. *Journal of the Atmospheric Sciences*, **46 (1)**, 163–174.

Held, I. M., R. L. Panetta, and R. T. Pierrehumbert, 1985: Stationary external Rossby Waves in vertical shear. *Journal of the Atmospheric Sciences*, **42 (9)**, 865–883.

Hoerling, M. P., and M. Ting, 1994: Organization of extratropical transients during El Niño. *Journal of Climate*, **7 (5)**, 745–766.

Horel, J. D., and J. M. Wallace, 1981: Planetary-scale atmospheric phenomena associated with the Southern Oscillation. *Monthly Weather Review*, **109 (4)**, 813–829.

Hoskins, B. J., and D. J. Karoly, 1981: The steady linear response of a spherical atmosphere to thermal and orographic forcing. *Journal of the Atmospheric Sciences*, **38 (6)**, 1179–1196.

Ji, X., J. D. Neelin, S.-K. Lee, and C. R. Mechoso, 2014: Interhemispheric teleconnections from tropical heat sources in intermediate and simple models. *Journal of Climate*, **27 (2)**, 684–697.

Ji, X., J. D. Neelin, and C. R. Mechoso, 2015: El Niño/Southern Oscillation Sea Level Pressure anomalies in the western Pacific: Why are they there? *Journal of Climate*, **28 (22)**, 8860–8872.

Kalnay, E., M. Kanamitsu, R. Kistler, W. Collins, D. Deaven, L. Gandin, M. Iredell, S. Saha, G. White, J. Woollen, Y. Zhu, A. Leetmaa, R. Reynolds, M. Chelliah, W. Ebisuzaki, W. Higgins, J. Janowiak, K. C. Mo, C. Ropelewski, J. Wang, R. Jenne, and D. Joseph, 1996: The NCEP/NCAR 40-year reanalysis project. *Bulletin of the American Meteorological Society*, **77 (3)**, 437–471.

Kiladis, G. N., and H. F. Diaz, 1989: Global climatic anomalies associated with extremes in the Southern Oscillation. *Journal of Climate*, **2 (9)**, 1069–1090.

Kumar, A., and M. P. Hoerling, 1998: Specification of regional sea surface temperatures in atmospheric general circulation model simulations. *Journal of Geophysical Research: Atmospheres*, **103 (D8)**, 8901–8907.

Kumar, A., and M. P. Hoerling, 2003: The nature and causes for the delayed atmospheric response to El Niño. *Journal of Climate*, **16 (9)**, 1391–1403.

Latif, M., D. Dommenget, M. Dima, and A. Grötzner, 1999: The role of Indian Ocean sea surface temperature in forcing east African rainfall anomalies during December—January 1997/98. *Journal of Climate*, **12 (12)**, 3497–3504.

Lau, N.-C., 1985: Modeling the seasonal dependence of the atmospheric response to observed El Niños in 1962–76. *Monthly Weather Review*, **113 (11)**, 1970–1996.

Lee, S.-K., C. Wang, and B. E. Mapes, 2009: A simple atmospheric model of the local and teleconnection responses to tropical heating anomalies. *Journal of Climate*, **22 (2)**, 272–284.

Lin, J. W.-B., and J. D. Neelin, 2000: Influence of a stochastic moist convective parameterization on tropical climate variability. *Geophysical Research Letters*, **27 (22)**, 3691–3694.

Lin, J. W.-B., and J. D. Neelin, 2002: Considerations for stochastic convective parameterization. *Journal of the Atmospheric Sciences*, **59 (5)**, 959–975.

Lin, J. W.-B., J. D. Neelin, and N. Zeng, 2000: Maintenance of tropical intraseasonal variability: Impact of evaporation—wind feedback and midlatitude storms. *Journal of the Atmospheric Sciences*, **57 (17)**, 2793–2823.

Lintner, B. R., and J. C. H. Chiang, 2007: Adjustment of the remote tropical climate to El Niño conditions. *Journal of Climate*, **20 (11)**, 2544–2557.

Ma, H. Y., X. Ji, J. D. Neelin, and C. R. Mechoso, 2011: Mechanisms for precipitation variability of the eastern Brazil/SACZ convective margin. *Journal of Climate*, **24 (13)**, 3445–3456.

Ma, H.-Y., C. R. Mechoso, Y. Xue, H. Xiao, J. D. Neelin, and X. Ji, 2013: On the connection between continental-scale land surface processes and the tropical climate in a coupled ocean–atmosphere–land system. *Journal of Climate*, **26 (22)**, 9006–9025.

Majda, A. J., and J. A. Biello, 2003: The nonlinear interaction of barotropic and equatorial baroclinic Rossby waves. *Journal of the Atmospheric Sciences*, **60 (15)**, 1809–1821.

Matsuno, T., 1966: Quasi-geostrophic motions in the equatorial area. *Journal of the Meteorological Society of Japan. Ser. II*, **44 (1)**, 25–43.

Mechoso, C. R., A. Kitoh, S. Moorthi, and A. Arakawa, 1987: Numerical simulations of the atmospheric response to a sea surface temperature anomaly over the equatorial eastern Pacific Ocean. *Monthly Weather Review*, **115 (12)**, 2936–2956.

Neelin, J. D., and H. Su, 2005: Moist teleconnection mechanisms for the tropical south American and Atlantic sector. *Journal of Climate*, **18 (18)**, 3928–3950.

Neelin, J. D., and N. Zeng, 2000: A quasi-equilibrium tropical circulation model—formulation. *Journal of the Atmospheric Sciences*, **57 (11)**, 1741–1766.

Reynolds, R. W., and T. M. Smith, 1994: Improved global sea surface temperature analyses using optimum interpolation. *Journal of Climate*, **7 (6)**, 929–948.

Ropelewski, C. F., and M. S. Halpert, 1987: Global and regional scale precipitation patterns associated with the El Niño/Southern Oscillation. *Monthly Weather Review*, **115 (8)**, 1606–1626.

Salby, M. L., and R. R. Garcia, 1987: Vacillations induced by interference of stationary and traveling planetary waves. *Journal of the Atmospheric Sciences*, **44 (19)**, 2679–2711.

Saravanan, R., and P. Chang, 2000: Interaction between tropical atlantic variability and El Niño/Southern Oscillation. *Journal of Climate*, **13 (13)**, 2177–2194.

Sardeshmukh, P. D., and B. J. Hoskins, 1988: The generation of global rotational flow by steady idealized tropical divergence. *Journal of the Atmospheric Sciences*, **45 (7)**, 1228–1251.

Simmons, A. J., 1982: The forcing of stationary wave motion by tropical diabatic heating. *Quarterly Journal of the Royal Meteorological Society*, **108 (457)**, 503–534.

Simmons, A. J., J. M. Wallace, and G. W. Branstator, 1983: Barotropic wave propagation and instability, and atmospheric teleconnection patterns. *Journal of the Atmospheric Sciences*, **40 (6)**, 1363–1392.

Stevens, B., J. Duan, J. C. McWilliams, M. Münnich, and J. D. Neelin, 2002: Entrainment, rayleigh friction, and boundary layer winds over the tropical Pacific. *Journal of Climate*, **15 (1)**, 30–44.

Su, H., and J. D. Neelin, 2002: Teleconnection mechanisms for tropical pacific descent anomalies during El Niño. *Journal of the Atmospheric Sciences*, **59 (18)**, 2694–2712.

Su, H., J. D. Neelin, and C. Chou, 2001: Tropical teleconnection and local response to sst anomalies during the 1997–1998 El Niño. *Journal of Geophysical Research: Atmospheres*, **106 (D17)**, 20 025–20 043.

Su, H., J. D. Neelin, and J. E. Meyerson, 2003: Sensitivity of tropical tropospheric temperature to sea surface temperature forcing. *Journal of Climate*, **16 (9)**, 1283–1301.

Su, H., J. D. Neelin, and J. E. Meyerson, 2005: Mechanisms for lagged atmospheric response to ENSO SST forcing. *Journal of Climate*, **18 (20)**, 4195–4215.

Taylor, K. E., R. J. Stouffer, and G. A. Meehl, 2012: An overview of CMIP5 and the experiment design. *Bulletin of the American Meteorological Society*, **93 (4)**, 485–498.

Ting, M., and I. M. Held, 1990: The stationary wave response to a tropical SST anomaly in an idealized GCM. *Journal of the Atmospheric Sciences*, **47 (21)**, 2546–2566.

Trenberth, K. E., 1997: The definition of El Niño. *Bulletin of the American Meteorological Society*, **78 (12)**, 2771–2777.

Trenberth, K. E., G. W. Branstator, D. Karoly, A. Kumar, N.-C. Lau, and C. Ropelewski, 1998: Progress during TOGA in understanding and modeling global teleconnections associated with tropical sea surface temperatures. *Journal of Geophysical Research*, **103 (C7)**, 14 291–14 324.

Walker, G. T., 1923: Correlation in seasonal variations of weather viii. a preliminary study of world weather. *Memoirs of the Indian Meteorological Department*, **24 (4)**, 75–131.

Wallace, J. M., E. M. Rasmusson, T. P. Mitchell, V. E. Kousky, E. S. Sarachik, and H. von Storch, 1998: On the structure and evolution of ENSO-related climate variability in the tropical Pacific: Lessons from TOGA. *Journal of Geophysical Research: Oceans*, **103 (C7)**, 14 241–14 259.

Wang, B., and X. Xie, 1996: Low-frequency equatorial waves in vertically sheared zonal flow. part i: Stable waves. *Journal of the Atmospheric Sciences*, **53 (3)**, 449–467.

Wang, C., S.-k. Lee, and D. B. Enfield, 2007: Impact of the Atlantic Warm Pool on the summer climate of the Western Hemisphere. *Journal of Climate*, **20 (20)**, 5021–5040.

Wang, C., S.-K. Lee, and D. B. Enfield, 2008: Climate response to anomalously large and small Atlantic Warm Pools during the summer. *Journal of Climate*, **21 (11)**, 2437–2450.

Wang, C., S.-K. Lee, and C. R. Mechoso, 2010: Interhemispheric influence of the Atlantic Warm Pool on the southeastern Pacific. *Journal of Climate*, **23 (2)**, 404–418.

Webster, P. J., 1972: Response of the tropical atmosphere to local, steady forcing. *Monthly Weather Review*, **100 (7)**, 518–541.

Zeng, N., J. D. Neelin, and C. Chou, 2000: A quasi-equilibrium tropical circulation model—implementation and simulation. *Journal of the Atmospheric Sciences*, **57 (11)**, 1767–1796.